National Library of Canada
Bibliothèque nationale du Canada

Canadian Theses Service
Service des thèses canadiennes

Ottawa, Canada
K1A 0N4

NOTICE

The quality of this microform is heavily dependent upon the quality of the original thesis submitted for microfilming. Every effort has been made to ensure the highest quality of reproduction possible.

If pages are missing, contact the university which granted the degree.

Some pages may have indistinct print especially if the original pages were typed with a poor typewriter ribbon or if the university sent us an inferior photocopy.

Reproduction in full or in part of this microform is governed by the Canadian Copyright Act, R.S.C. 1970, c. C-30, and subsequent amendments.

AVIS

La qualité de cette microforme dépend grandement de la qualité de la thèse soumise au microfilmage. Nous avons tout fait pour assurer une qualité supérieure de reproduction.

S'il manque des pages, veuillez communiquer avec l'université qui a conféré le grade.

La qualité d'impression de certaines pages peut laisser à désirer, surtout si les pages originales ont été dactylographiées à l'aide d'un ruban usé ou si l'université nous a fait parvenir une photocopie de qualité inférieure.

La reproduction, même partielle, de cette microforme est soumise à la Loi canadienne sur le droit d'auteur, SRC 1970, c. C-30, et ses amendements subséquents.

NL-339 (r. 88/04) c

Canada

UNIVERSITY OF ALBERTA

SORPTION RATES AND BANDBROADENING ON A POROUS POLYMERIC HPLC PACKING

BY

LAURIE M. LITWINSON

A THESIS SUBMITTED TO THE FACULTY OF GRADUATE STUDIES AND RESEARCH IN PARTIAL FULFILLMENT OF THE REQUIREMENTS FOR THE DEGREE OF

MASTER OF SCIENCE

DEPARTMENT OF CHEMISTRY

EDMONTON, ALBERTA

SPRING, 1992

National Library of Canada
Bibliothèque nationale du Canada

Canadian Theses Service
Service des thèses canadiennes

Ottawa, Canada
K1A 0N4

The author has granted an irrevocable non-exclusive licence allowing the National Library of Canada to reproduce, loan, distribute or sell copies of his/her thesis by any means and in any form or format, making this thesis available to interested persons.

L'auteur a accordé une licence irrévocable et non exclusive permettant à la Bibliothèque nationale du Canada de reproduire, prêter, distribuer ou vendre des copies de sa thèse de quelque manière et sous quelque forme que ce soit pour mettre des exemplaires de cette thèse à la disposition des personnes intéressées.

The author retains ownership of the copyright in his/her thesis. Neither the thesis nor substantial extracts from it may be printed or otherwise reproduced without his/her permission.

L'auteur conserve la propriété du droit d'auteur qui protège sa thèse. Ni la thèse ni des extraits substantiels de celle-ci ne doivent être imprimés ou autrement reproduits sans son autorisation.

ISBN 0-315-73107-9

Canada

UNIVERSITY OF ALBERTA

RELEASE FORM

NAME OF AUTHOR: LAURIE M. LITWINSON

TITLE OF THESIS: SORPTION RATES AND BANDBROADENING ON A POROUS POLYMERIC HPLC PACKING

DEGREE FOR WHICH THESIS WAS PRESENTED: M.Sc.

YEAR THIS DEGREE GRANTED: 1991

Permission is hereby granted to the University of Alberta Library to reproduce single copies of this thesis and to lend or sell such copies for private, scholarly or scientific purposes only.

The author reserves all other publication and other rights in association with the copyright in the thesis, and except as hereinbefore provided neither the thesis nor any substantial portion thereof may be printed or otherwise reproduced in any material form whatever without the author's prior written permission.

L.M. Litwinson

#301 - 555 Austin Ave.
Coquitlam, B.C.
V3K 6R8

DATE: 13 Nov. 1991

UNIVERSITY OF ALBERTA

FACULTY OF GRADUATE STUDIES AND RESEARCH

The undersigned certify that they have read, and recommed to the Faculty of Graduate Studies and Research for acceptance, a thesis entitled, SORPTION RATES AND BANDBROADENING ON A POROUS POLYMERIC HPLC PACKING submitted by LAURIE M. LITWINSON in partial fulfillment of the requirements for the degree of MASTER OF SCIENCE.

F.F. Cantwell, Supervisor

N. Dovichi

P. Huck

DATE: 6 Nov 1991

This thesis is dedicated to my mother and the memory of my father

"You are the wind beneath my wings"

ABSTRACT

Although the polymeric phase Hamilton PRP-1, which is a styrene-divinylbenzene copolymer, is chemically more stable than silica-based reversed phases, it produces broad asymmetric peaks with certain compounds, such as naphthalene and other polyaromatics. Slow sorption-desorption rates on PRP-1 are investigated as a possible cause of the inefficiency.

A shallow bed apparatus is designed to measure rates of sorption on microparticulate HPLC packings. Milligram amounts of sorbent are contained in a slider valve and are subject to exposure to a flowing sample solution for times greater than about 0.4 s. A sorption rate curve, a plot of the concentration of sample in the stationary phase against exposure time, is produced. For sorption of naphthalene on PRP-1, the curve rises sharply then approaches equilibrium at 60 s relatively slowly. It is well fit by a tri-exponential rate equation.

An HPLC analytical column containing PRP-1 is modelled by a series of three hypothetical columns, each corresponding to a separate kinetic process described by one of the terms in the tri-exponential rate equation. Each hypothetical column acts on an impulse function to produce a probability distribution referred to as P1, P2, and P3, corresponding to the broadening caused by the fastest, intermediate and slowest sorption processes respectively. If a sample is injected into a series of the hypothetical columns, the overall predicted elution profile is a convolution of the three distributions.

For PRP-1, the observed elution peak of naphthalene is semi-quantitatively predicted by P1 and P2. The tail of the peak, predicted by inclusion of P3, is not well modelled because of uncertainties in P3 and because the extent of tailing appears to be dependent on column history.

The sorption rate curve of naphthalene on Partisil-10 ODS-3, a silica-based

packing is very different from that on PRP-1. There is a marked absence of a very slow sorption process that, on PRP-1, is observed to affect the curve mainly after the 10 s time. Because the rates on Partisil are too fast to be accurately measured, the sorption rate data does not accurately predict real elution profiles in this case.

ACKNOWLEDGEMENTS

The author is sincerely grateful to Dr. F.F. Cantwell for his infinite patience and invaluable guidance which made this work possible. Many thanks are also owed to David Gowanlock who simplified everything by writing the computer programs used in the calculations. The author would also like to thank the staff of the Machine Shop in the Chemistry department for their wisdom and expertise in manufacturing the shallow bed apparatus. Finally, the support of my friends, who made the bad days not quite so bad and the good days better, is also gratefully acknowledged.

The author would also like to thank NSERC, the University of Alberta and the Department of Chemistry for financial assistance.

TABLE OF CONTENTS

1. INTRODUCTION 1

2. THEORY

2.1 Bandbroadening in Liquid Chromatography

2.1.1 Introduction 7

2.1.2 Longitudinal Diffusion 8

2.1.3 Eddy Diffusion 8

2.1.4 Resistance to Mass Transfer in the Mobile Phase 9

2.1.5 Coupling of H_{eddy} and H_m 10

2.1.6 Resistance to Mass Transfer in the Stationary Phase 11

2.1.7 Resistance to Mass Transfer in the Stagnant Mobile Phase 12

2.1.8 Total Plate Height 13

2.1.9 Rate Processes and Bandbroadening 15

2.2 Shallow Bed Theory 16

2.3 Analysis of Sorption Rate Data

2.3.1 Curve Fitting of Sorption Rate Data 22

2.3.2 Calculation of Elution Profiles from Sorption Rate Data 22

2.3.3 Data Treatment for Bi-Exponential Rate Curve 25

2.3.4 Assumptions in Generation of Elution Profiles from Sorption Rate Data 28

2.3.5 Data treatment for Bi-Exponential Rate Curve where Non-Interacting Fraction for One Sorption Step is Significant 30

2.3.6 Data treatment for Tri-Exponential Rate Curve where Non-Interacting Fraction for One Sorption Step is Significant 33

2.3.7 Description of Elution Chromatographic Peaks by Statistical

Moment Analysis..... 36

3. EXPERIMENTAL PROCEDURES

3.1 Reagents..... 39

3.2 Solvents and Mobile Phases..... 39

3.3 Packings..... 40

3.4 Measurement of Sorption Rate Using the Shallow Bed Apparatus

3.4.1 Apparatus for Sorption Rate Measurements..... 40

3.4.2 Experimental Procedure..... 51

3.4.3 Hold-up Volume Measurement..... 54

3.4.4 Measurement of the Sorption Isotherm..... 56

3.5 Elution Chromatography

3.5.1 Experimental Procedure..... 57

3.5.2 Correction for Extra-Column Bandbroadening..... 60

4. RESULTS AND DISCUSSION

4.1 Introduction..... 62

4.2 Hamilton PRP-1 as a Sorbent

4.2.1 Characterization of Experimental Elution Profiles on PRP-1

4.2.1.1 Numerical Integration..... 62

4.2.1.2 Non-linear Least Squares Curve Fitting 67

4.2.1.3. Efficiency of PRP-1 HPLC Columns..... 79

4.2.2 Equilibrium Sorption of Naphthalene on PRP-1

4.2.2.1 Measurement of the Sorption Isotherm of Naphthalene on PRP-1..... 82

4.2.2.2 Calculation of k' from Elution Profiles of Naphthalene on PRP-1..... 85

4.2.3 Sorption Rate of Naphthalene on PRP-1..... 88

4.2.4 Sources of Error..... 98

4.2.5 Prediction of Elution Profiles from Sorption Rate Curves of Naphthalene on PRP-1 104

4.2.6 Comparison of Predicted and Observed Elution Profiles of Naphthalene on PRP-1 113

4.3 Partisil-10 ODS-3 as a Sorbent

4.3.1 Introduction 149

4.3.2 Characterization of Elution Profiles on Partisil-10 ODS-3 149

4.3.3 Equilibrium Sorption of Naphthalene on Partisil-10 ODS-3

4.3.3.1 Measurement of the Sorption Isotherm of Naphthalene on Partisil-10 ODS-3 153

4.3.3.2 Calculation of k' from Elution Profiles of Naphthalene on Partisil-10 ODS-3 155

4.3.3.3 Effect of Changing the Solvent Composition on the Diffusion Characteristics and Bandbroadening of a Naphthalene Sample Zone 157

4.3.4 Sorption Rate of Naphthalene on Partisil-10 ODS-3 161

4.3.5 Prediction of Elution Profiles from Sorption Rate Curves of Naphthalene on Partisil-10 ODS-3 168

4.3.6 Comparison of the Predicted and Observed Elution Profiles of Naphthalene on Partisil-10 ODS-3 177

4.4. Summary 177

5. CONCLUSIONS AND FUTURE WORK 180

6. BIBLIOGRAPHY 183

* * * * * * *

APPENDIX 1: Calculation of Contributions to the Total Plate Height from Individual Rate Processes..... 189

APPENDIX 2: Calculation of Specific Pore Volume for Partisil-10 ODS-3.

APPENDIX 3: Exponentially Modified Gaussian Curve Fit Programs..... 192

APPENDIX 3.1: EXPGAUSS..... 194

APPENDIX 3.2: FITMY..... 196

APPENDIX 3.3: FZERO..... 197

APPENDIX 3.4: EXP_FIT_DIFF..... 200

APPENDIX 4: Programs to Calculate Elution Profiles from Rate Curve Data

APPENDIX 4.1: PEAK SHAPE CALC..... 201

APPENDIX 4.2: INTEGRATE_2PT..... 206

APPENDIX 4.3: PROBDIST..... 207

LIST OF TABLES

TABLE		PAGE
2.1	Summary of individual plate height contributions for a hypothetical HPLC column	14
3.1	Packing properties of PRP-1 and Partisil-10 ODS-3	41
3.2	Properties of shallow beds of PRP-1 and Partisil-10 ODS-3	45
3.3	Corrections for extra-column bandbroadening	61
4.1	Statistical moments of chromatograms of phloroglucinol	65
4.2	Z values for naphthalene profiles at different flow rates	69
4.3	Effect of changing subset used in EMG curve fit	72
4.4	Effect of changing subset from 0 to 10 % of the peak maximum on EMG curve fit	74
4.5	Effect of changing number of data points on EMG curve fit	76
4.6	EMG constants for three replicate injections of naphthalene on PRP-1 at mobile phase linear velocity (u_o) = 0.30 cm/s	77
4.7	EMG constants for naphthalene on PRP-1 at four different u_o	78
4.8	k' from elution chromatograms on PRP-1	86
4.9	Tri-exponential constants describing sorption rate curve of naphthalene on PRP-1	90
4.10	Statistical moments of replicate sorption rate curves of naphthalene on PRP-1	93
4.11	Individual contributions of each term to each statistical moment of the sorption rate curve of naphthalene on PRP-1	94
4.12	Tri-exponential constants describing four replicate sorption rate curves of naphthalene on PRP-1	96
4.13	Non-interacting fractions, Φ_i, for all three hypothetical columns at four different u_o	106

4.14	EMG characteristics of profiles predicted by constants of four replicate sorption rate curves.....	111
4.15	EMG characteristics of P1/2 predicted from sets of experimental and modified rate data.....	132
4.16	EMG characteristics of observed elution profile of naphthalene on PRP-1 at u_o = 0.10 cm/s with confidence limits.....	133
4.17	Experimental and modified tri-exponential constants used to predict the elution profile of naphthalene on PRP-1.....	140
4.18	EMG constants of three replicate injections of naphthalene on Partisil-10 ODS-3 at u_o = 0.167 cm/s.....	151
4.19	EMG constants for naphthalene on Partisil at three u_o.....	152
4.20	Bi-exponential constants describing sorption rate curve of naphthalene on Partisil-10 ODS-3.....	163
4.21	Bi-exponential constants describing three replicate sorption rate curves of naphthalene on Partisil-10 ODS-3.....	167
4.22	Φ_2 for three data sets of replicate sorption rate at u_o = 0.167 cm/s...	171
4.23	EMG constants of elution profiles of naphthalene on Partisil predicted from sorption rate data at u_o = 0.167 cm/s.....	176
4.24	EMG constants of elution profiles of naphthalene on Partisil predicted from sorption rate data at three u_o.....	178

LIST OF FIGURES

FIGURE		PAGE
1.1	Chromatograms of naphthalene on PRP-1 and Partisil-10 ODS-....	3
2.1	Schematic diagram of sorption on a spherical stationary phase particle.....	17
2.2	Breakthrough curve.....	21
2.3	Typical sorption rate curve.....	23
2.4	Prediction of elution peak for a sample which has a bi-exponential sorption rate curve.....	26
2.5.a	Output from a column on which Φ is significant.....	31
2.5.b	Prediction of elution peak for a sample which has a bi-exponential sorption rate curve and where Φ_i is significant.....	32
2.6.a	Prediction of elution peak for a sample which has a tri-exponential sorption rate curve and where Φ_i is significant.....	34
2.6.b	Overall elution peak from predicted profiles in Figure 2.6.a.....	35
3.1	Schematic diagram of sorption rate measurement apparatus.....	42
3.2.a	Schematic diagram of slider valve (side view).....	43
3.2.b	Schematic diagram of slider valve (end-on view).....	44
3.3	Schematic diagram of lever system to move slider valve.....	48
3.4	Sequence of positions of slider valve in sorption rate measurements	50
3.5	Schematic diagram of apparatus for elution chromatography.....	58
4.1	ASYST output - phloroglucinol signal on PRP-1 -unsmoothed.....	64
4.2	ASYST output - naphthalene signal on PRP-1 - unsmoothed.....	66
4.3	Elution Profile of naphthalene with EMG curve fit and chosen points.....	68
4.4	EMG curve fit of naphthalene signal showing results of truncation of subset.....	71

4.5	H vs. u_o for naphthalene on PRP-1	81
4.6	Sorption Isotherm of naphthalene on PRP-1 - extended range	83
4.7	Linear region of naphthalene sorption isotherm on PRP-1	84
4.8	Sorption rate curve of naphthalene on PRP-1	89
4.9	Contributions of exponential terms to the sorption rate curve of naphthalene on PRP-1	91
4.10	Initial sorption rates of naphthalene on PRP-1	101
4.11	Slope of initial rise of sorption rate curve of naphthalene on PRP-1 vs u	102
4.12	Linear region of initial rise of sorption rate curve of naphthalene on PRP-1 with linear regression lines at r = 0.999	103
4.13	Predicted elution profile of naphthalene on PRP-1 at u_o = 0.10 cm/s using Replicate 1 sorption rate data	108
4.14	Predicted elution profiles of naphthalene on PRP-1 at u_o = 0.10 cm/s using four replicate sets of sorption rate data	109
4.15	EMG fits to elution profiles using Replicate 1 and Replicate 4 sorption rate data	112
4.16	Predicted and observed elution profiles of naphthalene on PRP-1 at u_o = 0.10 cm/s using Replicate 1 sorption rate data	114
4.17	The probability distributions P1, P2 and P3 predicted from the sorption rate data of Replicate 1	115
4.18	The probability distributions P1/2/3 and P1/2 predicted from the sorption rate data of Replicate 1	117
4.19	The probability distribution P2 and the observed elution signal	119
4.20	The probability distribution P1/2 and the observed elution signal	120
4.21	The probability distribution P1 as a function of k_1	122
4.22	The EMG width characteristics of P1 as a function of k_1	123

4.23	The probability distribution P1 as a function of n_1	125
4.24	The EMG width characteristics of P1 as a function of n_1	126
4.25	The EMG width characteristics of P2 as a function of k_2	127
4.26	The EMG width characteristics of P2 as a function of n_2	128
4.27	The probability distribution P1/2 predicted from the modified set of constants and the observed elution signal	130
4.28	The probability distribution P3 as a function of n_3	135
4.29	The probability distribution P3 as a function of k_3	136
4.30	Chromatogram of naphthalene on PRP-1 with vertically offset baseline in tail	138
4.31	Predicted and Observed elution profiles of naphthalene on PRP-1 at u_o = 0.10 cm/s using set of modified sorption rate data	141
4.32	Sorption Rate curve of naphthalene on PRP-1 fitting the set of modified constants	143
4.33	Predicted and Observed elution profiles of naphthalene on PRP-1 at u_o = 0.20 cm/s using Replicate 1 sorption rate data	145
4.34	Predicted and Observed elution profiles of naphthalene on PRP-1 at u_o = 0.30 cm/s using Replicate 1 sorption rate data	146
4.35	Predicted and Observed elution profiles of naphthalene on PRP-1 at u_o = 0.40 cm/s using Replicate 1 sorption rate data	147
4.36	The probability distribution P2 at u_o = 0.10 cm/s using four replicate sets of sorption rate data	148
4.37	ASYST output - naphthalene on Partisil-10 ODS-3	150
4.38	H vs. u_o for naphthalene on Partisil-10 ODS-3	154
4.39	Sorption Isotherm of naphthalene on Partisil-10 ODS-3	156
4.40	Viscosity of MeOH/H_2O solvents	158
4.41	Diffusion coefficient of naphthalene in MeOH/H_2O solvents	160

4.42	Sorption rate curve of naphthalene on Partisil-10 ODS-3.....	162
4.43	Contributions of exponential terms to the sorption rate curve of naphthalene on Partisil-10 ODS-3.....	165
4.44	The probability distributions P1 and P2 predicted from three replicate sets of sorption rate data on Partisil-10 ODS-3.....	170
4.45	The probability distributions P1 and P1/2 for Replicates 1 and 3 on Partisil-10 ODS-3.....	172
4.46	Predicted and observed elution profile of naphthalene on Partisil at u_o = 0.167 cm/s using Replicate 1 sorption rate data.....	173
4.47	Predicted elution profiles of naphthalene on Partisil at u_o = 0.167 cm/s using results of three replicate sorption rate curves.....	175

LIST OF SYMBOLS

A	Pre-exponential factor in EMG function
$A_{hold\text{-}up}$	Area of peak due to amount of unretained compound in hold-up volume of shallow bed
A_{inj}	Area of peak due to amount of unretained compound in injection loop of valve V3
C	Concentration of sample injected, in elution experiments
C_e	Effluent sample concentration, in breakthrough experiment
C_m	Sample concentration in the mobile phase
C_s	Sample concentration in the stationary phase
d_f	Diffusion distance
d_p	Particle diameter
D	Slope of linear portion of a sorption isotherm
D_m	Diffusion coefficient in the mobile phase
erf	Error function
EMG	Exponentially modified Gaussian
f	Fraction of mobile phase in pores of a porous stationary phase
$h(t)$	Height of a chromatographic signal with respect to time
h_{EMG}	Height of an exponentially modified Gaussian signal
H	Height equivalent of a theoretical plate
H_{couple}	Plate height due to coupling between eddy diffusion and resistance to mass transfer in the mobile phase
H_{Eddy}	Plate height due to eddy diffusion
H_{LD}	Plate height due to longitudinal diffusion
H_m	Plate height due to resistance to mass transfer in the mobile phase
H_s	Plate height due to resistance to mass transfer in the stationary phase
H_{sm}	Plate height due to resistance to mass transfer in the stagnant mobile phase

H_T	Total plate height
j_m	species j in the mobile phase
j_s	species j in the stationary phase
k'	capacity factor
k_f	Irreversible sorption rate constant
$k_{f,i}$	Irreversible sorption rate constant associated with the ith sorption process
k_i	Measured sorption rate constant due to the ith sorption process
k_r	Irreversible desorption rate constant
$k_{r,i}$	Irreversible desorption rate constant associated with the ith desorption process
L	Length of chromatographic column
M_0	Zeroth statistical moment
$M_{0,i}$	Zeroth statistical moment contribution of the ith term of the multiexponential equation describing the sorption rate curve
M_1	First statistical moment
$M_{1,i}$	First statistical moment contribution of the ith term of the multiexponential equation describing the sorption rate curve
M_2	Second statistical moment
$M_{2,i}$	Second statistical moment contribution of the ith term of the multiexponential equation describing the sorption rate curve
MW_a	molecular weight of solute
n(t)	Concentration of sample sorbed at time t in the shallow bed experiment, in moles sample/g packing
n_i	Pre-exponential factor of ith term in the multiexponential equation describing the sorption rate curve
n_m	Number of moles of sample in the mobile phase
n_s	Number of moles of sample in the stationary phase
n_0	Concentration of sample sorbed at infinite exposure time in the shallow bed experiment, in moles sample/g packing

N_{dummy}	Number of moles contained in the dummy hole
N_{el}	Number of moles eluted from shallow bed
$N_{hold\text{-}up}$	Number of moles contained in hold-up volume in shallow bed
N_s	Number of moles adsorbed on the shallow bed
N_{sorb}	Number of moles sorbed on shallow bed
$P(ts)_i$	The probability distribution due to the ith sorption process with respect to time, ts
r	Radius of the shallow bed
t_f	Diffusion time
t_G	Centre of gravity of the parent Gaussian peak in an EMG function
t_m	Time to elute an unretained compound
$t_{m,i}$	Time to elute an unretained compound in a hypothetical column associated with the ith sorption process
t_r	Retention time of a sample
t_s	Time measured from the time to elute an unretained compound
T	Temperature, measured in Kelvin
u	Linear velocity through the shallow bed
u_o	Mobile phase linear velocity, in HPLC column experiments
v_{ip}	Specific interparticle volume
v_p	Specific pore volume
$v_{p,Si}$	Specific pore volume of underivatized silica
v_p'	Specific pore volume of bonded phase with respect to weight of original silica
V_a	Molar volume of solute a
$V_{hold\text{-}up}$	Actual hold-up volume of shallow bed
$V_{hold\text{-}up,T}$	Total hold-up volume of shallow bed
V_{inj}	Volume of injection loop in valve V3
V_m	Mobile phase volume
V_p	Pore volume in shallow bed

W	Weight of stationary phase in chromatographic column
Wt	Weight of packing in shallow bed
X	Distance travelled down a chromatographic column
Z	Variable in EMG function (see equation 2.31 for definition)
ε_{inter}	Fraction of bed volume between particles
γ	Obstruction factor
γ'	Tortuosity factor in resistance to mass transfer in the stagnant mobile phase term
η	viscosity of solvent
λ	packing factor in longitudinal diffusion term
ω	packing factor in resistance to mass transfer in the mobile phase term
ω'	density of solvent
Φ_i	Fraction of sample that passes through a hypothetical column in which the ith sorption process occurs without undergoing at least one sorption-desoption cycle; the non-interacting fraction
ρ	packing density
σ_G	Square root of the variance of the parent Gaussian peak of an EMG function
σ_x^2	Variance of a chromatographic zone in terms of distance
Ψ_s	Association factor of solvent S

LIST OF EQUATIONS

EQUATION		PAGE
2.1	Height equivalent of a theoretical plate	7
2.2	Plate height due longitudinal diffusion	8
2.3	Plate height due to eddy diffusion	9
2.4	Plate height due to resistance to mass transfer in the mobile phase	9
2.5	Coupling of plate height due to eddy diffusion and to resistance to mass transfer in the mobile phase	10
2.6	Plate height due to resistance to mass transfer in the stationary phase	12
2.7	Plate height due to resistance to mass transfer in the stagnant mobile phase	12
2.8	fct(f,k') for spherical particles	13
2.9	Einstein's equation for diffusion distance	13
2.10	Plate height due to resistance to mass transfer in the stagnant mobile phase in terms of diffusion time	13
2.11	Total plate height	13
2.12	Adsorption of species j	19
2.13	Relation of observed rate constant, k to k_f and k_r	19
2.14	General form of multi-exponential equation	22
2.15	Probability distribution due to ith kinetic process	24
2.16	Definition of t_s	24
2.17	General form of Bi-exponential equation	25
2.18	Relation of k_f and k_r by k'	25
2.19	Relation of k_f to measured rate constant	25
2.20	Relation of k_r to measured rate constant	27
2.21	Retention time for the ith column, $t_{m,i}$	27
2.22	The probability distribution $P(t_s)_1$	27

2.23	The probability distribution $P(t_S)_2$	27
2.24	The fraction Φ_i, of sample that passes through the column i without undergoing sorption-desorption	29
2.25	General form of Tri-exponential equation	33
2.26	Zeroth moment of a peak	37
2.28	First moment of a peak	37
2.29	Second moment of a peak	37
2.30	Exponentially modified Gaussian function	38
2.31	Definition of Z	38
2.32	Identity using erf function for solution of EMG function	38
2.33	First moment of an EMG function	38
2.34	Second moment of EMG function	38
3.1	Linear velocity through shallow bed, u	52
3.2	Number of moles sorbed by shallow bed, N_{sorb}	53
3.3	N_{sorb} with correction for presence of dummy hole	53
3.4	Specific number of moles sorbed by shallow bed, n(t)	54
3.5	Total hold-up volume in shallow bed apparatus, $V_{hold\text{-}up,T}$	54
3.6	Hold-up volume exclusive of pore volume in shallow bed apparatus, $V_{hold\text{-}up}$	54
3.7	Number of moles in hold-up volume, $N_{hold\text{-}up}$	55
3.8	Number of moles adsorbed, N_S, in isotherm measurement	56
3.9	Number of moles adsorbed, N_S, from N_{sorb}	56
3.10	Concentration in the stationary phase, C_S	56
3.11	Linear velocity through chromatographic column, u_O	59
4.1	Plate height from first and second moments of peaks	79
4.2	Plate height from EMG characteristics	80
4.3	Capacity factor, k', from slope of sorption isotherm	82

4.4	Capacity factor, k', from first moment of elution peak	85
4.5	Zeroth moment of tri-exponential curve	92
4.6	First moment of tri-exponential curve	92
4.7	Second moment of tri-exponential curve	92
4.8	ith contribution to zeroth moment of overall curve	95
4.9	ith contribution to first moment of overall curve	95
4.10	ith contribution to second moment of overall curve	95
4.11	Summation of contribution to the zeroth moment	95
4.12	Concentration in the stationary phase from n_0	98
4.13	Approximation of $P(t_s)_1$ when k_1 is large	121
4.14	Wilke-Chang equation	157
4.15	Molar volume, V_a of solute a	159
A2.1	Relationship of pore volume to carbon loading	192
A2.2	Number of grams of Si in packing	193
A2.3	Specific pore volume, v_p, in terms of weight of packing	193

CHAPTER 1

Introduction

Modern HPLC analyses have been made routine and reliable with the commercial availability of high quality, high efficiency columns. Most analyses are carried out in the reverse-phase mode on columns containing a non-polar stationary phase. The vast majority of reverse-phase columns are packed with a silica-based bonded phase [1.1]. The physical characteristics of the silica support, including excellent mechanical strength, excellent mass transfer properties in microparticulate packings and widely available reagents to modify the silica surface, make it a suitable material for manufacturing chromatographic packings [1.2]. The material does have some limitations, however, notably its relatively poor resistance to attack in acidic or basic solutions. The efficiency of silica-based packings also tends to deteriorate with use of mobile phases which have a high water content, such as are appropriate for ion-exchange separations.

Various alternate materials have been used as the support for bonded phases in an attempt to overcome the problems with the pH extremes. Other supports, such as alumina [1.3, 1.4] and zirconia [1.2] show greater chemical stability [1.5], but are still largely experimental as supports for RP-HPLC.

Non-polar adsorbents represent an alternate family of RP supports. This includes carbon and organic copolymers. Carbon, in its various forms has been shown to be energetically heterogeneous and, in the form of graphite, is mechanically fragile and subject to long term oxidation [1.2]. One common organic polymer is polystyrene-divinylbenzene (PS-DVB) which is marketed under trade names such as PRP-1 (Hamilton, Reno, NV), PLRP-S (Polymer Laboratories, Church Stretton, UK) and Rogel (RSL-Alltech Europe, Eke, Belgium). Other types of polymers such as

polyaromatic esters [1.6] have been synthesized.

Originally, the copolymers were successfully applied to problems such as the separation of amines at high pH, which produces ion suppression, and the resulting separations showed better efficiencies than the same separations on silica-based packings [1.7]. The use of macroporous polymers as a stationary phase for liquid chromatography has recently been reviewed [1.8]. They are applicable in areas where silica-based packings are inadequate and they have been used in the analysis of biologically active species such as tetracyclines [1.9, 1.10, 1.11], penicillins [1.11], proteins [1.12] and erythromycin [1.13]. Some successful assays, such as the separation of Rheumatoid drugs and their metabolites in blood and plasma [1.14] are carried out at elevated pH, in this case, at pH 11. The packing used in this study, PRP-1, has been successfully used as a dynamic cation [1.15, 1.16, 1.17] and a dynamic anion exchanger [1.18, 1.19]. PRP-1 has also been used in the analysis of S-triazine herbicides [1.20].

PS-DVB packings are neutral stationary phases which can be easily modified to produce cation- or anion-exchangers by derivatization with sulphonate or amino groups [1.21]. The underivatized support is stable from pH 1 to 14 [1.22]. The relatively high amount of cross-linking makes the supports mechanically rigid. Despite these ideal characteristics, columns of polymeric packings tend to demonstrate asymmetric peaks and poor efficiency [1.21,1.23]. The efficiency has been shown to be dependent on both the identity of the sample [1.23, 1.24] and the solvent [1.23]. For instance, a planar molecule, such as 9-hydroxymethylanthracene is associated with much lower efficiency than a compound with similar retention characteristics which is linear. Aromatic compounds, in general, tend to give poor efficiency on these packings [1.21].

Figure 1.1 shows the elution chromatograms for naphthalene on two different stationary phases. Partisil-10 ODS-3 is a silica-based bonded phase and the elution profile associated with this packing is symmetrical and narrow. PRP-1 is a PS-DVB

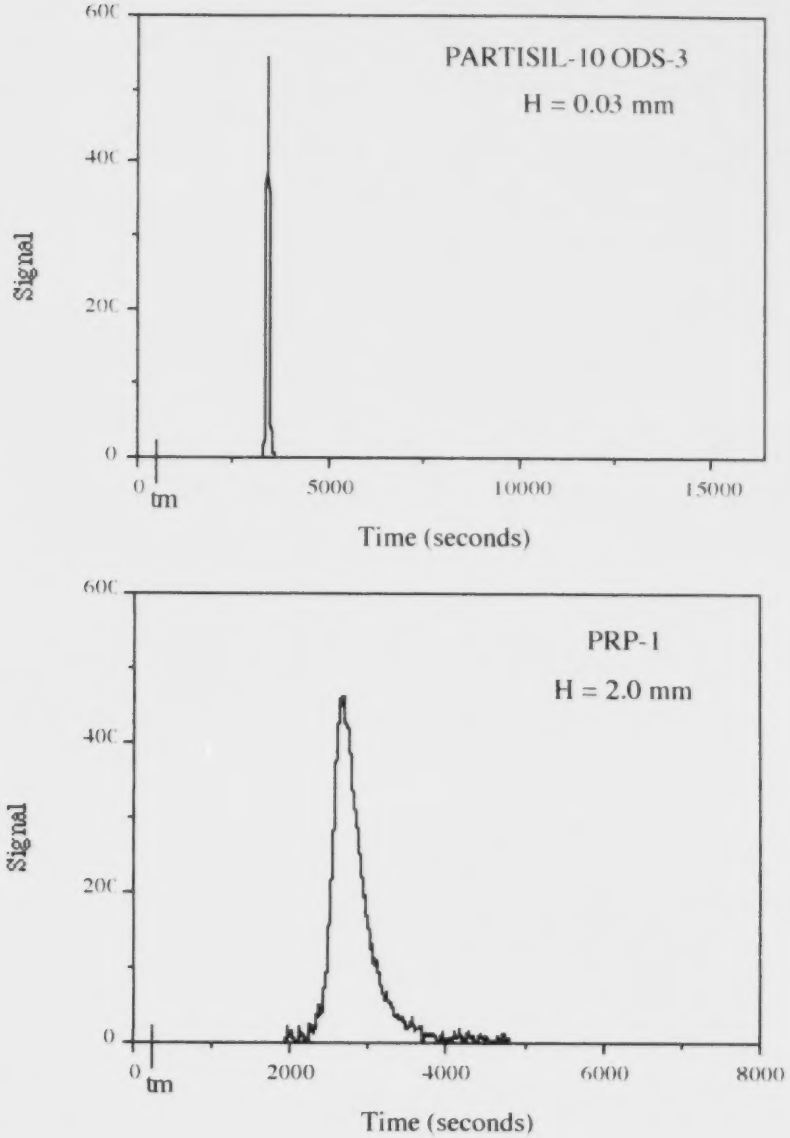

Figure 1.1 Chromatograms of naphthalene on two different kinds of HPLC packing. The time t_m is the retention time of an unretained compound. The signal eluting from a column containing the silica-based RP packing (Partisil-10 ODS-3, in this case) is symmetrical and narrow with a small plate height, H. The signal from a polymeric packing (PRP-1, in this case) is severely broadened and highly tailed, with a large plate height.

polymeric stationary phase and the elution profile associated with it is severely broadened and asymmetrical. These peak characteristics observed with PRP-1 lead to poor resolution, poor detection limits and anomalously long analysis times.

Two alternate explanations for this phenomenon have been given. Benson and Woo initially assumed that the poor efficiency was due to π electrons in the polystyrene chains of the support. These electrons might interact strongly with orbitals of solute species. These relatively strong interactions might lead to peak broadening and asymmetry [1.21] in the same way that compounds that are strongly attracted to residual silanols in silica-based columns show these elution characteristics. Copolymers which had been derivatized at the aromatic portion would show decreased π electron interaction and this would lead to decreased tailing. While increased efficiency has been claimed for PS-DVB derivatized with nitro groups [1.25], no plate heights or other similar measures of the quantity were quoted and conclusions are difficult from published information. Other chemically modified PS-DVB packings have been reported [1.21, 1.26].

An alternate explanation depends on the physical structure of the support. The physical characteristics, including the pore characteristics have been recently well studied for the polymeric systems [1.22, 1.24, 1.27]. These packings are termed "macroporous', and have rather large pores (>50 nm) due to the heterogeneity of the polymerization process. The average pore diameter of these packings is in the range of 5 - 10 nm and there are a large number of micropores (< 2 nm) as well [1.28]. The micropores are due to the spaces between the components of the copolymer. Poor efficiency has been linked to hindered diffusion of solutes in and out of these micropores [1.24]. This view explains not only the sample dependence but also the solvent dependence of column efficiency. For solvents like tetrahydrofuran (THF), much better efficiencies are generally obtained than if the solvent is methanol (MeOH) or acetonitrile (ACN) [1.23, 1.29]. There is also evidence that the void volume of a

column changes with the solvent, meaning that the support swells in solvents it is well wetted by, such as THF, which can interact with the aromatic rings in the polystyrene chains. As the support swells, the micropore volume increases and, with the larger pore, the hindered diffusion also decreases, leading to better efficiency.

This proposed effect of micropores on efficiency is supported by studies of porous polymer packings of varying mean pore dimensions which suggest that the efficiency is generally independent of this quantity [1.24], even though it would be reasonable to assume that with a larger pore size, diffusion rates would increase. The quantity however, does not deal with the existence of micropores which exist necessarily because of the structure of the polymer and which might be the cause of the rate limiting processes in the partition of solutes between the two phases.

This is not to suggest that only polymeric phases have micropores. Silica-based supports which are underivatized also have micropores but these are generally smaller than found in polymers because the functional groups, SiO_2, are smaller than the functional groups in the polymers. It is also conceivable that the micropores, which are already inaccessible to solute molecules in the underivatized support may be filled in the process of derivatization and/or endcapping. The mechanism of adsorption on silica-based RP-HPLC packings is probably more of a surface phenomenon than on the polymeric phases.

Whatever the physical process, there seems to be some excessive resistance to mass transfer of solutes in these packings which lead not only to peak asymmetry but also to increased peak widths for certain compounds. It is the origin of the poor efficiency which is the subject of this study.

Bandbroadening in chromatography is the result of physical processes which occur in the separation process. It is generally considered to be the result of a series of independent rate processes which affect the sample band, originally injected as an impulse, as it migrates along the column. The individual processes are examined

briefly in Chapter 2. The processes that may be dominant for the polymeric phases involve resistance to mass transfer within the particle. Included in this transfer are the rate of transfer through the stagnant mobile phase which fills the pores of the polymer and the rate of transfer between the stationary phase and the stagnant mobile phase. This rate of transfer, termed here the rate of sorption if we are describing the transfer of a solute from the mobile to the stationary phase, is of interest if we are to quantify the contribution of this transfer processes to the overall process of separation.

This study focuses on the possibility that a slow sorption rate is the major cause of the bandbroadening and tailing observed on PRP-1 when using polyaromatic sample species. The development of a technique to measure the rate of sorption is detailed and a model is used to relate the measured rate to experimental elution profiles of naphthalene. The results of the study on PRP-1 are compared to results for a parallel study on the silica-based packing, Partisil-10 ODS-3.

CHAPTER 2

Theory

2.1 Bandbroadening in Liquid Chromatography

2.1.1 Introduction

The phenomenon of bandbroadening has been extensively treated in the literature [2.1 to 2.3]. Only a brief discussion will be included here.

Ideally, sample solutions are injected onto chromatographic columns as an impulse. Physical rate processes on the column affect the sample zone and lead to non-uniform flow profiles and non-equilibrium between the various phases in the column. The relative magnitudes of these rate processes are affected by the characteristics of the experiment, such as the particle size of the packing, the diffusion characteristics of the sample molecule and the linear velocity of the mobile phase. The relative effect of various parameters on the bandbroadening can be predicted by assuming that several independent physical processes contribute to the sample zone broadening. The contribution of each process to zone broadening is equivalent to the relative plate height contribution of that process to the overall plate height for the column. The usual treatment, described below assumes that as independent processes, the effect of each is superimposed on the moving zone centre to describe the overall observed peak shape.

The height equivalent of a theoretical plate is the quantitative measure of the contribution to zone broadening. This quantity, H, is defined in equation 2.1.

$$H = \frac{\sigma_X^2}{X} \qquad \text{eqn. 2.1}$$

The variance produced by the process, σ_X^2, in units of distance, is related to the width of the chromatographic peak. X is the distance travelled; for a sample eluting from a

column X is equal to the length of the column. Equation 2.1 can be easily converted into time or volume units.

2.1.2 Longitudinal Diffusion

If the sample zone is initially an impulse of infinitely narrow width, as it moves down a column, molecules in the band will tend to diffuse along the axis of the column in two directions, backward and forward. This diffusion is inversely proportional to the linear velocity of the mobile phase, u_o; the faster the stream is flowing, the less time available for the sample molecules to diffuse from the front. The contribution to plate height is directly proportional to the diffusion coefficient of the sample molecule, D_m; as the diffusion coefficient increases, the molecule diffuses faster and the longitudinal diffusion becomes more extreme. The plate height contribution due to longitudinal diffusion, H_{LD} is given by equation 2.2 [2.4].

$$H_{LD}=\frac{2\gamma D_m}{u_o} \qquad \text{eqn. 2.2}$$

In packed beds, the longitudinal diffusion tends to be smaller than that found in open tubes of similar diameters. In packed beds, diffusion is obstructed by the particles and an unitless obstruction factor, γ, is introduced. The value of the obstruction factor is approximately 0.5 to 0.7. The obstruction factor accounts for the overall effect of packing on the diffusion characteristics of the sample molecule. More detailed accounts of the origin of the obstruction factor are available elsewhere [2.5]. In HPLC, this term tends to be negligibly small [2.6].

2.1.3 Eddy Diffusion

This term arises from changes to the sample band resulting from non-uniformity in flow of the mobile phase. The presence of particles in a column creates velocity differences of various types especially when particles are not uniformly packed or of a

large distribution of sizes. The different velocity flow streams carry along molecules, leading to broadening of the zone. The broadening, however, is not as severe as it would be in an open tube. This is a result of the lateral convective mass transfer of molecules between the flow streams of different linear velocities which tends to relax the non-uniform flow profile. The value of the contribution to the plate height can be calculated from equation 2.3 [2.7].

$$H_{eddy}=2\lambda d_p \qquad \text{eqn. 2.3}$$

This term is dependent on particle diameter, d_p; when the particle diameter is small, the sample molecule may spend less time in a flow stream which is faster or slower than average. The packing factor, λ, relates to the uniformity of packing of the bed and generally increases as the particle size decreases. Large particles are easier to pack uniformly in a chromatographic column [2.8]. Modern packing techniques result in columns which generally have a packing factor much less than 10. It has been measured to be approximately 2.5 for spherical particles in the particle diameter range of 5 to 35 μm [2.9]. However, λ can vary significantly from column to column [2.2].

2.1.4 Resistance to Mass Transfer in the Mobile Phase

In the mobile phase, radial diffusion of the sample across the column leads to a relaxing of the effects of non-uniform flow profile of the mobile phase on the sample zone. The finite rate of diffusional mass transfer across the column means that the non-uniform flow profile will be only partially relaxed. The plate height contribution due to this effect is calculated by equation 2.4 [2.10].

$$H_m = \frac{\omega d_p^2 u_o}{D_m} \qquad \text{eqn. 2.4}$$

The process is related to the diffusion characteristics of the sample; as the diffusion coefficient, D_m increases, the relaxation of the non-uniform profile is more

efficient . The term depends directly on the linear velocity, u_o; if the sample spends more time in the flowing stream while travelling a given distance along the column, then diffusion across the column becomes more efficient. For small particle sizes, the plate height contribution tends to be relatively small. The contribution is also directly proportional to ω , a packing factor. As the uniformity of the bed increases, ω decreases since the various streams of moving phase become more uniform in velocity. ω is dependent on the column packing and can also vary from column to column [2.2].

In gas chromatography, where the mobile phase is a gas, the value of the diffusion coefficient is on the order of 10^{-2} to 10^{-1} cm^2/s, the plate height contribution due to resistance to mass transfer in the mobile phase is considered negligible [2.11]. In liquid chromatography, however, the diffusion coefficient of sample molecules is on the order of 10^{-6} to 10^{-5} cm^2/s and the contribution calculated from equation 2.4 is much larger.

2.1.5 Coupling of H_{eddy} and H_m in HPLC

These two contributions are associated with lateral convection and lateral diffusion respectively. Both contribute to relaxation of the flow profile established by non-uniform velocity profile. These terms are said to be coupled and the overall contribution, H_{couple}, is given by Giddings as equation 2.5 [2.12].

$$H_{couple} = \left[\frac{1}{H_{eddy}} + \frac{1}{H_m} \right]^{-1} \qquad \text{eqn. 2.5}$$

The validity of the coupling term has been questioned by several researchers including Giddings himself [2.13] who states that "The coupling expression is simply an approximation to a very complex interaction between diffusion and convection. The process has been formulated rigorously but the boundary conditions for real granular beds are so complex that meaningful solutions have not yet been obtained." Equation

2.5 along with equations 2.3 and 2.4 allow one to predict the relative effect of changing the variables in the column (for example, d_p). The values of the constants γ, λ and ω are only estimates and the value of the plate height calculated from the above equations may be significantly different from actual plate height of a column. The contribution due the processes covered in the previous sections can be measured directly in silica columns for affinity chromatography using totally unretained compounds, which neither interact with the stationary phase by adsorption or enter the pores. The bands of these totally unretained compounds will be subject to broadening due to longitudinal diffusion and to the coupled mobile phase processes. These contributions were measured on silica gel packings which had been derivatized with an immobilized ligand for use in affinity chromatography. On 10 μm particles, these contributions are on the order of 10 to 100 μm at the usual linear velocities used in HPLC [2.14].

2.1.6. Resistance to Mass Transfer in the Stationary Phase

Bandbroadening occurs whenever sample molecules fail to move with the centre of the sample plug. The physical or chemical reactions of adsorption and desorption can be a source of bandbroadening if they requires a finite time. As a sample zone moves down the column, the mobile phase will contain a concentration of sample that is higher than the equilibrium concentration. This provides the driving force for adsorption but if this step takes time, the sample will continue down the column without reaching equilibrium, causing the front end of the peak to stretch out. The sample zone in the stationary phase will, at this point contain a concentration less than that at equilibrium. Once the band centre passes, however, the mobile phase will contain a concentration of sample less than that predicted by the equilibrium distribution coefficient. If desorption takes time, this cause the back end of the peak to stretch out. Overall, the peak is broadened by the non-equilibrium processes associated with slow sorption-desorption kinetics.

The bandbroadening contribution is related to the rate constant for the sorption or desorption reaction. The process is often considered in terms of the irreversible desorption rate constant, k_r. The random walk model was used by Giddings to derive equation 2.6 [2.15].

$$H_s = 2 \frac{k'}{(1 + k')^2} \frac{u_o}{k_r} \qquad \text{eqn. 2.6}$$

The time associated with this process is only the time necessary to undergo reaction, not time required to diffuse to the surface. For reverse phase packings used in HPLC, this term is often considered to be negligible [2.3].

2.1.7 Resistance to Mass Transfer in the Stagnant Mobile Phase

Porous particles are filled with mobile phase but the solution does not undergo the various convection processes associated with the flowing mobile phase. The stagnant mobile phase is probably not quickly exchanged with fresh mobile phase. Sample molecules which enter the pores of a particle must diffuse into the stagnant mobile phase to reach the surface of the stationary phase where adsorption actually occurs. The bandbroadening associated with this process must depend on the diffusion characteristics of the sample molecule. Equation 2.7 calculates the plate height contribution for this process [2.16].

$$H_{sm} = \frac{fct\ (f, k')\ d_p^2\ u_o}{\gamma' D_m} \qquad \text{eqn. 2.7}$$

The tortuosity factor, γ', accounts for the increased path length the sample molecules must follow due to the winding channels within the particles. It has a value less than 1. The variable fct (f, k') is a function of f, the fraction of the mobile phase in the pores of the packing and of k', the capacity factor. The function has different forms depending on the type of stationary phase used. For spherical particles, the function is given by equation 2.8 [2.16].

$$fct(f,k') = \frac{(1 - f + k')^2}{30(1 - f)(1 + k')^2} \qquad \text{eqn 2.8}$$

Einstein's equation, shown in equation 2.9 which relates the square of the diffusion distance, d_f^2, to the time of diffusion, t_f, can be used to replace d_p^2 and D_m in equation 2.7 with diffusion times as shown in equation 2.10 [2.17].

$$d_f^2 = 2D_m t_f \qquad \text{eqn 2.9}$$

$$H_{sm} = 2\, fct(f,k')\, \gamma'\, t_f = \frac{2\, fct(f,k')\, \gamma'}{k_f} \qquad \text{eqn 2.10}$$

Equation 2.10 relates the band broadening due to resistance to mass transfer in the stagnant mobile phase to a first-order rate constant, k_f, for diffusion through the pores of the packing.

2.1.8 Total Plate Height

The previous discussion for the estimation of plate heights for chromatographic columns can be summarized in equation 2.11.

$$H = H_{LD} + \left[\frac{1}{H_{eddy}} + \frac{1}{H_m} \right]^{-1} + H_s + H_{sm} \qquad \text{eqn 2.11}$$

The relative contributions to the plate height have been calculated for a hypothetical HPLC column containing 10 µm spherical, porous particles for a sample having a k' = 35. The calculations used a linear velocity of 0.4 cm/s which corresponds to a realistic flow rate of about 2 mL/min. Detailed calculations are shown in Appendix 1. Table 2.1 summarizes the results.

The overall plate height for this column then is 0.073 mm, with the majority of the band broadening originating with the mobile phase effects in the coupled term. The parameters discussed in Appendix 1 were chosen to closely parallel parameters for the polymeric packing PRP-1 and for typical HPLC experiments on that packing.

Table 2.1 Summary of individual plate height contributions in a typical HPLC experiment with conditions described in Appendix 2.

term	plate height contribution (cm)
H_{LD}	3×10^{-5}
H_{eddy}	0.005
H_m	0.052
H_{couple}	0.0046
H_{sm}	0.0027
H_s	4.3×10^{-5}
H_{total}	0.0073

However, the predicted value of 0.073 mm grossly underestimates the observed plate height for PRP-1 columns with certain kinds of samples. This study will investigate the possibility that the some combination of the H_{sm} term and the H_s term underestimates the contribution to bandbroadening of slow mass transfer in the porous structure of the polymer. For certain molecules which are of the molecular dimensions of the micropores, their behaviour in the micropores may be lead to large values of H_{sm} and/or H_s.

2.1.9 Rate Processes and Bandbroadening

PRP-1 was previously described as a macroporous packing. Each particle has an extensive network of pores of a variety of sizes. Mercury porosimetry studies on a related macroporous polymer, Amberlite XAD-2, suggests that micropores are present [2.18]. The pores probably range in size from macropores to micropores. It has also been observed that PRP-1 is an exceptionally poor stationary phase for certain kinds of compounds, especially polyaromatics. After eliminating other possible causes for the severely broadened peaks such as high longitudinal diffusion and a non-uniform flow profile [2.19], the slow adsorption-desorption kinetics was suspected to be the primary cause of the inefficiency. Typically, adsorption onto non-polar stationary phases is considered to be a fast process since there tends to be only a small activation energy associated with the weak dispersion forces which are the primary retention mechanism. If, however, we consider the total sorption process to include the diffusion of the sample through the interior pores of the particle it is not difficult to imagine that the overall process may be slow and may lead to non-equilibrium between the mobile phase and the particle phase (including the stagnant mobile and the stationary phases).

The shallow bed method described in this thesis is designed to measure the overall rate of the total sorption process of a sample compound onto a stationary phase. The measured rate may be limited by slow diffusion through the pores and/or by

adsorption onto the actual surface.

2.2 Shallow Bed Theory

Sorption of a sample from a liquid solution onto a porous solid particle involves several steps as illustrated in Figure 2.1 [2.20, 2.21]. Film diffusion is the diffusion of sample from the bulk solution across a concentration gradient to the particle surface. For porous particles, particle diffusion involves the movement of the sample through the pores in the particle. The final step is the actual physical or chemical reaction involved in surface adsorption. Desorption can be considered occur as the reverse of the above steps [2.21].

In chromatographic columns, the manifestation of these processes will be bandbroadening if the processes are time-consuming. If film diffusion is slow, this results in a plate height contribution due to slow mass transfer in the mobile phase according to equation 2.4. In fact, film diffusion relates to only one of the physical processes included in the H_m term. The individual processes refer to mass transfer over various distances in the column; film diffusion corresponds to so-called "trans-channel" mass transfer. This is the mass transfer between flow streams of different linear velocities in the channel between two particles. This contribution is actually small at normal HPLC linear velocities [2.10]. If particle diffusion is slow, it might be expected that the contribution from resistance to mass transfer in the stagnant mobile phase according to equation 2.7 will be large. If the chemical or physical adsorption is slow, a large contribution due to resistance to mass transfer in the stationary phase calculated according to equation 2.6 will be expected. The slowest of the three steps illustrated in Figure 2.1 is considered to be the rate-limiting step in the overall sorption process. At this point, however, it may be noted that in the "shallow bed method", described below, film diffusion is very fast because the particle outer film is very thin so that only particle (pore) diffusion and surface adsorption-desorption are potentially

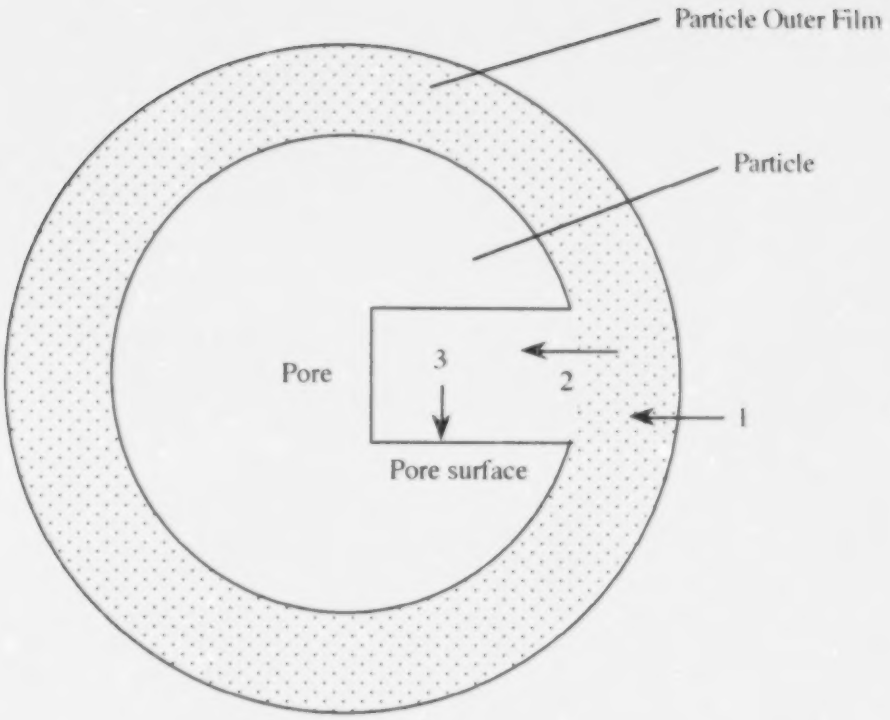

Figure 2.1 Schematic diagram of a spherical porous stationary phase particle. Three steps in the sorption process are illustrated. (1) Sample diffuses from the bulk solution across the concentration gradient surrounding the outer surface of the particle. This process is termed "film diffusion". (2) Sample diffuses through the stagnant mobile phase contained in the pore. This process is termed "particle diffusion". (3) Physical or chemical adsorption occurs onto the pore surface. Desorption can be considered to occur by the reverse of these steps.

involved. It is not necessary to determine which of these two steps is the slower, and, for convenience, the terms "sorption" and "desorption" will be used to refer to the combined process of pore-diffusion and surface adsorption-desorption.

Whatever the actual rate limiting process, the measurement of the rate of the overall sorption process is dependent on measuring the amount sorbed by an adsorbent with respect to an exposure time to a solution. For very large particles where the overall sorption rate is small, the experiment may be as technically simplistic as shaking a known amount of sorbate in a solution of known concentration for variable amounts of time and analyzing either phase for changes in concentration. This type of experiment becomes more challenging as the sorption rate becomes faster and the necessary exposure times decrease.

The rate of sorption on HPLC stationary phases has been the subject of relatively few studies. It has proven to be a bit more technically challenging. Marshall et.al. [2.22] measured the sorption rate constant in an octadecylsilica, ion pairing chromatographic system using the pressure-jump relaxation kinetics method. While the rate constant for the ion-pairing reaction preceding the adsorption was too fast to measure with the system, the adsorption step was determined also determined to be very fast. Reciprocal relaxation times for adsorption on bonded phases were determined to be of the order of 500 to 700 s^{-1}.

In this laboratory, a technique based on a fixed-bed adsorber, termed the shallow bed method, has been developed to accommodate exposure times of less than 1 s. The basic technique was originally described in 1947 [2.23] and has been used to study the kinetics of sorption on ion-exchange resins [for example, 2.24]. The design of the apparatus will be discussed in detail in Section 3.4.1. Briefly, the fixed bed consists of milligram amounts of HPLC stationary phase material held in a modified slider valve. This small bed, termed a shallow bed, can be exposed to a flowing sample stream for variable amounts of time. The sorbed sample is then eluted from the shallow

bed and the sorbed amount is plotted vs exposure time to generate a sorption rate curve.

The experiment is designed to measure the rate constant for the reversible sorption of species j from the mobile phase, designated j_m onto the stationary phase where the species is designated j_s.

$$j_m \underset{k_r}{\overset{k_f}{\rightleftharpoons}} j_s \qquad \text{eqn. 2.12}$$

The forward reaction is the sorption reaction and has an irreversible rate constant of k_f while the reverse reaction, desorption, has an irreversible rate constant of k_r. Under reversible conditions, the observed rate constant, k can be shown to be the sum of the two aforementioned irreversible constants [2.25] as shown in equation 2.13.

$$k = k_f + k_r \qquad \text{eqn. 2.13}$$

The success of the experiment depends on achieving so-called shallow bed conditions. Shallow bed conditions are said to exist when the sample concentration in the mobile phase is constant at all times including exposure time = 0. To fulfill this condition, the sample solution passes through the bed at a rapid rate. When sample is sorbed by the bed, the local concentration in the flowing sample solution will not decrease because the flow flushes the bed at a rapid rate. Shallow bed conditions simplify assumptions necessary to data analysis. No concentration gradient exists in the shallow bed either longitudinally or radially.

The fulfillment of shallow bed conditions is accomplished by the combination of two experimental conditions. First, a small length of packing is used in the shallow bed. This assures that by the time a volume element of solution reaches the lower portion of the bed, it will not have been in contact with much overlying packing and at most only a very small amount of solute will have been sorbed. The more sample sorbed by the bed, the harder it will be to maintain a constant sample concentration in the flowing phase. A concentration gradient might be established. The second

experimental consideration is the use of a high linear velocity of the sample solution through the shallow bed. This is accomplished using a constant pressure system. Minimization of resistance to flow is also necessary. The use of a very short (shallow) bed is therefore indicated.

The shallow bed method can be compared to frontal chromatography [2.26]. In frontal chromatography, which is schematically illustrated in Figure 2.2, a sample solution of concentration C_m is pumped continuously through a column. A plot of the sample concentration in the effluent, C_e, vs time is called a breakthrough curve. The shape of the breakthrough curve is often sigmoidal. The variable t_m, illustrated in Figure 2.2, is the finite time that is necessary to sweep out the void volume of the column with sample solution. In the shallow bed experiment, this step is assumed to occur instantaneously because of the very high linear velocity and very small void volume of the bed. The breakthrough curve in Figure 2.2 continues along the baseline, then rises in the typical S shaped pattern. In this region, there is a concentration gradient established longitudinally in the column. At the top of the column, the packing sorbs sample decreasing its concentration in the flowing phase. As this gradient moves down the column, the concentration continually decreases due to the sorption process. As the packing reaches equilibrium with the flowing sample, the concentration of the mobile phase approaches a constant and the breakthrough curve levels off when all packing has reached equilibrium. The retention time of the sample, t_r, is located at the midpoint of the rising part of the elution curve. In the shallow bed experiment, the effluent concentration can be considered to be a constant at all times. In other words, the values of t_m and t_r approach zero. The curve in Figure 2.2 would therefore be inapplicable to the shallow bed. All particles in the shallow bed experience the same solution conditions at all times and will therefore undergo sorption processes at the same rate regardless of geographical location in the column.

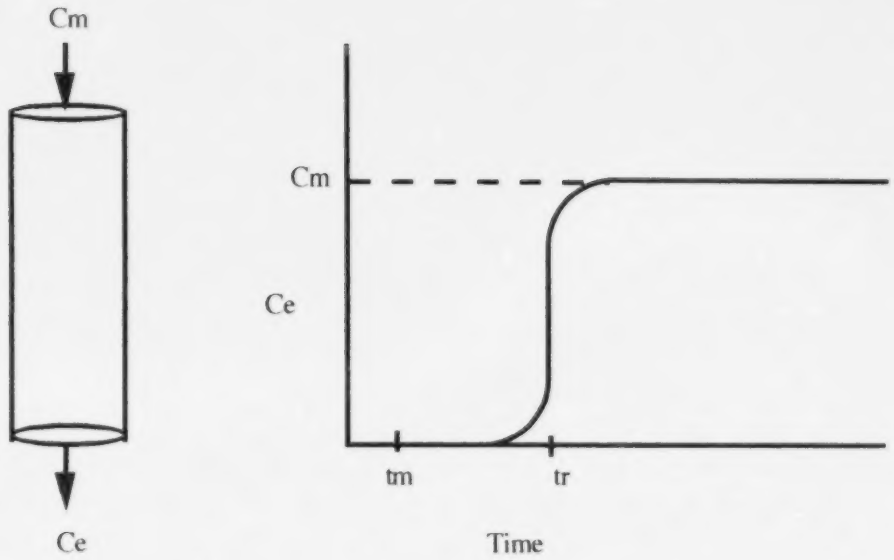

Figure 2.2 Column for frontal chromatography and breakthrough curve. A sample solution of concentration C_m is pumped continuously through the chromatographic column and the concentration in the effluent, C_e is monitored. C_e is plotted as a function of time in the breakthrough curve. The time t_m is the time for the solution to rinse out the void volume of the column. The time t_r is the retention time for the sample on the column. Equilibrium exists between the stationary and mobile phases in the plateau region of the breakthrough curve. If the column is replaced by a shallow bed, breakthrough is assumed to be achieved instantaneously. On the very short shallow bed, both t_m and t_r approach zero.

2.3 Analysis of Sorption Rate Data

2.3.1 Curve Fitting of Sorption Rate Data

The sorption rate data that result from the experiment described in this thesis can be fit, using non-linear least squares analysis, to a multi-exponential curve as shown in equation 2.14.

$$n(t) = n_0 - \sum_{i=1}^{j} n_i e^{-k_i t} \qquad \text{eqn. 2.14}$$

The use of a multi-exponential equation was suggested by the shape of the plot of the experimental data points and not by theoretical considerations. It is important to note that this curve fitting is empirical. Typical sorption rate data, a plot of moles of sample sorbed vs sorption time is shown in Figure 2.3. The solid line is a best-fit to a tri-exponential equation. Multi-exponential curves are observed in luminescence decay data for species in heterogeneous environments such as inhomogeneous surfaces [2.27]. In these situations, the various terms are associated with independent kinetic processes, each associated with different activation energies. Such curves may also be of the continuous exponential variety. In these types of curves, there is a range of rate constants instead of a set of discrete rate constants. The statistical considerations necessary to distinguish the situations are fully explored in Reference 2.28. The sorption rate data described in this thesis gave good fits to the discrete multi-exponential function and the possibility of a continuous distribution of sorption rate constants was not explored.

2.3.2 Calculation of Elution Profiles from Sorption Rate Data

We are primarily interested in predicting the shape of the profile of a sample peak eluted from a long chromatographic column packed with sorbent based on

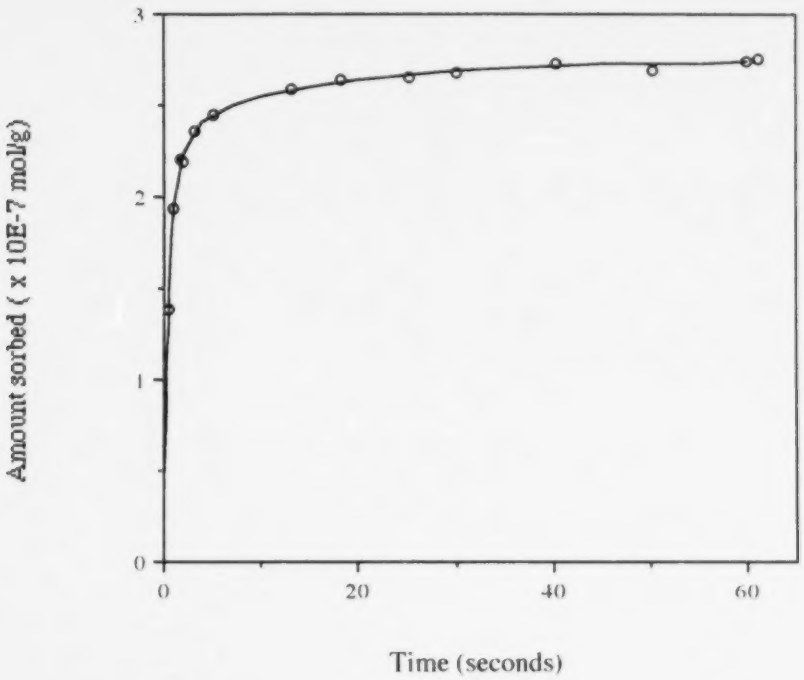

Figure 2.3 Sorption rate curve for Naphthalene on PRP-1 in 85 % MeOH. The experimental data point (o) are overlaid by a solid line representing the tri-exponential function that fits them.

information from the sorption rate curve for the sample obtained by the shallow bed experiment performed on the sorbent. In order to correctly predict the shape of the elution curve, it is necessary to treat each term of the multi-exponential as though it represented the rate of an independent first-order sorption process. For most of the sorption rate curves that will be presented here, there are three terms in the multi-exponential equation. This number is not imposed arbitrarily but rather is the number of terms that gives the best fit to the data points. Each of the i individual processes is associated with a first-order rate constant, k_i, and with a pre-exponential multiplier, n_i, which can be considered to be related to the number of sites associated with the ith process.

One can imagine that a chromatographic column filled with the packing of interest could be treated as a series of smaller columns in which only one of the sorption processes occurs. Each of the hypothetical smaller columns will have a length proportional to n_i/n_0, the fraction of sites associated with the process given in the multi-exponential equation. In each of the small columns, only a single first-order sorption process occurs, associated with a single sorption rate constant. Giddings has given a general equation which gives the probability distribution $P(t_S)_i$ associated with a single first-order sorption-desorption kinetic process, as shown in equation 2.15 [2.29].

$$P(t_S)_i = \left(\frac{k_{f,i} k_{r,i} t_m}{t_s} \right)^{0.5} e^{-(k_{f,i} t_m + k_{r,i} t_s)} I_1 \sqrt{4 k_{f,i} k_{r,i} t_s t_m} \qquad \text{eqn. 2.15}$$

The probability distribution plot of $P(t_S)_i$ vs t_S corresponds to an elution chromatogram for a sample on the hypothetical column associated with the ith process.

Equation 2.15 is expressed in terms of the variable t_S, which is time measured from the time an unretained compound takes to elute from the column, t_m.

$$t_s = t - t_m \qquad \text{eqn 2.16}$$

In a column, the sample is injected as an impulse. As the sample passes through the column, any physical process which results in certain molecules moving at a different velocity than the centre of the sample zone results in zone broadening. In our imaginary columns, the only source of zone broadening is slow sorption; we imagine that all other processes are negligible.

2.3.3 Data treatment for a Bi-exponential Rate Curve

The data treatment can be more easily understood by first considering the case where the sorption rate curve is in the form of a bi-exponential shown in equation 2.17.

$$n(t) = n_o - n_1 e^{-k_1 t} - n_2 e^{-k_2 t} \qquad \text{eqn. 2.17}$$

We then suppose that there are two independent sorption processes (i = 1 or 2) and treat the chromatographic column as if it were two smaller columns in tandem. This thought experiment is illustrated in Figure 2.4.

In hypothetical column 1, the only sorption process that occurs is one corresponding to the first term of the bi-exponential. The process has a reversible rate constant k_1 (as obtained by non-linear least squares fit of the sorption rate curve). The value of k_1 can be used to calculate the irreversible rate constants for sorption and desorption, $k_{f,1}$ and $k_{r,1}$, which are needed to calculate the probability distribution given by equation 2.15. Using equation 2.13 and equation 2.18, the values of the two reversible rate constants can be calculated using data for k' as shown in equations 2.19 and 2.20.

$$k' = \frac{k_{f,1}}{k_{r,1}} \qquad \text{eqn. 2.18}$$

So

$$k_{f,1} = k_1 \frac{k'}{1 + k'} \qquad \text{eqn. 2.19}$$

and

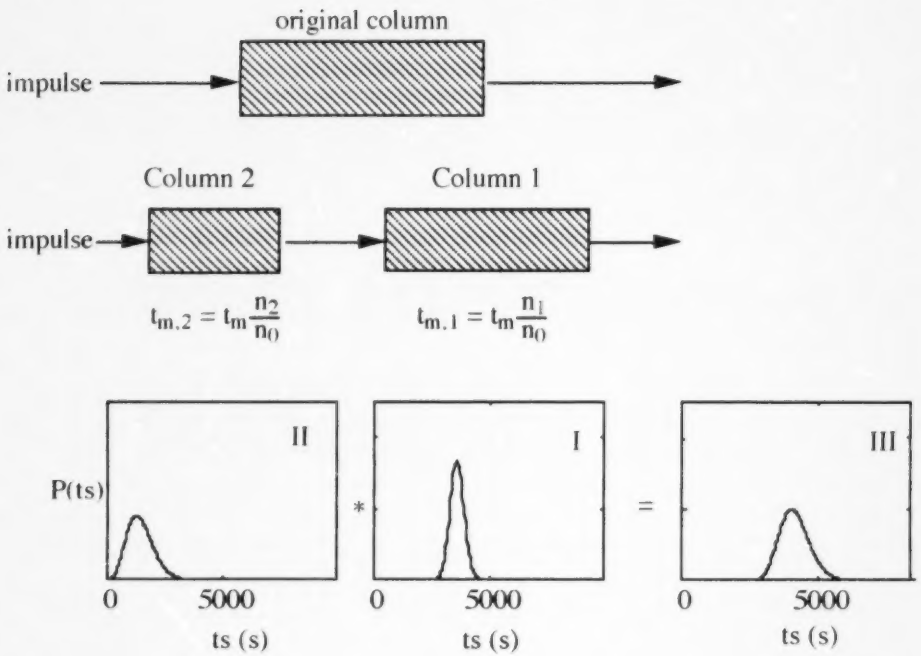

Figure 2.4 Prediction of elution peaks for a sample which has a bi-exponential rate curve on the packing in the column. The analytical column is modelled by two columns in which the two different sorption processes occur. The effect of these processes on a sample injected as an impulse is calculated for each column by equation 2.15, resulting in the profiles I and II. The overall elution peak, labelled III, is the result of the convolution of the probability distributions associated with the kinetic processes. Note that the distributions are a function of t_s which is zero at the time an unretained compound elutes from the column. In order to compare the peak III with an experimental elution profile, t_m must be added to the time axis. Details are found in Section 2.3.3.

$$k_{r,1} = k_1 \frac{1}{1 + k'} \qquad \text{eqn. 2.20}$$

Also required for calculation of the probability distribution associated with sorption onto the sites of hypothetical column 1 is a measure of the time the mobile phase takes to pass through the column, $t_{m,1}$. It is equal to the time the mobile phase takes to pass through the entire column, t_m, multiplied by a fraction of the number of sites, n_1/n_o as shown in equation 2.21.

$$t_{m,1} = t_m \frac{n_1}{n_o} \qquad \text{eqn. 2.21}$$

An analogous set of equation describes the hypothetical column 2. For the two columns the sum of $(t_{m,1} + t_{m,2})$ is equal to t_m for the original column.

From equation 2.15, the probability distribution associated with the sorption process in hypothetical column 1 is shown in equation 2.22.

$$P(t_s)_1 = \left(\frac{k_{f,1} k_{r,1} t_{m1}}{t_s} \right)^{0.5} e^{-(k_{f,1} t_m + k_{r,1} t_s)} I_1 \sqrt{4 k_{f,1} k_{r,1} t_s t_{m,1}} \qquad \text{eqn 2.22}$$

Similar calculations can be done for a second column having only sites that undergo the second sorption process which has an observed reversible rate constant k_2.The rate constants $k_{f,2}$ and $k_{r,2}$ can be calculated from k_2 using equations analogous to equations 2.19 and 2.20 and the quantity $t_{m,2}$ can be calculated using an equation analogous to equation 2.21 along with data for n_2. The probability distribution associated with slow sorption on the second hypothetical column has the form shown in equation 2.23.

$$P(t_s)_2 = \left(\frac{k_{f,2} k_{r,2} t_{m,2}}{t_s} \right)^{0.5} e^{-(k_{f,2} t_m + k_{r,2} t_s)} I_1 \sqrt{4 k_{f,2} k_{r,2} t_s t_{m,2}} \qquad \text{eqn. 2.23}$$

If these two hypothetical columns are now imagined to be attached in tandem as illustrated in Figure 2.4 and an injection is made into column 2, the sample band will undergo broadening in both columns due to the kinetic processes. (Note that the

sample band is initially considered to be an impulse of infinitely narrow width.) As the sample passes through column 2, broadening due to the slower kinetic process results in profile II. If the effluent from column 2 is directed into column 1, where broadening due to the faster kinetic process occurs, the profile exiting column 1 will be the convolution of the two distributions I and II. This profile is designated III.

One final correction to this predicted profile must be made before comparison to real chromatograms. Distribution III in Figure 2.4 is expressed in terms of t_s (defined in equation 2.16). To be expressed in real time units, the peak must be shifted down the time axis an amount t_m corresponding to the retention time of an unretained compound in the original column.

The convolution of the two probability distributions is valid providing the absolute values of $k_{f,1}$ and $k_{f,1}$ are large enough that virtually all molecules in the sample zone undergo at least one sorption-desorption cycle in each of the hypothetical columns 1 and 2, as described in Section 2.3.4, below.

2.3.4 Assumptions in Generation of Elution Profiles from Sorption Rate Data

The distributions calculated above will be the resulting profile of the effluent under two conditions:

1. if all other bandbroadening processes are negligible
2. if all molecules in the sample zone undergo the sorption-desorption processes at least once in each column.

Each of these conditions can be examined separately as follows:

Condition 1:

As was previously mentioned, slow sorption-desorption kinetics is assumed to be the major contributor to zone broadening. The relative contributions from other processes such as those described in Sections 2.1.2 to 2.1.5 can be calculated using equations shown in the above sections.

Condition 2:

Usually in chromatography, any given sample molecule will undergo the sorption-desorption cycle many times on a column. However, if sorption is particularly slow, it is conceivable that, depending on how much time the molecules spend in the mobile phase of a column, some of the molecules in the sample zone will pass through the column without undergoing the slow physical process even once. In an ideal column, these molecules would then elute as an impulse, having the same shape as the injected impulse if all other bandbroadening processes are negligible. The fraction of molecules that do not undergo the ith slow sorption process, Φ_i, is given by Giddings [2.29].

$$\Phi_i = e^{-k_{f,i}t_{m,i}} \qquad \text{eqn. 2.24}$$

The fraction Φ_i is the "non-interacting fraction" of sample on the column in question. It is related to the adsorption rate constant, $k_{f,i}$; as the process becomes slower and the rate constant decreases, the fraction of molecules that passes through the column without undergoing the process will necessarily increase. The fraction is also related to $t_{m,i}$ which is a measure of how long the sample molecules stay in the mobile phase. As the linear velocity of the mobile phase increases, t_m decreases. Because the sample molecules spend less time in the column, they have less time to undergo the slow sorption process. On any particular hypothetical column which has a single k_i and n_i, equation 2.15 describes the distribution only of the fraction of molecules ($1 - \Phi_i$) which elutes with a retention time of $t_{s,i}$. The fraction Φ_i elutes as an impulse at time $t_{m,i}$. In the discussion in Section 2.3.3, above, it was assumed that $\Phi_i \sim 0$ for both hypothetical columns 1 and 2. As this fraction Φ_i increases in one or both of the hypothetical columns, the above data treatment will fail to predict reasonable elution curves. The following section describes the data treatment procedure for a bi-exponential sorption rate curve where k_i and/or $t_{m,i}$ are small in one of the columns so

that a significant fraction of molecules pass through that column without undergoing the zone broadening process.

2.3.5 Data Treatment for Bi-exponential Rate Curve where Non-interacting Fraction for One Sorption Step is Significant.

The discussion in this section draws heavily on the two-site sorption model of kinetic tailing developed by Giddings [2.29]. Consider the situation illustrated in Figure 2.5.a. A single column contains a stationary phase on which the sorption rate is sufficiently slow as to violate condition 2 described in the previous section. In this column, the rate constant k_f, is small enough to make Φ_1, the non-interacting fraction of a sample zone significant. If sample is injected into this column as an impulse, the non-interacting fraction passes through the column without being sorbed onto the stationary phase. These molecules elute in one dead volume of the column (profile I in Figure 2.5.a) at the time t_m and the shape of the zone is unchanged except for the height. The height of this impulse is Φ of the height of the original impulse. A second fraction, $(1 - \Phi)$ is shown as profile II in Figure 2.5.a, which does interact with the stationary phase in the column. This fraction will elute as a peak with a distribution $P(t_S)$, given by equation 2.15. Note that as k_f and k_r decrease, the distribution becomes increasingly broadened and increasingly asymmetrical.

Now consider the situation illustrated in Figure 2.5.b.The column described above is designated Column 2 . The characteristics of this hypothetical column are determined by the constant in the second exponential term of the bi-exponential equation (ie. n_2 and k_2). The only process that occurs in this column is the slower sorption-desorption. The sample exits Column 2 in two zones. The first is an impulse from the fraction of sample that has not yet undergone sorption. The second is a broadened zone described by $P(t_S)_2$ (equation 2.23). Both of these zones enter Column 1 which is associated with the faster sorption process and the first exponential term of

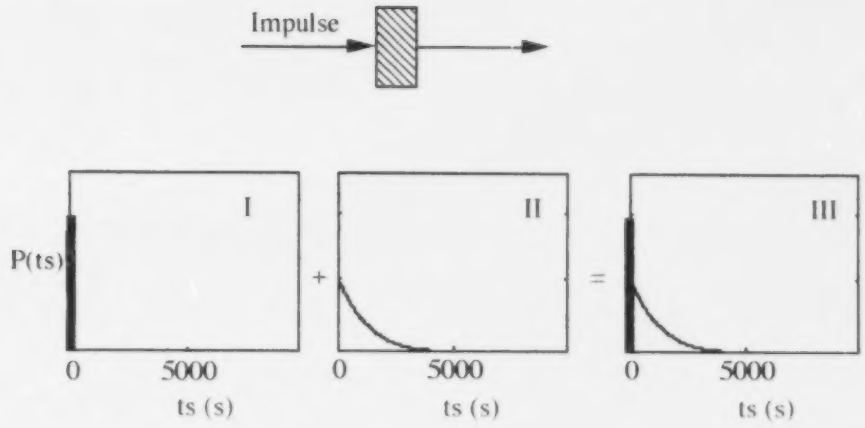

Figure 2.5.a The output of a column in which a significant fraction of sample does not undergo at least sorption-desorption cycle. The non-interacting fraction elutes as a spike at $t_s = 0$. The profile illustrated I represents this impulse, assumed to have the same width as the injected impulse which is considered to be infinitely narrow. Note that the time $t_s = 0$ corresponds to t_m, the retention time for an unretained compound in the column. The interacting fraction has a probability distribution that can be calculated by equation 2.15. The resulting profile is labelled II in the diagram above. The overall profile of a sample is the sum of the two fractions, labelled III above.

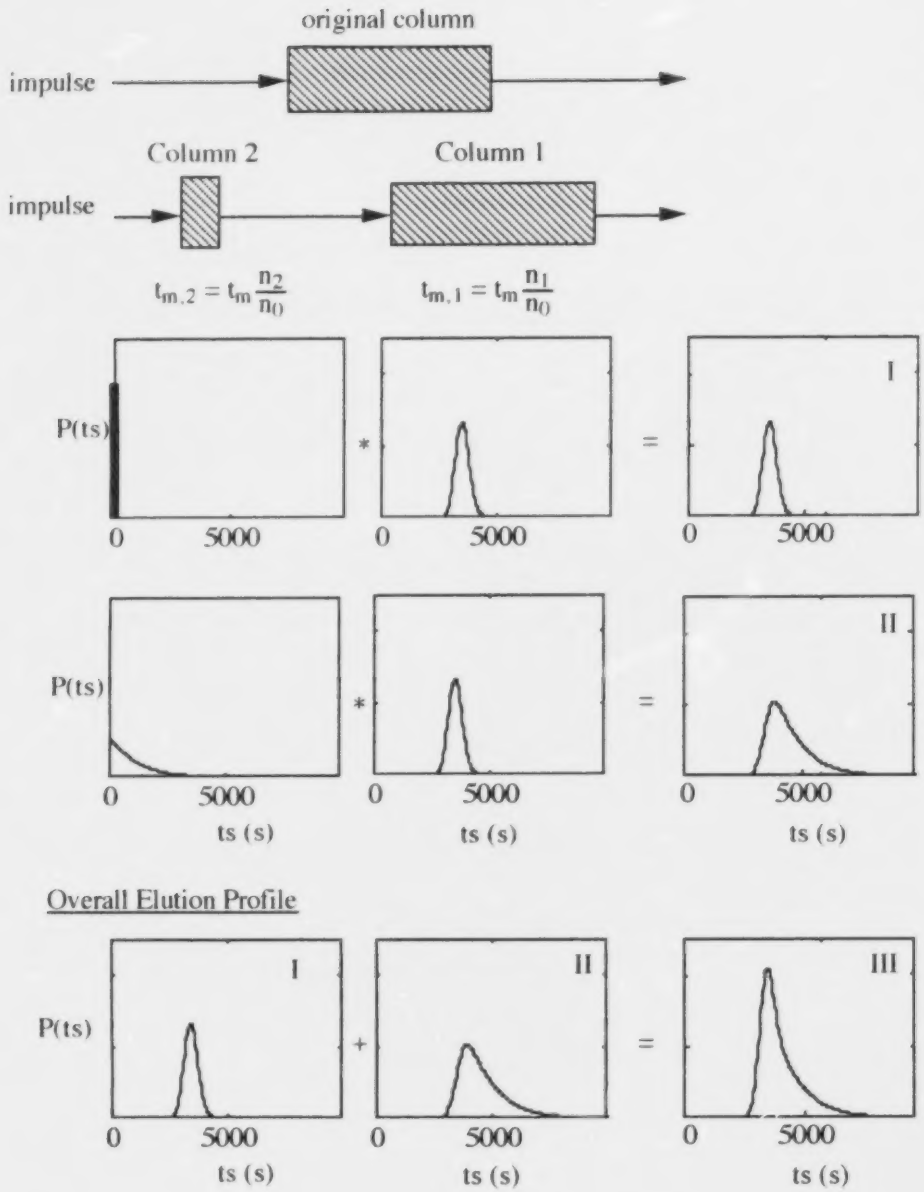

Figure 2.5.b Prediction of the elution peak for a sample which has a bi-exponential rate curve on the packing in the analytical where there is some fraction that does not undergo the slowest sorption process. See Section 2.3.5.

the tri-exponential equation. Both of the incoming sample zones undergo broadening which is equivalent to convolution with the distribution $P(t_s)_1$ (equation 2.21). Profile I is the result of convolution of the impulse with $P(t_s)_1$ and profile II is the result of convolution of $P(t_s)_2$ with $P(t_s)_1$.

In order to predict the real chromatogram from the profiles I and II, two additional calculations are made. First, the profiles are scaled according to the non-interacting fraction. This scaling is done according to area (ie. if $\Phi_2 = 0.3$, the area under profile I must be 30 % of the total area.) The scaled profiles are then summed to form III. Once the time correction is made by adding t_m on the time axis (as discussed in Section 2.3.3), this profile is then comparable to the elution profile of the sample from a real chromatographic column containing a stationary phase whose sorption rate curve is modelled by a bi-exponential equation containing one relatively small and one relatively large sorption rate constant.

2.3.6 Data Treatment For Tri-exponential Rate Curve Where Non-interacting Fraction for One Sorption Step is Significant.

The data treatment actually used for the majority of rate curves described in this thesis falls under this category. Generally, the rate curves are tri-exponential in nature, which has the form shown in equation 2.25.

$$n(t) = n_0 - n_1e^{-k_1t} - n_2e^{-k_2t} - n_3e^{-k_3t} \qquad \text{eqn. 2.25}$$

The thought experiment previously described is modified so that the chromatographic column is modelled by a series of three columns of varying lengths. This situation is illustrated in Figure 2.6. In the first column, labelled Column 3, the sorption rate is the slowest and a significant fraction of a sample zone will not interact with the stationary phase in this column. The output from the first column is as

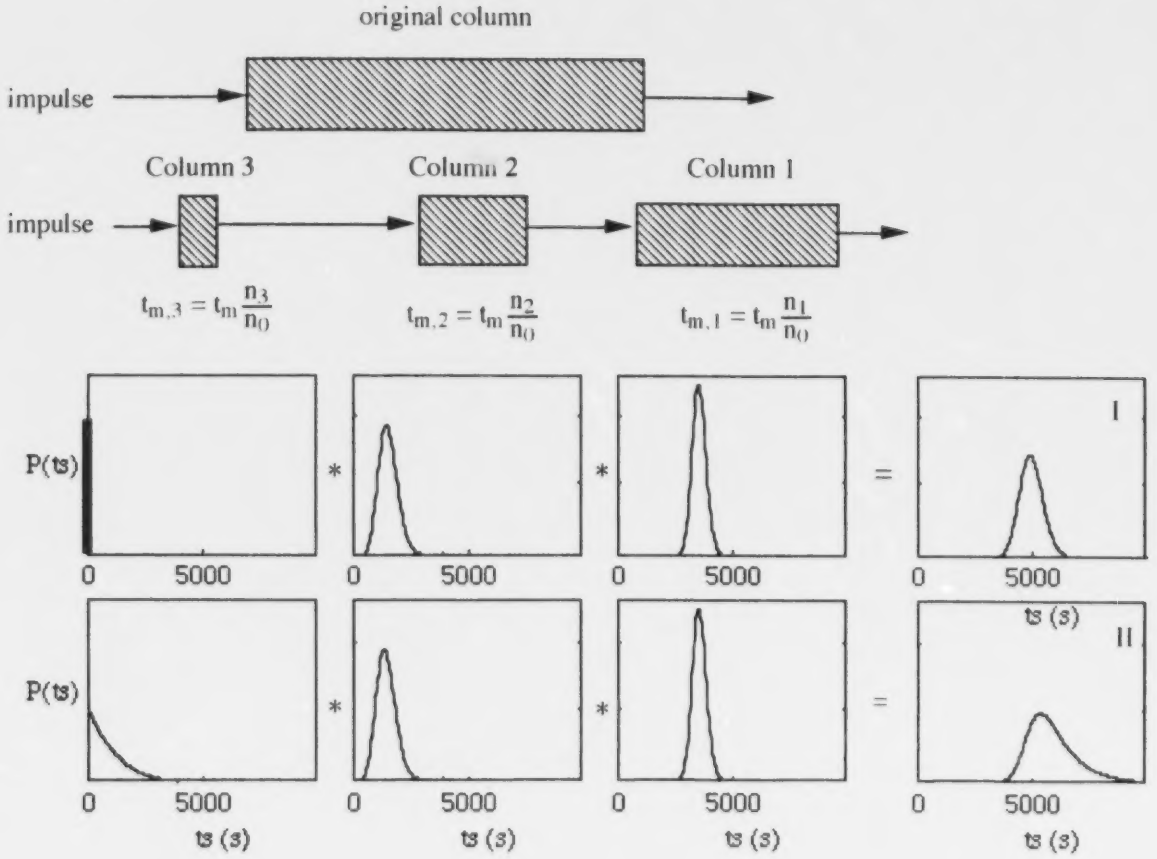

Figure 2.6.a See caption for Figure 2.6.b for explanation.

Overall Elution Profile

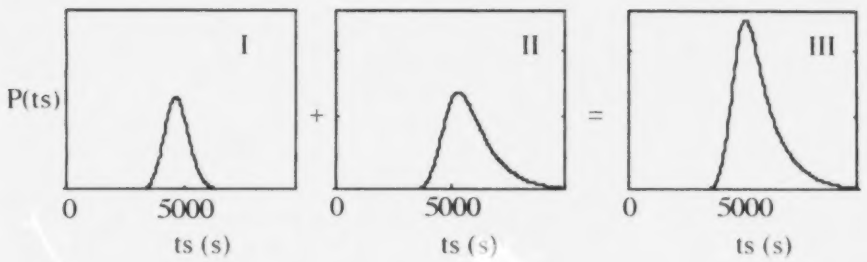

Figure 2.6.b Prediction of the elution profile for a sample which has a tri-exponential sorption rate curve on the packing in the analytical column. The profiles I and II represent the two sample zones which elute from the series of hypothetical columns, as shown in Figure 2.6.a. Profile I is broadened due to kinetic processes occurring only on columns 1 and 2. Profile II is broadened due to interaction on columns 1, 2 and 3. The peaks are scaled according to area and added to get the overall profile III. After correction for t_m on the time axis, the peak III may be compared to a real chromatogram. See Section 2.3.6 for a complete description.

described in Section 2.3.5, consisting of sample eluting in two zones. Each of these zones will enter the next column, Column 2, where they will be modified by slow sorption-desorption kinetics associated with the stationary phases contained therein. The zones exiting Column 2 will then enter Column 1 to be further broadened. Column 1 is taken to be associated with the fastest sorption process and the constants n_1 and k_1. Column 2 is associated with the intermediate process and the constants n_2 and k_2. Each of these two columns would therefore act on injected impulses to give the distributions $P(t_S)_1$ and $P(t_S)_2$. In this case, however, the zones entering in these columns are not impulses, but are sample zones which have already undergone broadening.

In Figure 2.6, distribution I is the output from the series considering only the non-interacting fraction of sample molecules which eluted from the Column 3 as an impulse. Notice that the impulse is, in turn, convolved with the distributions $P(t_S)_2$ and $P(t_S)_1$. Distribution II in the illustration is the output from the series considering the sample zone that was broadened by slow sorption-desorption kinetics in Column 3 as well as in the Columns 1 and 2. After scaling (as described in Section 2.3.5), the overall elution profile is the summation of distributions I and II. Once the overall profile, III, is corrected along the time axis (Section 2.3.3), it is the comparable to the elution profile of the sample from a real chromatographic column containing a stationary phase whose sorption rate curve is modelled by a tri-exponential equation containing one relatively small and two relatively large sorption rate constants.

2.3.7 Description of Elution Chromatographic Peaks by Statistical Moment Analysis

The ideal elution profile in chromatography follows a Gaussian distribution. If a profile is Gaussian, it is symmetrical and the peak is easily described or characterized. The time for elution of the peak maximum is the retention time or centre of gravity of the peak. The variance is related to the peak width and can be easily calculated by

graphical methods [2.30]. These quantities are used to calculate the overall column efficiency (see equation 2.1). Most chromatographic peaks are not described by a Gaussian distribution and various schemes have been developed to adequately measure the peak characteristics mentioned above. Estimates of the characteristics can be obtained using graphical methods (summarized in Reference 2.30). For asymmetric peaks, these have proven to be unreliable. Instead, asymmetric peaks are best characterized by their statistical moments. The zeroth, first and second moments, designated as M_0, M_1, and M_2 , are integrals defined by equations 2.26, 2.27 and 2.28 respectively. M_0 is the area under the peak and is used in the calculation of other moments. M_1 is the centre of gravity and M_2 is the variance of the peak [2.31].

$$M_0 = \int_0^\infty h(t)dt \qquad \text{eqn. 2.26}$$

$$M_1 = \frac{\int_0^\infty t * h(t)dt}{M_0} \qquad \text{eqn. 2.27}$$

$$M_2 = \frac{\int_0^\infty (t-M_1)^2 * h(t)dt}{M_0} \qquad \text{eqn. 2.27}$$

In equations 2.26 to 2.28, h(t) is the peak height at time t.

If chromatographic data are collected digitally, the moments can be calculated either using summations as approximations of the integrals or using the computer languages which contain integration functions, such as ASYST (see Section 3.5.1). Results of numerical integration for experimental elution profiles are discussed in Section 4.2.1.1.

An alternate method of characterizing elution profiles which are asymmetric is to fit the profile to an exponentially-modified Gaussian (EMG) function. This fit

simplifies the calculation of the moments which characterize the peak because the moment equations (ie. 2.26, 2.27 and 2.28) can be applied analytically. The EMG function is shown in equation 2.29 [2.32].

$$h_{EMG}(t) = A\frac{\sigma_G}{\tau}\sqrt{2}\exp\left[\frac{1}{2}\left(\frac{\sigma_G}{\tau}\right)^2 - \frac{t - t_G}{\tau}\right]\int_{-\infty}^{Z}\exp(-x^2)dx \qquad \text{eqn. 2.29}$$

where $$Z = \frac{t - t_G}{\sigma_G} - \frac{\sigma_G}{\tau} \qquad \text{eqn 2.30}$$

The EMG function is defined by three parameters. The constants t_G and σ_G are the centre of gravity and the variance of the parent Gaussian peak. The parameter τ is the centre of gravity of the modifying exponential function. The factor A in the pre-exponential term determines the amplitude of the function. The function has been shown to be a good approximation of chromatographic peak shapes [2.33].

In order to evaluate the integral contained in the EMG function, the identity shown in equation 2.31 [2.32] is used to take advantage of the built-in error function (erf) routine in the language.

$$\int_{-\infty}^{x}\exp(-y^2)dy = \frac{\sqrt{\pi}}{2}[1 + \mathrm{erf}(x)] \qquad \text{eqn 2.31}$$

At values of $Z \leq -3$, techniques utilizing the error function have previously been shown to be inaccurate in evaluating the integral in equation 2.29 [2.32].

The moments of an EMG profile can be calculated from the constants of the function as shown in equations 2.32 and 2.33.

$$M_1 = t_G + \tau \qquad \text{eqn. 2.32}$$

$$M_2 = \sigma_G^2 + \tau^2 \qquad \text{eqn. 2.33}$$

CHAPTER 3

Experimental Procedures

3.1 Reagents

Naphthalene, supplied by Coleman and Bell (Norwood, OH), was recrystallized from methanol before use as the sample. Phloroglucinol (1,3,5-trihydroxybenzene), obtained form Fisher Scientific Co. (Fairlawn, NJ), was recrystallized from water and was used to determine hold-up volumes and mobile phase linear velocity in the elution experiments on PRP-1. Analytical reagent grade $Ca(NO_3)_2.4H_2O$ was used as supplied by BDH Chemicals (Poole, England) in the elution experiments on Partisil-10 ODS-3 to measure the mobile phase linear velocity.

3.2 Solvents and Mobile Phases

Doubly-distilled water was obtained from a Barnstead (Dubuque, IA) Nanopure water filtration/distillation system (part D4741). Reagent grade methanol was obtained from two suppliers, Anachemica Ltd. and Mallinckdrot and was distilled before use. Eluents and solvents were made by measuring appropriate volumes of methanol into a 2L volumetric flask and diluting to volume with doubly distilled water. For all experiments in which the stationary phase was PRP-1, 85% MeOH/H_2O was used as the solvent and eluent. This solvent was made by diluting 1700 mL of MeOH to a volume of 2000 mL. Because Partisil-10 ODS-3 is not as strong a sorbent as PRP-1, 52.5% MeOH/H_2O was used as the solvent and eluent for this packing. This solvent was made by diluting 1050 mL MeOH to 2000 mL. Before use, the mixed solvents were vacuum filtered through Nylon 66 membrane filters of 0.45 μm porosity (part 00140, Schleicher & Schuell, Keene, NH).

3.3 Packings

Two types of stationary phase packings were used in this experiment. PRP-1 (lot 372), a polystyrene-divinylbenzene copolymer, was donated by Hamilton Co. (Reno, NV). The second material was the silica-based Partisil-10 ODS-3 (part 4128-010, Whatman, Clifton, NJ, batch 100763). The characteristics of both packings are shown in Table 3.1.

3.4 Measurement of Sorption Rate using the Shallow Bed Apparatus

3.4.1 Apparatus for Sorption Rate Measurements

Figure 3.1 provides a schematic diagram of the apparatus. The centre of the system is a slider valve V2, illustrated in Figures 3.2.a and 3.2.b. The basic design of the valve follows the design of commercially available slider valves with some important distinctions. The valve is constructed mainly of stainless steel. The valve body, as shown in Figure 3.2.b, is basically a stainless steel box with sides approximately 1/4" thick. The valve body disassembles to allow access to the slider. The slider is a 2 mm thick stainless steel plate with four holes of 3 mm diameter drilled at 3/8" intervals on centres. At the bottom of each of the holes is a stainless steel mesh screen of 2 μm pore size. One of the holes contains the shallow bed, a small "column" of packing material approximately 0.5 mm in height. The bed is held in place on the bottom by the metal screen and on the top by a 3 mm diameter Zitex Teflon porous plug. This material, available in sheets (part K1064-122D, Chemplast, Wayne, NJ), is approximately 0.6 mm thick and of 30-60 μm pore diameter. Typical shallow bed characteristics are shown in Table 3.2.

The slider is mounted in a stainless steel assembly between two Teflon face plates. The Teflon face plates provide low friction for the sliding action. The actual surface area contacting the slider is decreased by milling grooves along the sides of the

Table 3.1 Packing properties of PRP-1 and Partisil-10 ODS-3. Properties of the Partisil marked with an asterisk (*) are data given by the manufacturer for the underivatized silica gel. Further information about the pore volume of the derivatized packing is given in Appendix 2.

Packing Property	PRP-1	Partisil-10 ODS-3
Material	Poly(Styrene Divinylbenzene)	C_{18} groups bonded to Partisil Silica Gel
Particle Shape	spherical	irregular
Particle Size	10 ± 2 μm	10 μm
Packing Density	0.42 g/mL	0.45 g/mL*
Avg. Pore Diameter	7.5 nm	6.8 nm*
Specific Pore Volume	0.79 mL/g	0.796 mL/g*
Specific Surface Area	415 m^2/g	467 m^2/g*
% C Loading	N/A	10.5

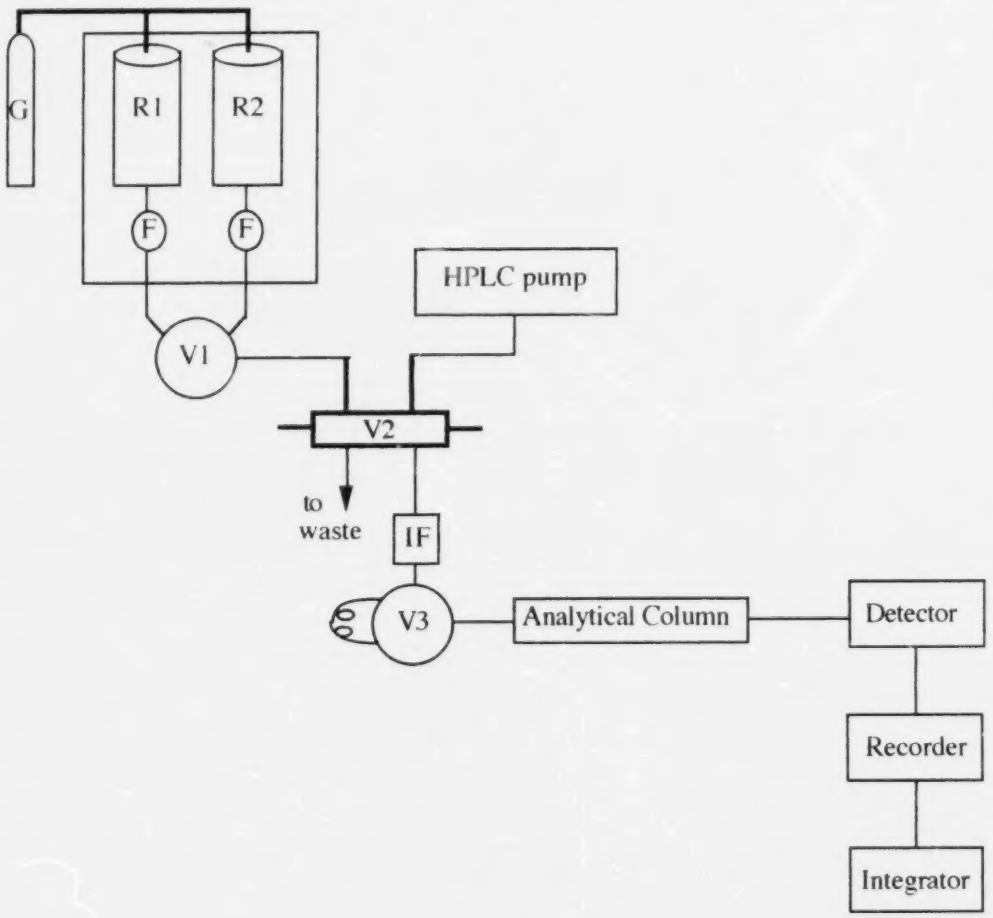

Figure 3.1 Schematic diagram of apparatus used for sorption rate measurements. G: Gas cylinder (N_2). R1 and R2: solvent and sample solution reservoirs of constant pressure pumps. F: Millipore solution filter holders. V1: Rheodyne six-way valve. R1, R2 and the filters F are immersed in a constant temperature bath. V2: Slider valve. IF: Rheodyne in-line filter. V3: Rheodyne injection valve. The system is described in detail in Section 3.4.1.

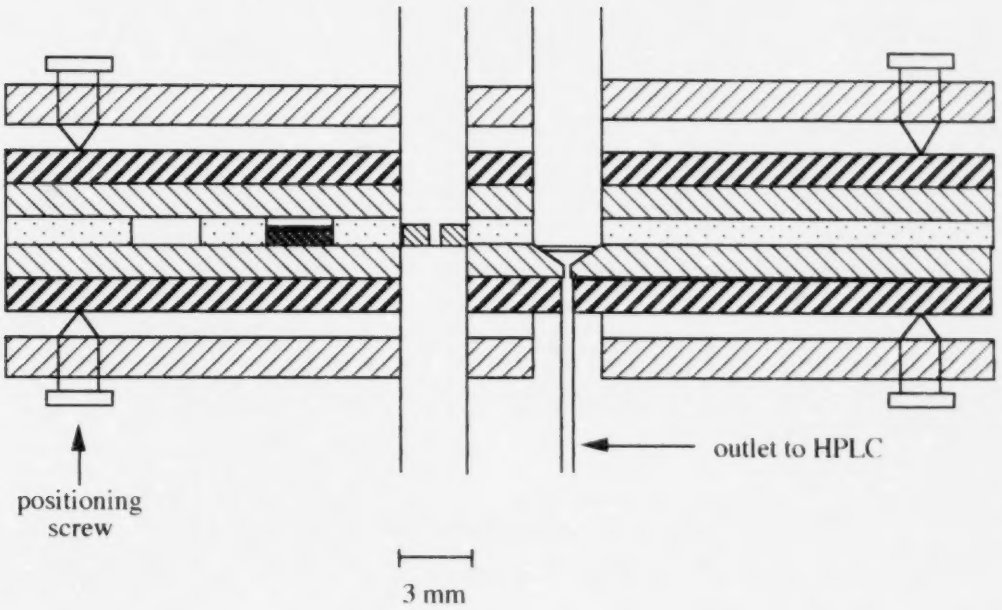

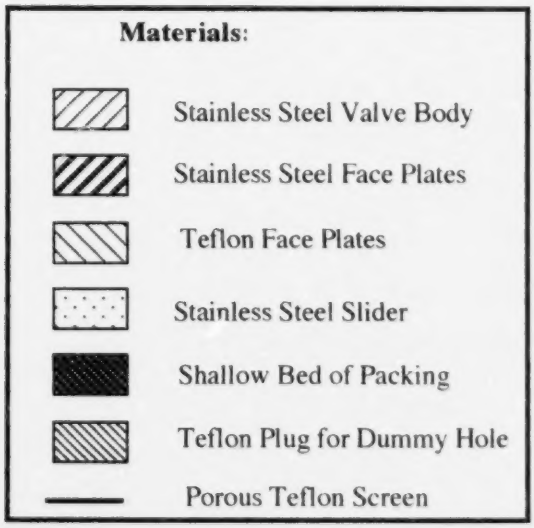

Figure 3.2.a Schematic diagram of slider valve (side view). The valve is more fully described in Section 3.4.1.

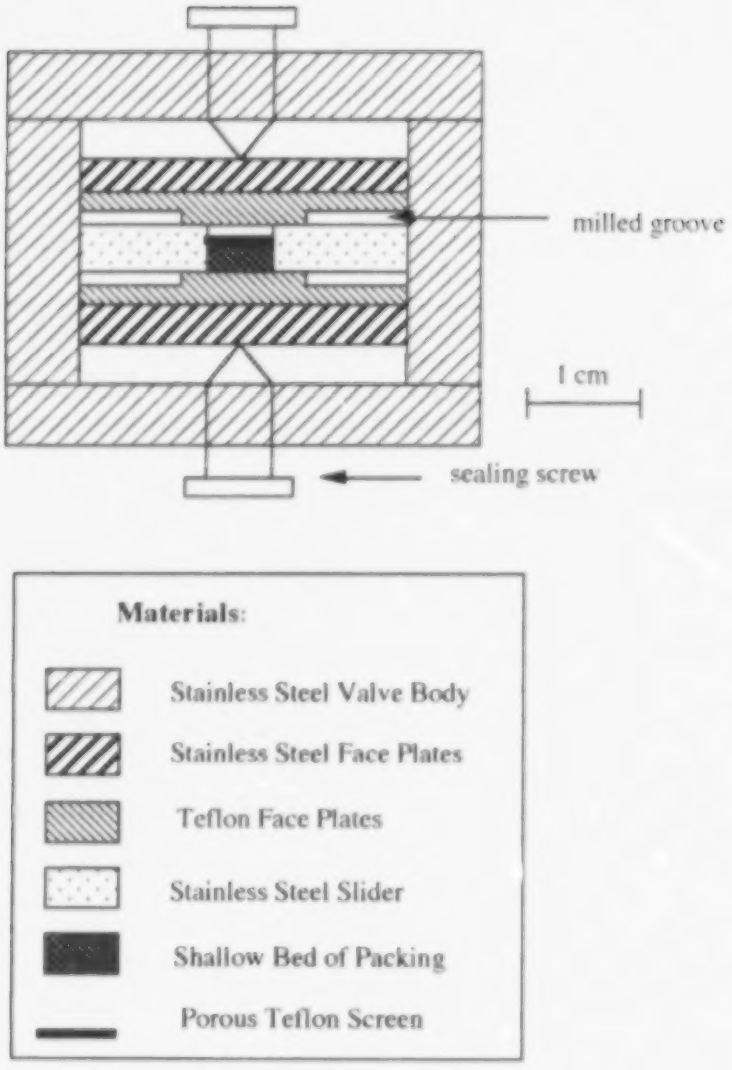

Figure 3.2.b Schematic diagram of slider valve (end-on view). A complete description of the slider valve is given in Section 3.4.2.

Table 3.2 Properties of shallow beds of PRP-1 and Partisil-10 ODS-3 used in sorption rate experiments. The weight of the shallow beds are measured directly and the error is the absolute error. The $V_{hold\text{-}up,T}$ and $V_{hold\text{-}up}$ are measured as in Section 3.4.3. The error values are calculated by propagation and are expressed as ± one standard deviation. All other characteristics are estimated from manufacturer's information concerning the packing. The pore volume for the Partisil shallow bed uses the specific pore volume calculated in Appendix 2.

Shallow Bed Property	PRP-1	Partisil-10 ODS-3
weight packing	1.82 ± 0.05 mg	1.06 ± 0.05 mg
bed height	~ 0.6 mm	~ 0.3 mm
packing volume*	~ 4.3 µL*	~ 2.3 µL*
V_{pore}	1.44 ± 0.04 µL	0.64 ± 0.03 µL
$V_{hold\text{-}up,T}$	13.88 ± 0.07 µL	15.17 ± 0.44 µL
$V_{hold\text{-}up}$	12.44 ± 0.12 µL	14.53 ± 0.46 µL

*Based on bulk density

Teflon face plates as shown in Figure 3.2.b so that only the small area around the holes in the slider are contacted. The decreased area of contact leads to a better seal of the Teflon/stainless steel surfaces.

Screwed to the Teflon plates is a set of stainless steel plates. At four sites, positioning screws through the valve body contact these steel plates. These four positioning screws provide the forces necessary to seal the valve. The steel plates prevent the Teflon plates from being deformed by the sealing screws. Pieces of Teflon tape are placed between the steel and Teflon plates before attachment to assure a good seal between them.

The slider valve has 2 inlets, both of which are stainless steel tubes of 3 mm i.d. which are silver-soldered to the steel plates. The first inlet, shown on the left side of valve V2 in Figures 3.1 and 3.2.a, is connected to a system of constant pressure pumps consisting of two aluminum cylinders, R1 and R2, pressurized by N_2. R1 and R2 contain a solvent and sample solution respectively. The solutions pass through in-line stainless steel filter holders labelled F in Figure 3.1 (part XX44 047 00, Millipore, Mississauga, Ont.) containing Durapore HV membrane filters of 0.45 μm pore diameter (part HVLP 047 00, Millipore, Mississauga, Ont.) before reaching a Cheminert 6-way valve, V1 (part 414 2530, LDC, Riviera Beach, FA). The setting of V1 determines which solution enters the first inlet of the slider valve. R1 and R2 are immersed in a constant temperature bath thermostated by a circulating Haake D3 temperature controller which is set to 25.0 ± 0.1 °C. This left-side inlet of the slider valve has an outlet to waste. Moving the slider to the right, from the position shown in Figure 3.2.a places the shallow bed in the sample flow stream to initiate the timed "exposure step". The exposure time refers to the time the shallow bed spends in the second position, during which the sample stream passes through it.

The second inlet, located on the right side of the slider valve, as shown in Figures 3.1 and 3.2.a is fed by an SP 8000 HPLC pump (Spectra-Physics, Santa

Clara, CA) in constant flow mode. When the bed is moved out of the sample flow stream into this flow stream, any sample which was sorbed in the previous exposure step will be eluted and analyzed using conventional HPLC as follows. The right-hand outlet of V2 is directed to narrow-bore (.002" i.d.) stainless steel tubing leading to a Rheodyne in-line filter (part 7315, Rheodyne, Berkeley, CA) and an analytical HPLC column. The analytical column (part 086680, Waters, Mississauga, Ont.) used in the sorption rate experiments is packed with μBondapak Phenyl and is 15 cm in length and 4.6 mm i.d. A Rheodyne injection valve, V3 (part 7010, Rheodyne, Berkeley, CA) with a sample loop of a previously measured volume of 23.88 ± 0.02 μL [3.1] is located upstream of the analytical column and is used to construct a calibration curve, as explained in Section 3.4.2.

The slider can occupy one of three positions which are illustrated in Figure 3.3 and further described in Section 3.4.2. The exposure time (illustrated in Figure 3.3.d) is measured using a small infra-red generator/detector unit which is attached to the lever system. The exposure time is displayed on a modified Hewlett Packard 5321B electronic counter set to display to ± 0.1 msec.

Sample eluted from the shallow bed in the elution step (Figure 3.3.e) passes through the analytical column into a Kratos 757 Variable Wavelength UV detector (λ = 276 nm). The resulting peaks are recorded on a Fisher Recordall Chart Recorder and integrated by an HP 3390A Integrator.

Good temperature control was found to be of some importance for reducing scatter in the sorption rate measurements. The body of valve V1 and connecting tubing leading from the thermostated reservoirs were both insulated with asbestos tape. Monitoring the temperature of the flowing streams proved to be problematic. Since the slider and slider valve body were for the most part metal, heat conduction between the various valve parts was considered to be good. The temperature of the valve body and of the metal inlet tubing near the slider were monitored with a contact K-type

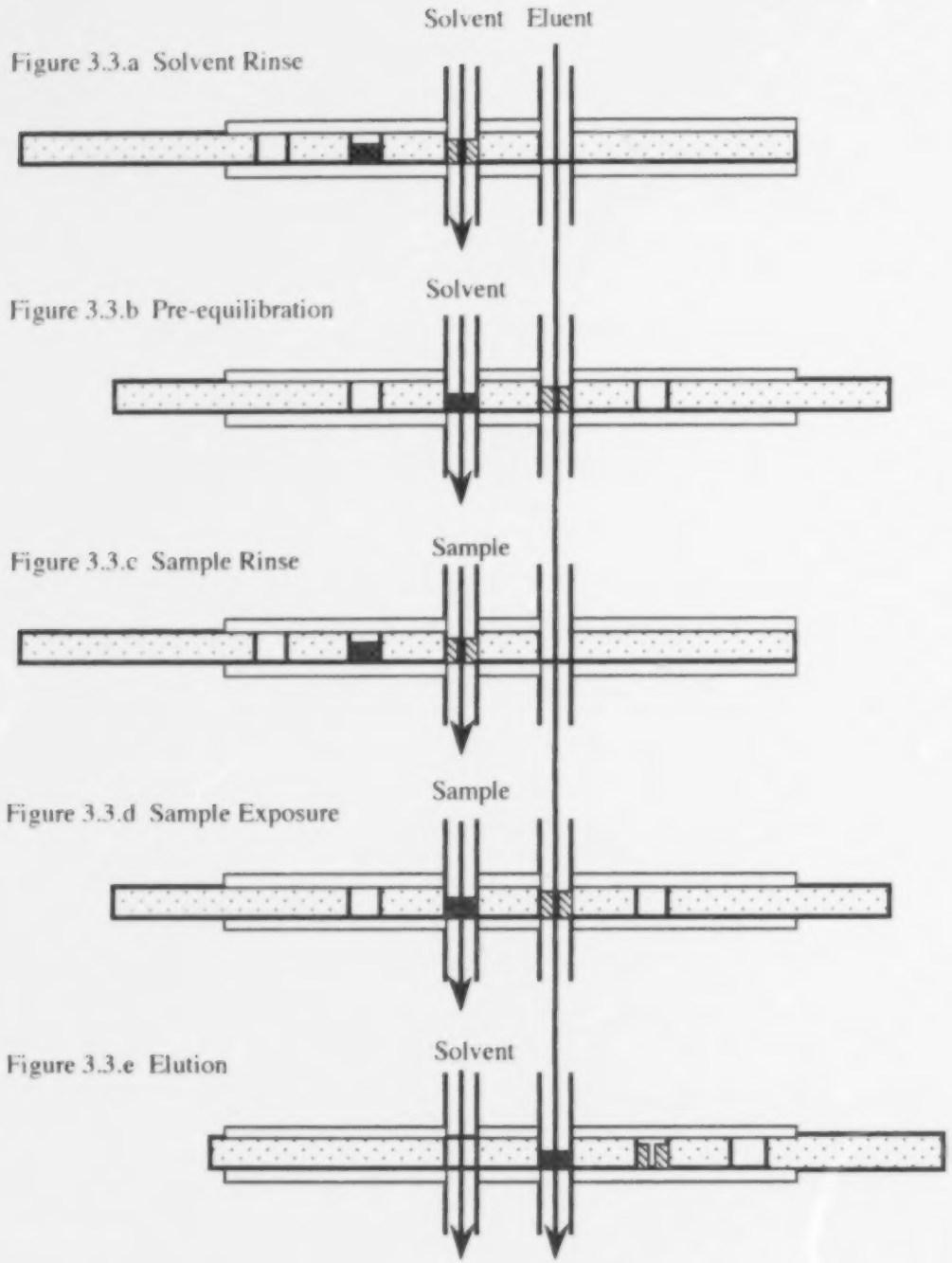

Figure 3.3 The sequence of positions of the slider valve in the sorption rate experiment as described in Section 3.4.2.

thermocouple and Digi-Sense JTK thermometer readout (part N-08528-20, Cole-Parmer) set to read ± 0.1 °C.

The valve is mounted on an aluminum back plate, not shown in the figures, which is mounted on the top of a lab bench. Also mounted on the back plate is a lever assembly which is used to move the slider, as shown in Figure 3.4. The slider is attached at one end to a lever via a brass bar. The lever uses a hinged hook to catch notches in the bar. To change the position of the slider, the lever is pushed forward (to the left in Figure 3.4) until the hook catches the next notch in the bar, then is pulled back until it hits a stop. The stop and the notches in the bar are carefully calibrated so that the slider falls into a position where the holes are aligned directly under the inlet of interest. To return the slider to the original position, it is necessary to pull the slider back manually using a handle (not shown in the schematics) on the left end of the slider. At present, this results in some stress on the slider and a tendency for the slider to twist out of shape. A lever, built on the same principle as the one described above, attached to this end of the slider would be of great help in prolonging the life of the slider.

The valve in its present form provides little back pressure. For example, a flow rate of about 12 mL/min can be achieved in the exposure step with 120 psi for the shallow bed of PRP-1. An HPLC pump is used in the elution step because of the presence of the analytical column which provides most of the back pressure for the system. Relatively low flow rates of the eluent (eg. 0.4 ml/min) are used. The valve seals well up to about 600 psi but is more usually used in the range of 300 psi or less.

The slider is made of stainless steel and should be handled carefully to avoid scratching the polished surface. One persistent problem with the valve is that the sliding action tends to shave off the Teflon surface of the face plate. The sharp edges of the holes in the slider drag across the Teflon surface as the slider moves, planing off flakes of Teflon. The flakes of Teflon become lodged in the empty holes of the slider

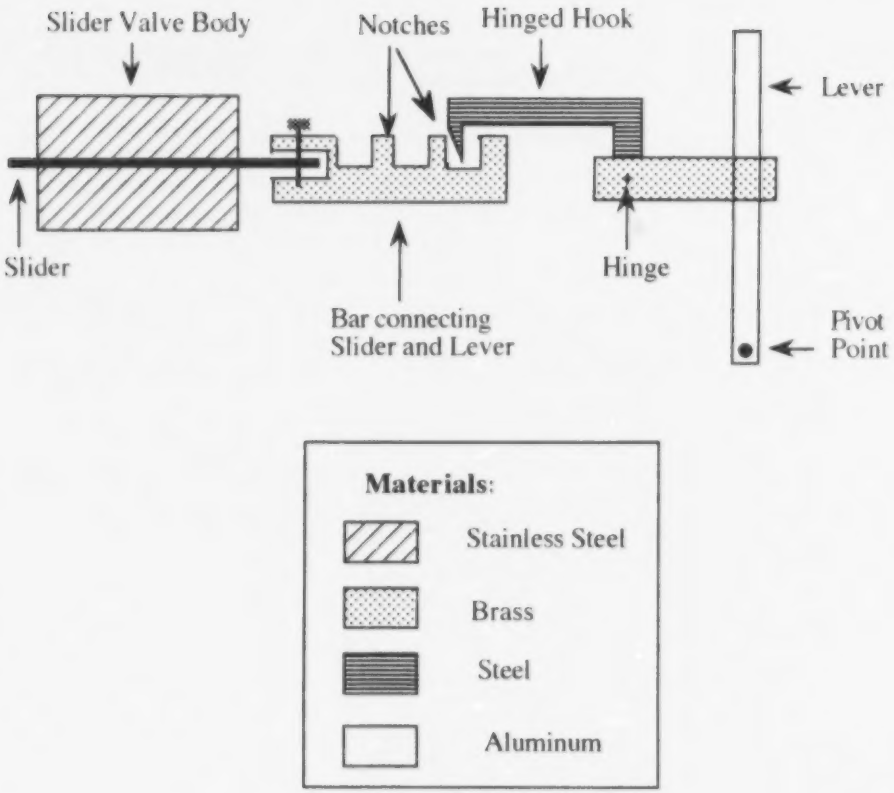

Figure 3.4 Lever System used to move slider in sorption rate experiment. The lever system is described in detail in Section 3.4.2

and on top of the Zitex retaining screen of the shallow bed. This results in an increase in back pressure. The edges of the holes on the underside of the slider also produce flakes of Teflon which tend to lodge in the inlet to the HPLC. Since the outlet tubing to the HPLC is narrow bore, even a small piece or amount of Teflon can severely increase the system back pressure. This problem is prevented by the use of a stainless steel mesh screen with 2 μm porosity placed over the outlet to the HPLC in the bottom Teflon plate. This is illustrated in Figure 3.2.a. The down stream in-line filter also provides protection against particulate matter but mainly for the analytical column.

The inlets to the slider valve were designed to produce a flow stream having the same 3 mm in diameter as the shallow bed. If the inlet were of a smaller diameter than the shallow bed, a radial flow velocity gradient might be established. The flow through the bed would probably be too fast to allow lateral diffusion to completely relax this gradient. If this were the case, parts of the bed at different radial locations would experience different sample concentrations and the criteria for establishing shallow bed conditions would not be met.

3.4.2 Experimental Procedure

The measurement of the rate of sorption onto a packing involves a series of experiments in which the shallow bed of the packing of interest is exposed to a relatively fast stream of a sample solution for variable amounts of time.

In each run of the series, the bed is initially located in the first position of the slider as illustrated in Figure 3.3.a. The first step in the experiment is the pre-equilibration of the shallow bed with solvent which is being pumped through the left-hand inlet to the slider valve. This solvent is stored in R1 and 25 mL of it is allowed to flow through connecting tubing to adequately rinse the system. Pre-equilibration of the shallow bed begins when the bed is pulled into the solvent stream as shown in Figure 3.3.b. The time needed to collect 10 mL of solvent after it passes through the bed is

measured and recorded. The superficial linear velocity, u, through the bed is calculated from this time, Δt, using equation 3.1.

$$u = \frac{10\ mL}{\pi\ r^2\ \varepsilon_{inter} \Delta t} \qquad \text{eqn. 3.1}$$

r is the radius of the shallow bed which is 0.15 cm. ε_{inter} is the fraction of bed volume contained between the particles. For PRP-1, the quantity was calculated using manufacturer's information concerning the specific interparticle volume and the bed density. For PRP-1, ε_{inter} was calculated to be 0.31. For the silica-based packing, similar information was not available and ε_{inter} was assumed to be 0.4 [3.2, 3.3].

Once pre-equilibration is complete, the shallow bed is pulled back into its initial position as seen in Figure 3.3.c and the rotary valve V1 is used to change the liquid flowing through the left hand tube from solvent to sample solution. The connecting tubing is flushed with approximately 25 mL of sample solution before the bed is pulled back into the sample stream to initiate the exposure step (Figure 3.3.d). In the exposure step, the bed is left in the flowing stream for the desired amount of time. The slider is then pulled to the third position (Figure 3.3.e) in which the shallow bed is located in the eluent stream fed by the HPLC pump. Once elution is complete, the slider is pulled back to the first position (Figure 3.3.a) and the experiment is repeated with a different exposure time. The minimum exposure time used in this experiment (> 0.3 s) was determined by the minimum time required by the lever and hinged hook assembly to move the slider from the position shown in Figure 3.3.d to that shown in Figure 3.3.e. Each repetition of the sequence shown in Figure 3.3 results in a detected peak with area proportional, after corrections described below, to the number of moles sorbed by the shallow bed.

A calibration curve is constructed by injecting solutions of known concentration into the analytical column using the injection valve V3 (in Figure 3.1) and plotting the integrated area against the number of moles injected. Next, the area of the peak eluted

from the shallow bed is used to calculate the total moles of sample eluted, N_{el} . In order to calculate the number of moles sorbed, N_{sorb}, the number of moles eluted from the shallow bed must be corrected for $N_{hold\text{-}up}$, the moles of sample contained in the hold up volume of the shallow bed (see Section 3.4.3) as shown in Equation 3.2 .

$$N_{sorb} = N_{el} - N_{hold\ up} \qquad \text{eqn. 3.2}$$

For short exposure times, an additional correction is necessary. The 3 mm hole to the right of the shallow bed in the slider (see Figure 3.3) is filled with a Teflon plug with a very small hole (~0.3 mm diameter and volume 0.37 μL) drilled through it. The plug was installed to decrease the volume in this dummy hole. The hole in the centre of it is necessary to allow flow through the valve when the valve is in any of the positions illustrate in Figure 3.3. During the step in which the connecting tubing is rinsed with sample solution (see Figure 3.3.c), this dummy hole is located in the sample stream and is thus filled with sample solution. When the valve is switched into the next position (see Figure 3.3.d), the dummy hole lies in the eluent stream and the sample solution it contains is injected into the analytical column. For very long exposure times, the sample peak resulting from sample solution in the dummy hole will elute from the analytical column well ahead of the sample peak resulting from elution from the shallow bed. However, as the exposure time for the shallow bed is decreased, the two sample peaks are injected closer and closer together. When the eluent flow rate is 0.4 mL/min, the two peaks were found to overlap when the exposure time was less than about 20 sec. In this case, the integrator treats them as one peak. The number of moles of sample contained in the dummy hole, N_{dummy}, must therefore also be subtracted from the number of moles eluted from the shallow bed for these short exposure times.

$$N_{sorb} = N_{el} - N_{hold\text{-}up} - N_{dummy} \qquad \text{eqn 3.3}$$

Once N_{sorb} is calculated, the data are normalized to Wt, the weight of packing in the shallow bed.

$$n(t) = \frac{N_{sorb}}{Wt} \qquad \text{eqn 3.4}$$

The units of n(t) are mol/g. The quantity n(t) is a function of exposure time, t, so the experiment results in a sorption rate curve which is the plot of n(t) vs exposure time. A typical sorption rate curve is illustrated in Figure 2.3.

3.4.3 Hold-up Volume Measurement

The procedure used for measuring the sorption rate was, with a few modifications, also used to measure the hold-up volume for the shallow bed. The sample for these experiments was phloroglucinol in 85% MeOH/H_2O which was shown to be unretained on chromatographic columns of both sorbents. The exposure time was 60 s. The result of this procedure was a peak of area $A_{hold\text{-}up}$. For detector calibration, the phloroglucinol solution was then injected onto the analytical column using the injection valve V3 with an injection volume of V_{inj} giving a peak of area A_{inj}. The measured total hold-up volume of the bed, $V_{hold\text{-}up,T}$ was calculated by equation 3.5.

$$V_{hold\text{-}up,\,T} = V_{inj}\,\frac{A_{hold\text{-}up}}{A_{inj}} \qquad \text{eqn. 3.5}$$

The measured hold-up volume was corrected by subtracting the pore volume, V_p, of the packing in the shallow bed. This correction, shown in equation 3.6, was necessary because diffusion of the sample into the pores of the packing must be considered to be part of the overall time consuming process of sorption.

$$V_{hold\text{-}up} = V_{hold\text{-}up,\,T} - V_p \qquad \text{eqn. 3.6}$$

The quantity $V_{hold\text{-}up}$ is the volume associated with interparticle space as well as space within and below the retaining screen and within and above the porous Teflon plug in the 3 mm hole in the slider containing the shallow bed. The pore volume V_p is calculated by multiplying the specific pore volume of the product by the weight of

packing used in the shallow bed. The specific pore volume, in ml/g, of Hamilton PRP-1 is a packing characteristic listed in Table 3.2 and found in the manufacturer's information accompanying the product. The specific pore volume of Partisil-10 ODS-3 was calculated according to information described in the literature for silica based bonded phase packings [3.4] The authors found that as silica was derivatized, the decrease in the pore volume related only to the carbon loading and not the phase type. Since the specific pore volume for the original silica and the resulting % C loading were available (see Table 3.2), the specific pore volume, v_p, was calculated by using the linear relation described in Reference 3.4, substituting the appropriate value for the specific pore volume of the silica out of which the Partisil-10 ODS-3 was synthesized. Detailed calculations are found in Appendix 2.

Since the concentration of the naphthalene sample solution C_m, is constant in a particular shallow bed experiment, the moles of naphthalene present in the hold-up volume, $N_{hold\text{-}up}$, can be calculated according to equation 3.7.

$$N_{hold\text{-}up} = V_{hold\text{-}up}\, C_m \qquad \text{eqn 3.7}$$

This quantity is needed for equations 3.2 and 3.3.

As discussed, the hold-up volume of the Partisil-10 ODS-3 shallow bed is determined using phloroglucinol in 85 % MeOH/H_2O and sorption rates are measured with naphthalene in 52.5 % MeOH/H_2O. Ideally, the hold-up volume should be determined in the same eluent as used for a sample. In this case, that was not possible since phloroglucinol was retained on Partisil in 52.5 % MeOH/H_2O. Certain kinds of packings such as ion-exchangers and agarose swell as the water content of the mobile phase increases. Swelling would lead to an increase in the hold-up volume of the packing. Silica-based packings are rigid, however, so the hold-up volume should not vary with water content of the mobile phase. Therefore, the hold-up volume as

determined with phloroglucinol in 85% MeOH should be applicable when the 52.5 % MeOH solvent is used.

3.4.4 Measurement of the Sorption Isotherm

The sorption isotherms for naphthalene on the two packings were studied using the shallow bed apparatus as illustrated in Figure 3.1 in a procedure developed by May, Hux and Cantwell [3.1] called the 'column equilibration method'. In the experiment, the shallow bed is exposed to the sample solution until the stationary and mobile phases are in equilibrium. The exposure time in this experiment was 60 seconds. After this time, the shallow bed is slid under the eluent stream from the HPLC pump and the number of moles eluted is determined as described above. This quantity must be corrected for the sample contained in the hold-up volume. The quantity of interest in this case is the number of moles of sample actually adsorbed on the stationary phase. (In the shallow bed experiment, the quantity of interest is the amount adsorbed as well as the amount located in the pores of the packing.) In this case, therefore, the necessary calculation used the total hold-up volume $V_{hold\text{-}up,T}$, not $V_{hold\text{-}up}$ which was defined in Section 3.4.3.

$$N_s = N_{el} - C_m V_{hold\text{-}up} \qquad \text{eqn. 3.8}$$

The quantity N_s differs from N_{sorb} by the number of moles in the pore volume of the packing.

$$N_s = N_{sorb} + C_m V_{pore} \qquad \text{eqn. 3.9}$$

The sorption isotherm is a plot of C_s, the concentration in the stationary phase, in mol/g vs C_m, the concentration in the mobile phase. C_s is determined by dividing N_s by the weight of packing in the shallow bed.

$$C_s = \frac{N_s}{Wt} \qquad \text{eqn. 3.10}$$

3.5 Elution Chromatography

3.5.1 Experimental Procedure

The purpose of measuring the sorption rate (kinetic) curves for naphthalene on a particular packing by the shallow bed experiment is to allow prediction of the chromatographic peak shape expected when naphthalene is eluted from a long column of the packing. The experimental elution chromatograms needed for comparison with those predicted by the calculations given in Section 2.3.7 were collected using the instrument illustrated in Figure 3.5. The HPLC pump, run in constant flow mode, the in-line filter, the injection valve and the UV detector are the same components mentioned above. The columns used were commercially available HPLC analytical columns. The PRP-1 column (part 79425, Hamilton, Reno, NV) was 4.6 mm i.d. and 15 cm long and packed with 10 μm spherical particles. The Partisil-10 ODS-3 column (part 1P9913, Whatman, Clifton, NJ) was 4.6 mm i.d. and 25 cm long and was packed with 10 μm irregular particles. The absorbance signals of the eluted peaks were fed into an analog-to-digital converter (Lab Master, TM-40-PGL, Tecmar, Cleveland, OH) in an IBM-XT microcomputer. Peak characteristics were calculated using ASYST Version 2.0 (McMillan Software Co., New York, NY). The programs, previously described in detail [3.5] permit the calculation of peak area, peak retention time, t_r, and peak variance, s^2, using statistical moment analysis. The experimental plate height is then determined using equation 2.1. Several problems with the ASYST software had to be overcome. The problems encountered with the moment analysis for naphthalene on PRP-1 are discussed in Section 4.2.1.1.

An alternate method of analysis was developed to compensate for some of the problems encountered in attempting to use numerical methods to calculate the moments of the elution peaks. Data were collected using the above instrument and the digital data

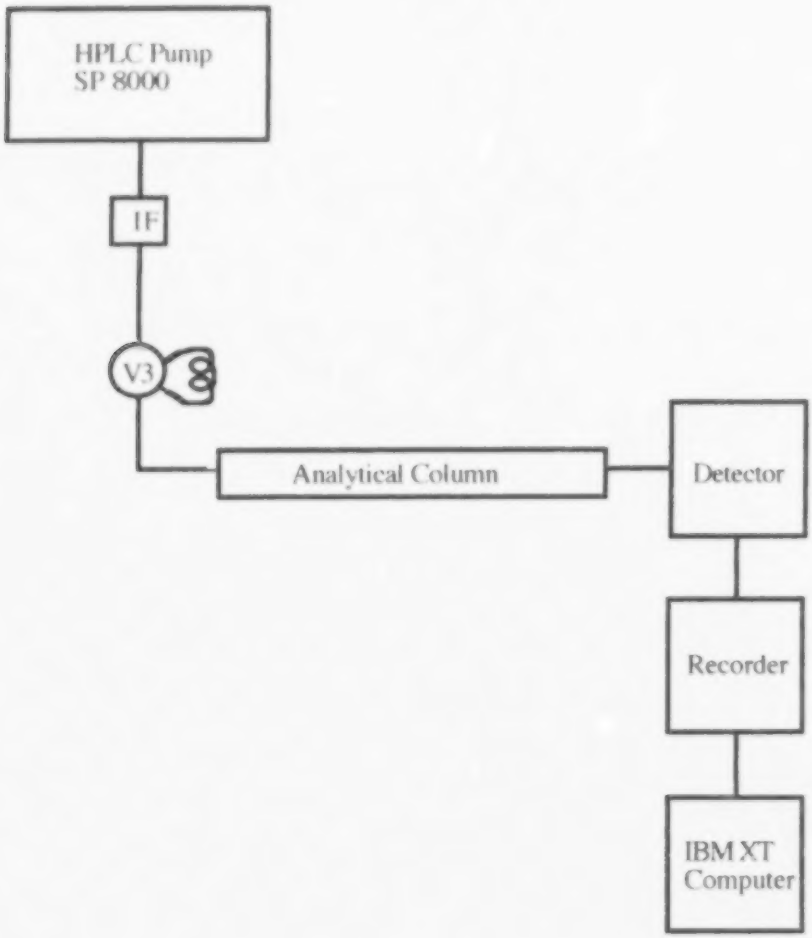

Figure 3.5 Schematic diagram of the apparatus used to collect experimental elution profiles as described in detail in Section 3.5.1. IF: Rheodyne In-line filter. V3: Rheodyne injection valve.

was smoothed using the smoothing function in the ASYST program. The data were saved in a data file which was then converted to MS-DOS format using a routine written in ASYST. This routine can be found in Appendix 3.1. The DOS file was then converted to a MacWrite (Claris Corp., 1988) format using Apple File Exchange software (Apple Computers Inc., 1990) on a Macintosh IIsi. The data were then copied to an Excel (Microsoft, 1991) data file. The data was easy to manipulate and view in this format. A data subset was chosen from each data file with limits as discussed in Section 4.2.1.2 and the subset transferred to a home-grown non-linear least squares fit program called EXPGAUSS written in Matlab (MathWorks, Inc., Natik, MA.). The program EXPGAUSS then chooses a user specified number of equally spaced data points within the subset which are used to fit the elution profile to an exponentially modified Gaussian (EMG) function. Statistical moments were then calculated analytically for the EMG function, as discussed in Section 2.3.7. Discussions of the limitations of this program including the effect of the number of data points chosen and the effect of uncertainty in the location of the baseline are discussed in Section 4.2.1.2.

On PRP-1, the linear velocity of the mobile phase, u_o, in the elution chromatography was measured by injecting a 10^{-3} M solution of phloroglucinol and calculating the first moment of the eluted peak. The first moment was corrected for extra-column effects as described in Section 3.5.2. The corrected first moment, t_m, is the time to elute the void volume of the chromatographic column. The linear velocity can be calculated from equation 3.11, where L is the column length.

$$u_o = \frac{L}{t_m} \qquad \text{eqn. 3.11}$$

On Partisil-10 ODS-3, the phloroglucinol proved to be retained in 52.5 % MeOH which was the eluent for this packing. Therefore, a 10^{-3} M solution of

$Ca(NO_3)_2$ was used as the unretained compound to measure the linear velocity in this solvent system.

3.5.2 Correction for Extra-Column Bandbroadening

The contribution to the centre of gravity and the variance of elution profiles is evaluated using the instrument illustrated in Figure 3.5 with the chromatographic column removed. Broadening of the sample zone can occur due to effects in the injector, detector and connecting tubing [3.6]. The extra-column contributions were evaluated using approximately 10^{-5} M naphthalene in 85 % MeOH and collecting data as described in section 3.5.1. The elution profiles were then analyzed using the ASYST program previously discussed and the averages of the first and second moments were calculated to estimate the extra-column effects. At the four flow rates studied, the contribution was relatively small, as shown in Table 3.3. These corrections have been subtracted in all values of the first and second moments as reported in this thesis, no matter what method was used to calculate the moments.

The same data were used to correct for extra-column effects in 52.5 % MeOH. Some error would be involved in this since the effects are dependent on the diffusion properties of the sample in the mobile phase. 52.5 % MeOH has a higher viscosity and the diffusion coefficient will be less. The extra-column effects would therefore be expected to be lower in this second solvent system. Since the corrections are small in relation the peak profile characteristics, the error associated with the change in solvent is expected to be small.

Table 3.3 Corrections for extra-column bandbroadening at four different flow rates. The extra-column contributions are first moments (retention times) and second moments (variances) that are present due to components of the chromatographic system like the injector, detector and connective tubing. The experimental details can be found in Section 3.5.2. The confidence limits shown are at the 95 % level.

Flow rate (mL/min)	M_1 (s)	M_1 (s^2)
2.0	2.15 ± 0.05	0.349 ± 0.011
1.5	2.56 ± 0.07	0.459 ± 0.023
1.0	3.88 ± 0.10	1.81 ± 0.29
0.5	7.35 ± .07	10.3± 0.8

CHAPTER 4

Results and Discussion

4.1 Introduction

In this chapter, the sorption characteristics of two HPLC packings, the polymeric PRP-1 and the silica-based bonded phase Partisil-10 ODS-3, are measured and discussed. In Section 4.2, the sorption characteristics of PRP-1 are considered, including: the problems involved in characterizing the broadened elution profiles of naphthalene; the measurement of k' by two separate methods; the rate of sorption of naphthalene onto PRP-1; the relationship between the measured sorption rate and elution profiles; and comparison to observed chromatographic elution peaks. A similar series of investigations is discussed in Section 4.3 for the sorption of naphthalene on Partisil-10 ODS-3. Finally, in Section 4.4, the major differences between the sorption characteristics of naphthalene on PRP-1 and on Partisil-10 ODS-3 as found in this investigation are summarized.

4.2 Hamilton PRP-1 as a Sorbent

4.2.1 Characterization of Experimental Elution Profiles On PRP-1

The characterization of elution profiles (ie. elution chromatographic peaks) was discussed in Section 2.3.7. The details of obtaining the data and analyzing it according to two methods were described in Section 3.5.1. The following discussion presents the results of using these two methods of describing elution profiles collected from PRP-1.

4.2.1.1 Numerical Integration

The first method was that of numerical integration using the digitally recorded data and a program written in ASYST. The program uses Simpson's rule [4.1] to numerically integrate a data set between chosen limits. The program performs well for peaks which are relatively noise-free (some smoothing capability is built in). For example, phloroglucinol is the unretained compound and elutes very quickly from the column. Its chromatogram, an example of which is shown in Figure 4.1, is fronting and elutes over a short period of time. The signal to noise ratio of phloroglucinol at the peak maximum is approximately 20 and there was no difficulty in collecting sufficient data to adequately define both the starting and the ending limits of the peak. Consequently, no difficulties were encountered in using the ASYST program to numerically integrate the phloroglucinol peaks. The first moments or centres of gravity for phloroglucinol peaks obtained at four different linear velocities of the mobile phase are shown in Table 4.1. The first moment is used to calculate the linear velocity of the mobile phase using equation 3.11. Good precision is obtained using these values and no other method was used to characterize phloroglucinol peaks.

The numerical integration method proved less successful for characterizing the elution peaks of naphthalene, a compound which is retained on PRP-1. Naphthalene peaks were difficult to characterize for a variety of reasons. Because the compound is highly retained and the resulting peaks are tailed, as shown in Figure 4.2, data had to be collected over a long period of time so that the signal was affected by baseline drift. Data sets were plagued by an uncertainty in the location of the baseline in the tailing portion of the peak because of problems with premature termination of data collection and because of the presence of noise, especially for low concentrations. For the profile shown in Figure 4.2, the signal to noise ratio is 10 at the peak maximum, which is only a factor of 2 below the S/N ratio of the phloroglucinol peak. Nevertheless, there were major difficulties in using the ASYST program, with less than half of the collected profiles leading to successful moment analysis. It was difficult by visual inspection to

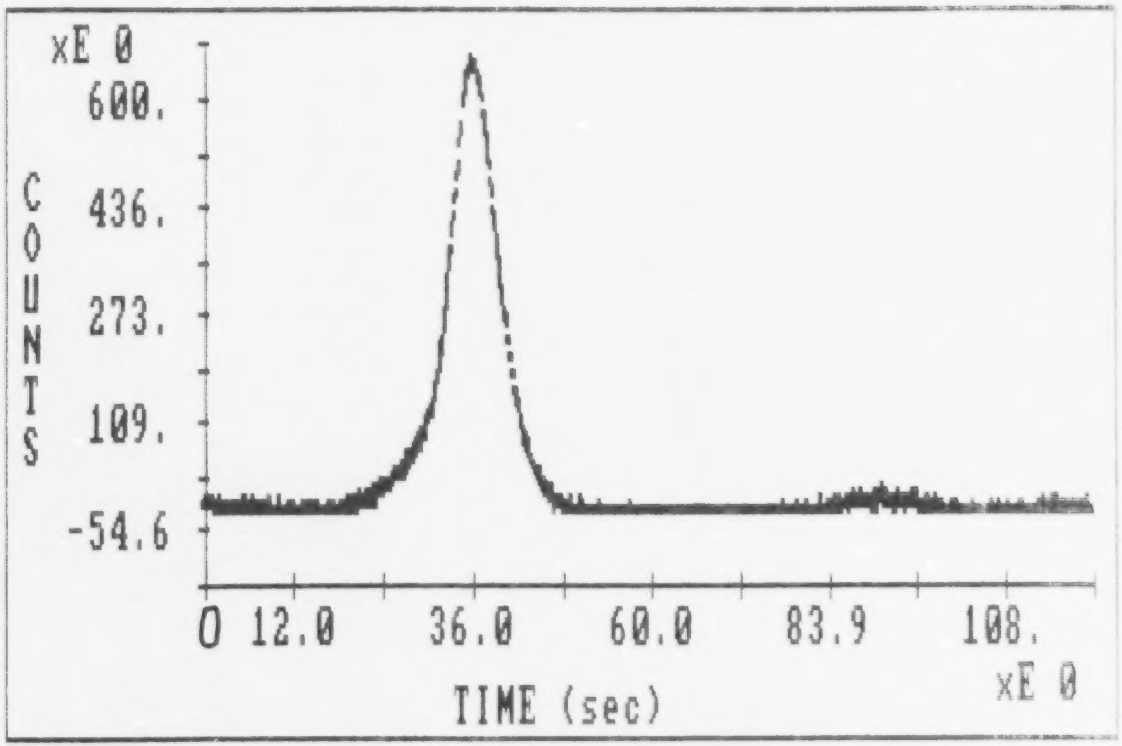

Figure 4.1 Chromatogram of 5.92 ± 0.12 x 10^{-6} M phloroglucinol in 85 % MeOH on PRP-1 with a mobile phase flow rate of 0.5 mL/min. The chromatogram in shown as the unsmoothed output from the data collection program written in ASYST. The zero mark on the time axis corresponds to a time of 2 minutes after injection. The u_o in this case is 0.10 cm/s.

Table 4.1 First moments of phloroglucinol elution profiles on PRP-1 and calculation of linear velocity of the mobile phase, u_o. The sample concentration was 5.92 ± 0.12 x 10^{-5} M in 85% MeOH. Other conditions are described in Section 3.5.1. The confidence limits shown for the first moment values are calculated at the 95 % confidence level. The variable s is the standard deviation in the linear velocity, calculated by propagation of error.

Flow Rate (± 0.1 mL/min)	number of repetitions	M_1(s)	u_o (cm/s)	s (cm/s)
2.0	5	37.32 ± 0.92	0.40	0.03
1.5	4	49.08 ± 0.40	0.30	0.02
1.0	4	74.56 ± 0.86	0.20	0.01
0.5	5	148.2 ± 1.1	0.101	0.006

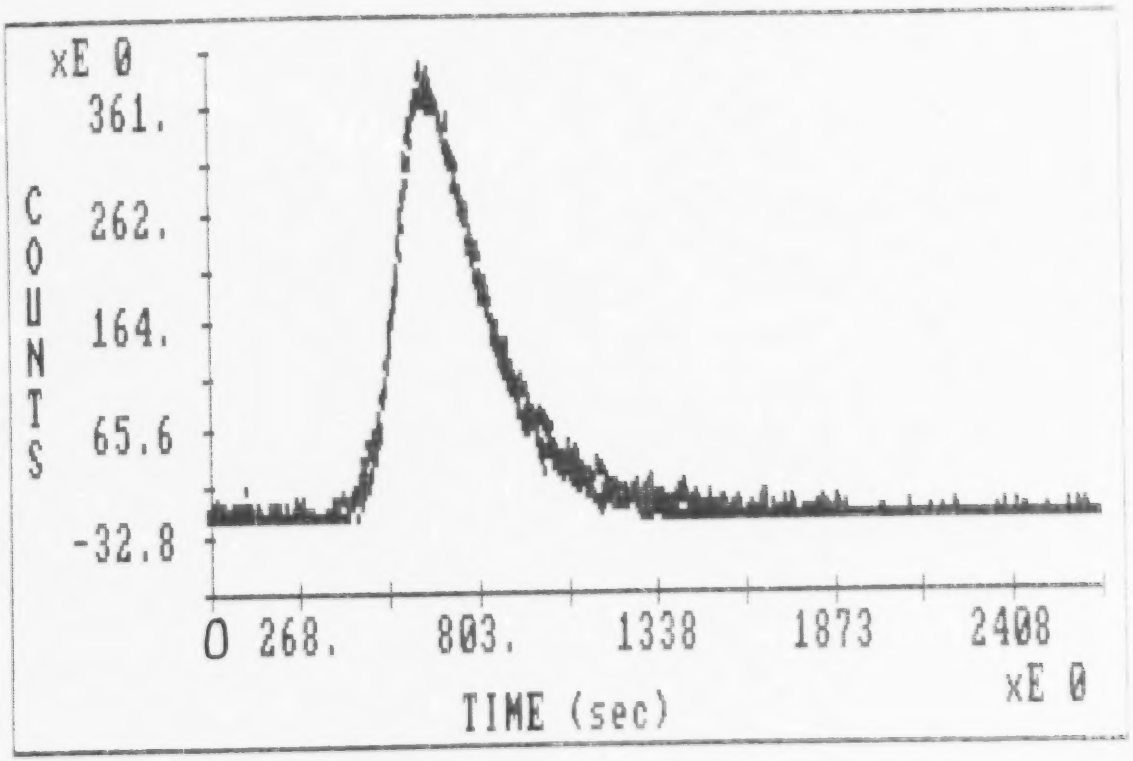

Figure 4.2 Chromatogram of 2.504 ± 0.099 x 10^{-6} M naphthalene in 85 % MeOH on PRP-1 with a mobile phase flow rate of 0.5 mL/min. The chromatogram in shown as the unsmoothed output from the data collection program written in ASYST. The zero mark on the time axis corresponds to the initiation of data collection. This zero is actually 60 minutes after injection. The u_0 in this case is 0.10 cm/s.

predict which data sets could be successfully analyzed. These problems were not unexpected. Numerical integration methods have been shown to be sensitive to noise [4.2 to 4.4], baseline drift [4.2], premature termination of data collection [4.2 to 4.6] and number of data points [4.5]. The higher moments are most sensitive to problems with data in the tailing portion of the peak [4.2]. A more reliable method of peak characterization was sought.

4.2.1.2 Non-linear Least Squares Curve Fitting

The second method described in Section 3.5.1 to characterize chromatograms involved first using a non-linear least squares program to fit the experimental elution profiles to an exponentially-modified Gaussian (EMG) function (equation 2.30). An example of the result of using such an approach is shown in Figure 4.3. The EMG curve gives a good fit for the tailing portion of the peak. The very early data in the rising part of the peak are not very well fit by the EMG function. There are two possible reasons for this. First, the elution peaks may not have a truly Gaussian parent profile. In fact, the phloroglucinol peak in Figure 4.1 shows that fronting profiles may be expected. Alternatively, the reason for the poor fit in the rising part of the peak may lie in the use of the identity given in equation 2.31. Use of an error function in EMG curve fitting has been shown to lead to inaccuracies when $Z \leq -3$ [2.32]. To test this possibility, the Z values were calculated for the subsets of data used for the curve fit. The results of this calculation are shown in Table 4.2. The values of Z_i, early in the peak, are, indeed, less than the prescribed value of -3.

Regardless of its origin, the poor fit in the early portion of the curve is not much of a concern since the peaks are so asymmetrical that the variance is due mainly to the broad tailing portion and the EMG function seems to adequately describe the peaks in this region.

The EMG curve-fitting program was evaluated for sensitivity to various user

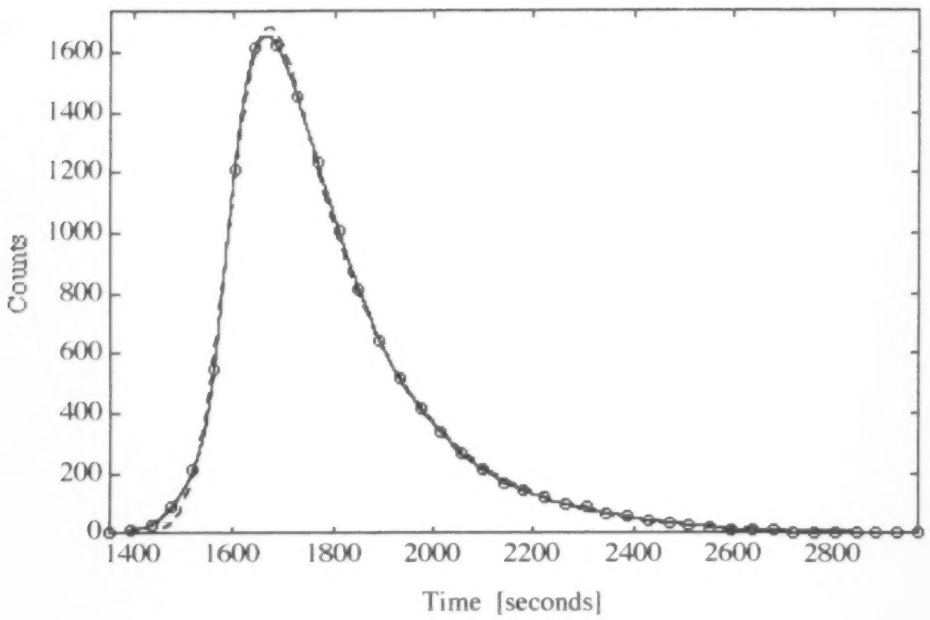

Figure 4.3 Elution profile of 1.002 x 10^{-3} M Naphthalene in 85 % MeOH on PRP-1 at u_o = 0.30 cm/s. The solid line shows the experimental data points. The open circles illustrate the data points chosen by the EXPGAUSS program to fit to an EMG function. The dashed line is the resulting EMG function. The EMG constants for this function are shown in Table 4.5 where the number of data points is 40.

Table 4.2 Calculated Z values at the beginning and end of the subset used for fitting experimental elution profiles of naphthalene in 85 % MeOH on PRP-1. t_i is the time of the first data point included in the subset and Z_i is the value of Z at this time as calculated from equation 2.30 using the EMG constant t_G, σ_G, and τ which are defined in Section 2.3.7. Z_f is the Z value calculated from equation 2.30 at time t_f, the time of the last data point included in the data subset. Results for two concentrations C, of naphthalene are shown. The standard deviation of the concentration is given in brackets following the concentration values. Other information regarding the chromatographic experiment is given in Section 3.5.1.

Run no.	C (x10 $^{-5}$M) (std. dev.)	t_i (±1.05 s)	t_f (±1.05 s)	t_G (s)	σ_G (s)	τ (s)	Z_i	Z_f
1	1.002 (.003)	964.20	2013.15	1157	42.01	143.8	-4.9	20
2	1.002 (.003)	987.83	2050.43	1154	41.92	141.5	-4.3	21
3	1.002 (.003)	988.52	2066.87	1176	43.06	141.2	-4.7	20
1	2.504 (.099)	1051.65	1921.05	1258	57.98	128.7	-4.0	11
2	2.504 (.099)	1077.97	1890.97	1248	52.16	144.5	-3.6	12
3	2.504 (.099)	1088.29	1912.54	1248	50.89	132.5	-3.5	13

input parameters. Two key parameters are of interest. First of all, the raw data collected by the ASYST program described in Section 3.5.1 must somehow be truncated into a data subset. The criteria for choosing points for this subset are examined below. Secondly, the user specifies the number of equally-spaced data points within the subset which the program will use to fit the EMG curve. The sensitivity of the goodness of fit to the number of these data points is also discussed.

The elution data were collected for each peak over a relatively long period of time so some of the data points at the beginning and end of the raw data set lie on the baseline. In transferring the data from the raw set into a subset to be used in the the curve-fitting program, a decision about the initial and final points of the subset had to be made. The fit was shown to be greatly affected if a very large number of data points in the tailing portion of the profile were included in the subset. For instance, Figure 4.4 shows the results of the analysis of the same raw data using two subsets which differ in the times chosen to limit the set. The peak shown is for the elution of naphthalene from PRP-1 at a linear velocity of 0.40 cm/s. Curve A is the EMG curve fit when the 40 data points are chosen from a subset which begins at 987.83 s and ends at 2050.43 s. The curve is well fit except for the beginning of the peak; the portion of the peak of greatest interest in this discussion, the tailing portion, is well-fit. The constants of the fit curve are shown in Table 4.3. Curve B in Figure 4.4 is the result of the EMG curve fit when the 40 data points are chosen by the routine from a subset which begins at 987.83 s and ending at 2363 s. The fit is very poor and the constants in Table 4.3 are radically different from results of the first analysis. The EMG constants were originally defined in Section 2.3.7. The fit is therefore sensitive to employing data points that lie too far out along the baseline on the trailing edge of the peak.

Some criteria must therefore be established for choosing points to include in the subset. If including too many points in the tailing portion results in a poor fit, it is

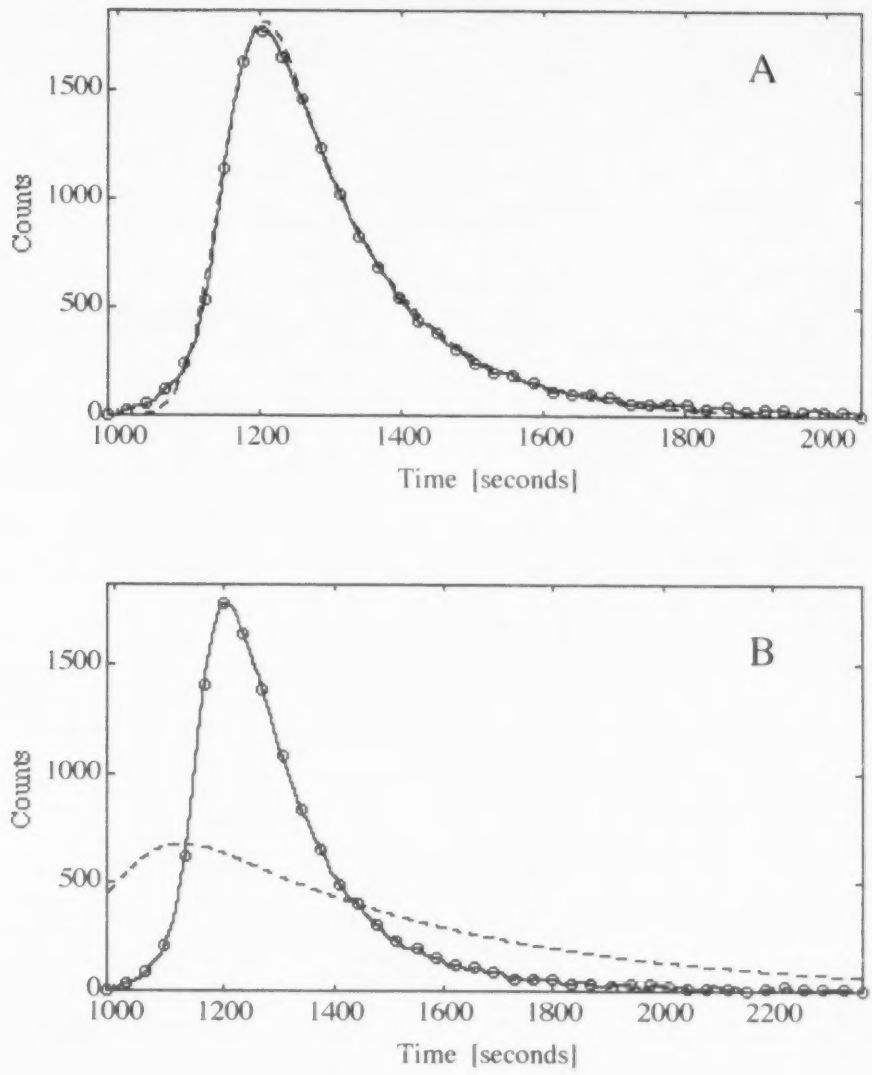

Figure 4.4 EMG fit of an elution profile of 1.002 x 10^{-3} M Naphthalene on PRP-1 at 0.40 cm/s. The solid line represents the experimental profile while the dashed line is the EMG function fit to the chosen data points (o). Figure A and B are the same peak except that fewer data points in the tailing section of the profile are included in the data set in Curve A.

Figure 4.44. Note that although k_2 for the second term is on the same order of magnitude as found on PRP-1, the distributions P2 on the two packings appear to be much different. This is due primarily to the small fraction of sites associated with this term on the ODS. The distributions P1 and P2 are then convolved to get P1/2, the distribution profile of sample that passes through both columns after undergoing at least one sorption-desorption cycle of each type of process. However, because some sample will pass through the column without undergoing the slowest process, the distribution P1 is scaled and added to P1/2 to obtain the final predicted elution profile.

Table 4.22 shows the Φ_2 values for the three replicate experiments at the lowest linear velocity studied, 0.167 cm.s. For Replicates 1 and 3, 7 and 29 % of the sample respectively will not interact with the second column and for Replicate 2 only 0.26 % does not interact with the second column. As the value of Φ_2 decreases, the method of predicting elution profiles will still be valid because of the scaling of the area of the profiles. If Φ_2 is very small, almost all the sample will undergo both sorption processes and, because of the scaling of the profiles P1/2 and P1 before addition, the overall profile will approach that of P1/2. This is illustrated in Figure 4.45 where graph A shows the scaled distribution P1 and P1/2 for Replicate 1 where $\Phi_2 = 0.07$ and graph B shows the same distributions for Replicate 3 where $\Phi_2 = 0.29$. By inspection, it is obvious that the addition of P1 in either of these cases alters the shape of P1/2 very little. Note that as u_o increases, the fraction Φ_2 will also increase because at higher linear velocities, the samples stay in the column for less time and are therefore less likely to be sorbed.

The overall elution profiles calculated from these sorption rate curves show the same basic characteristics as those predict by the sorption on PRP-1 in comparison to actual observed elution peaks. The profile predicted using the constants for Replicate 2 (see Table 4.21) is shown in Figure 4.46 along with the observed elution profile. Once again, the predicted profile is much wider than the observed signal. While the time of

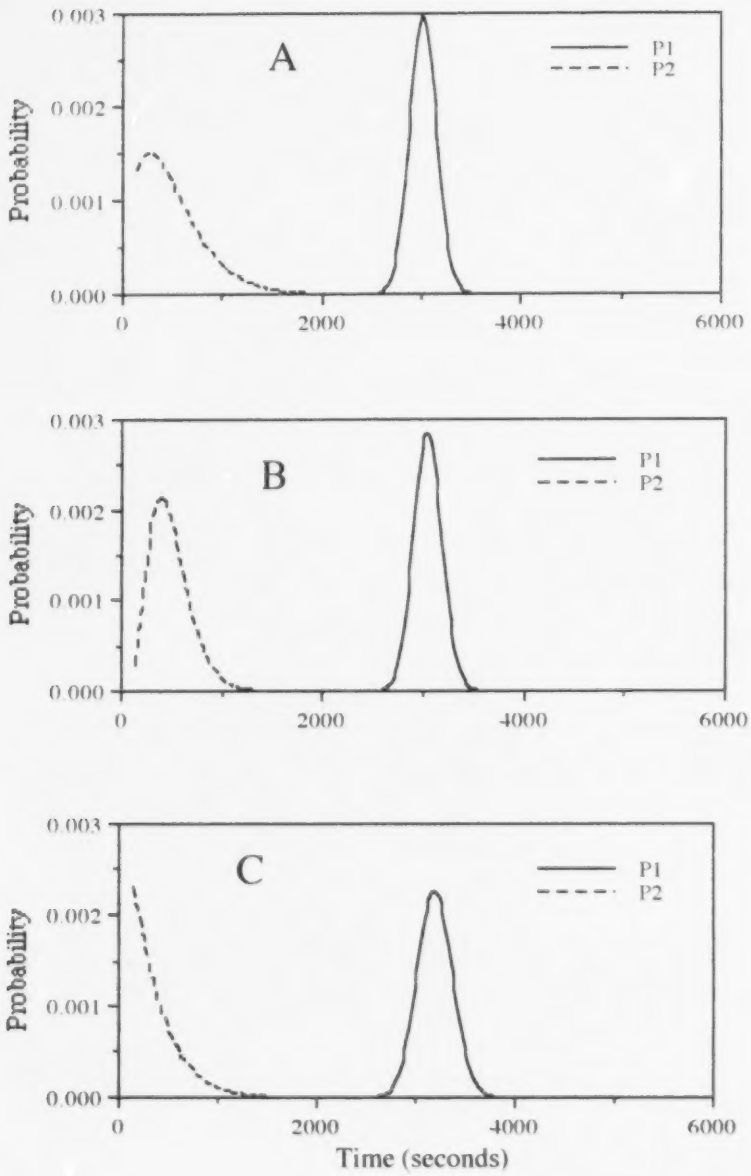

Figure 4.44 The probability distributions P1 and P2 for napthalene on Partisil. Curves A, B and C correspond to the results using the constants for Replicates 1, 2 and 3 from Table 4.21 respectively.

Table 4.22 The fraction Φ_2, which represents the fraction of sample which does not undergo at least one sorption-desorption cycle in the hypothetical column 2 representing the slowest sorption process at $u_o = 0.167$ cm/s. The sorption process discussed here is for naphthalene on Partisil-10 ODS-3. The values of the fraction are significant and the data treatment process is therefore applicable at this lowest linear velocity studied.

Replicate	Φ_2
1	0.0707
2	0.00257
3	0.293

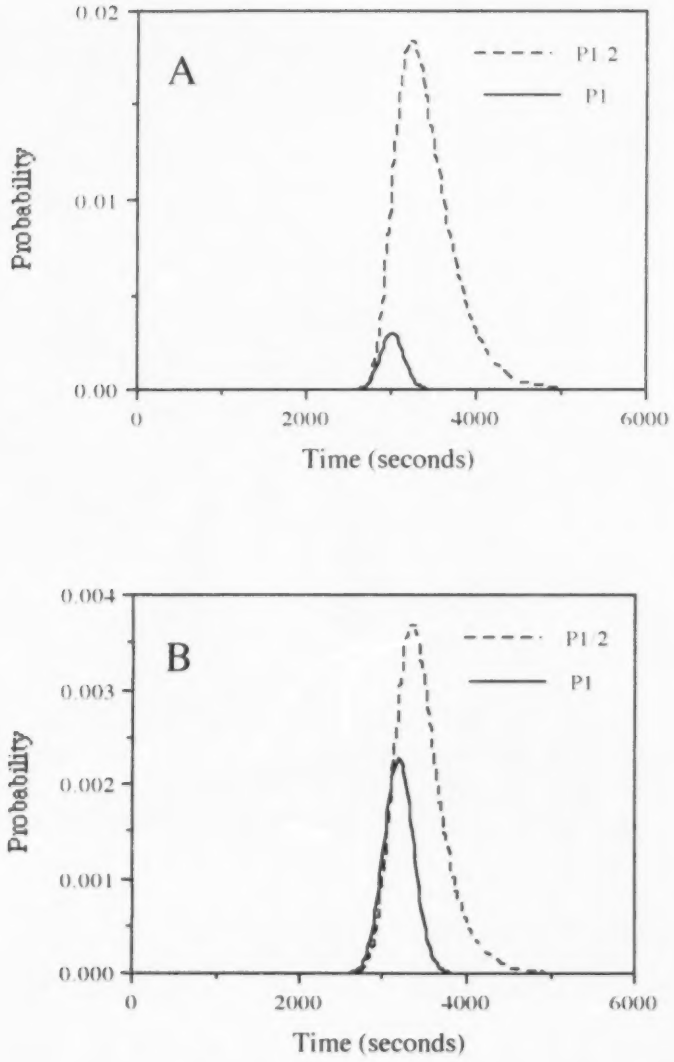

Figure 4.45 The probability distributions P1 and P1/2 for napthalene on Partisil. Curves A and B uses the exponential constants for Replicates 1 and 3 respectively. The non-interacting fraction Φ_2 for Curves A and B are 0.707 and 0.293 respectively.

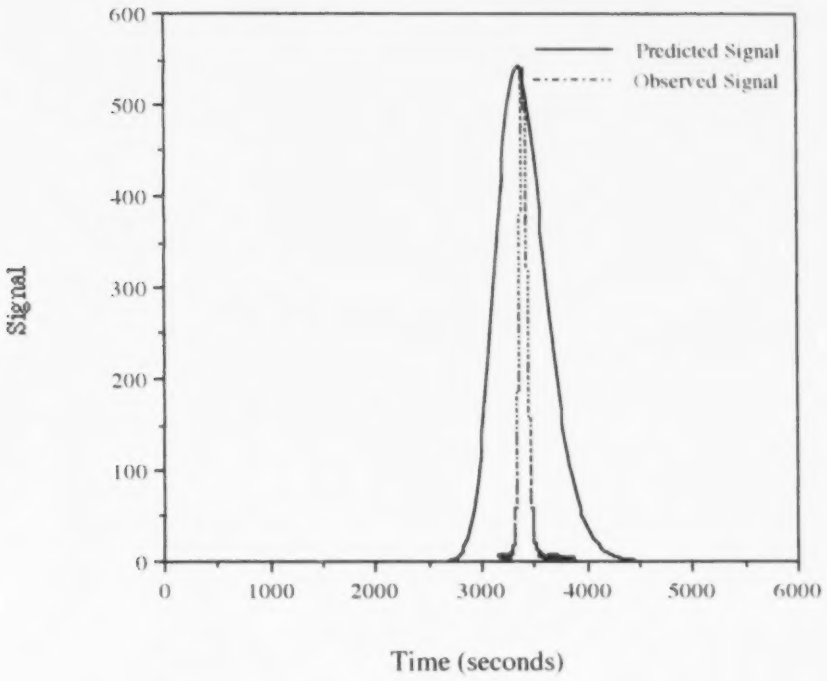

Figure 4.46 The predicted elution profile for naphthalene in 52.5 % MeOH on Partisil-10 ODS-3 at a mobile phase linear velocity of 0.167 cm/s. The profile is predicted using the bi-exponential constants for Replicate 2 as shown in Table 4.21. The observed signal results from the injection of 2.574×10^{-4} M naphthalene under the same elution conditions.

peak maxima are not coincident, they are close although this time is consistently shifted to the left for the predicted profile. It should be recalled that the profile was predicted on the basis of the actual elution conditions, that is, for a 25 cm long column packed with the same stationary phase as was used in the sorption rate experiment) at a linear velocity of 0.167 cm/s.

The three replicate rate curves predict elution profiles having somewhat differing shape. This is illustrated in Figure 4.47, for a mobile phase linear velocity of 0.167 cm/s. The elution profile predicted by Replicate 1 is less symmetrical and more tailed than the other profiles. This may be associated with the relatively small k_2 value combined with the relatively large n_2. The tailing of the profile predicted by Replicate 2 is much less because the value of k_2 here is relatively large. The profile of Replicate 3 is intermediate; although the value of k_2 is relatively small, the fraction of "sites" associated with the slow process (expressed by the fraction n_2/n_0) is much less than for the other two replicates (by about a factor of 2). As a result the influence of the second slower process is less.

The magnitude of these differences can be seen in the EMG characteristics of the predicted profiles. For $u_0 = 0.167$ cm/s, these characteristics are shown individually in Table 4.23. For all u_0 of interest, the averages from the peaks predicted by the three replicates are shown in Table 4.24. In general, the characteristics describing the character of the parent Gaussian peak are fairly reproducible, with the centre of gravity having less than 4 % RSD at all three flow rates. Less reproducible is the tailing characteristic, τ, which has a RSD greater than 25 %. This leads to a large uncertainty in the M_2 values which depend on the square of τ. It is not surprising that the tailing portion of the peak is associated with the most uncertainty, considering that it is determined mostly by the slowest rate constant and also the relatively large error in that quantity as calculated by the non-linear least squares fit program.

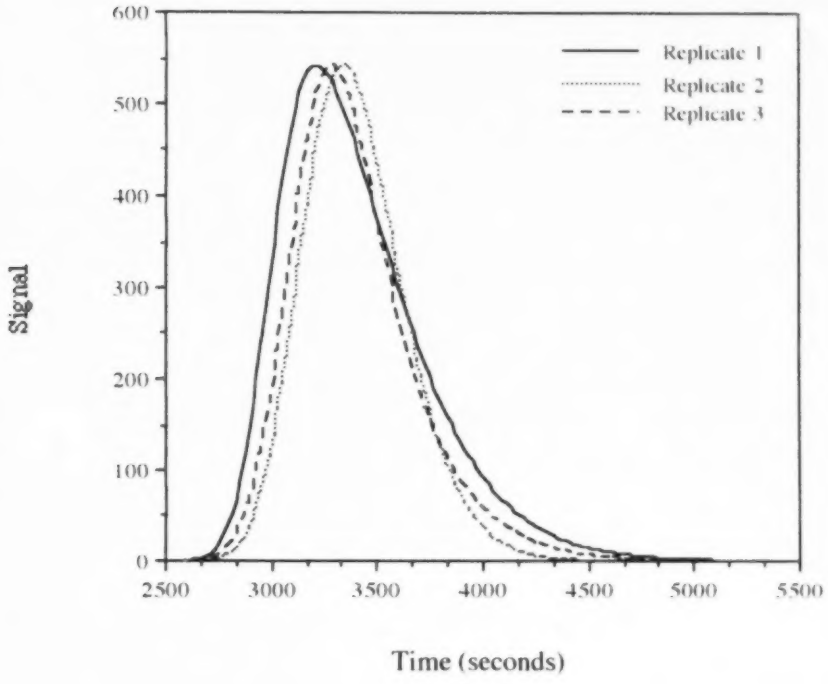

Figure 4.47 The elution profiles predicted by the three replicate bi-exponential sorption rate curves for naphthalene on Partisil-10 ODS -3 in 52.5 % MeOH. The individual sets of constants are shown in Table 4.21. The profiles are predicted for a mobile phase linear velocity of 0.167 cm/s in a 25 cm long column. The EMG characteristics of these three profiles are shown in Table 4.23. This plot illustrates the difference in the shape of the overall profiles.

Table 4.23 EMG characteristics of the elution profiles predicted by the three replicate bi-exponential sorption rate curves for naphthalene on Partisil-10 ODS-3 in 52.5 % MeOH for a mobile phase linear velocity of 0.167 cm.s. The elution profiles are modelled on a column which is 25 cm long containing a stationary phase identical to that used in the shallow bed experiment. Also shown are the observed values for a real elution profile acquired by the injection of 2.574×10^{-4} M naphthalene. See Table 4.24 for error estimates. The data in this table can be compared to data in Table 4.18 which shows the EMG characteristics of real elution profiles of naphthalene on Partisil-10 ODS-3.

Replicate	1	2	3	Observed
t_G (s)	3052	3223	3141	3270
σ_G (s)	168.2	185	165.8	29.25
τ (s)	373.1	184.5	262.9	16.52
M_1 (s)	3425	3408	3404	3286
M_2 ($\times 10^4$ s^2)	16.75	6.826	9.661	0.1128

4.3.6 Comparison of the Predicted and Observe Elution Profiles of Naphthalene on Partisil-10 ODS-3

Tables 4.19 and 4.24 show the EMG characteristics of the observed and predicted elution profiles of naphthalene on Partisil-10 ODS-3, respectively. The only parameters which are comparable are the centres of gravity which are fairly close. The parameters which are associated with the width of the main part of the peak, namely σ_G and with the asymmetry and tailing, namely, τ, are much larger for the predicted profiles at all flow rates. Once again, the sources of error which include the possibility of not meeting shallow bed conditions, inability to measure the fastest sorption rates and the possible overestimation of the effect of slow sorption-desorption kinetics on elution profiles using the proposed model, are consistent with the large width characteristics for predicted profiles.

4.4 Summary

The work presented here has demonstrated that PRP-1 and Partisil-10 ODS-3 differ as sorbents in at least two major areas. First, the efficiency of PRP-1, as demonstrated by the elution of naphthalene, is much lower than the efficiency of the silica-based packing. Secondly, the sorption rate of naphthalene on the polymeric phase was much slower than the rate on ODS, as measured by the shallow bed method. Specifically, the ODS packing reaches equilibrium with a naphthalene solution fairly quickly, at measured times of about 10 seconds whereas PRP-1 approaches equilibrium asymptotically after 60 seconds. In the absence of other differences in these packings and using information from the model use here to predict the shape of elution profiles on the two packings, the difference in efficiency in the two packings is due primarily to the difference in rate of sorption. In other words, the slow sorption (which includes

Table 4.24 Average EMG characteristics of elution profiles predicted by the three replicate bi-exponential sorption rate curves for naphthalene on Partisil-10 ODS-3 in 52.5 % MeOH. The characteristics are shown for three different mobile phase linear velocities, u_0, which is shown ± one standard deviation. The information in this table can be compared to that found in Table 4.19 which shows the analogous quantities for real elution profiles of naphthalene on Partisil-10 ODS-3.

u_0 (cm/s) ± s	0.167 ± 0.009	0.27 ± 0.01	0.35 ± 0.01
t_G (s)	3155	1864	1451
RSD t_G (%)	2.9	3.25	3.27
σ_G (s)	173	116.74	98.09
RSD σ_G (%)	6.0	15.3	17.4
τ (s)	274	211	180
RSD τ (%)	34.6	31.3	26.6
M_1 (s)	3412.2	2074.9	1634.7
RSD M_1 (%)	0.33	0.42	0.41
M_2 (x 10^5 s^2)	1.1079	0.61209	0.43891
RSD M_2 (%)	46.1	42.3	35.2

adsorption and diffusion through the pores of the polymeric packing) is the primary cause of the broadened and tailed elution profiles observed when naphthalene is eluted off PRP-1. At this point, however, it is not possible to use the sorption rate information as measured to accurately predict the shape of the elution profile. It is unclear whether this is the result of inaccurate sorption rate determinations (due to failure to meet shallow bed conditions and to the inability to measure sorption at very short exposure times) or whether this is the result of failure of the model. This question and a possible approach to its solution are addressed in Chapter 5.

CHAPTER 5

Conclusions and Future Work

The work presented in this thesis concentrated on three major areas including: (1) the characterization of elution peaks; (2) the development of the shallow bed apparatus an its use to measure sorption rates on HPLC stationary phases; and (3) the use of a model based on probability theory to predict elution profiles based on sorption rate data acquired in the shallow bed experiment. The conclusions and future work associated with these areas are discussed below.

First, experimental HPLC peaks which were broadened and severely tailed, such as those of naphthalene on PRP-1, were shown to be well fit by an EMG function, despite problems with baseline errors such as noise. The EMG characteristics of peaks can be used to characterize the efficiency of an HPLC column. One improvement to the data processing as described in this thesis would be the development of a data collection system for the Macintosh, where the EMG curve fit program is used. The current system requires transfer of data between an IBM clone to a Macintosh, which is tedious and prone to errors in translation.

The major undertaking of the research was the design and development of the shallow bed apparatus. This apparatus has been shown to give reproducible sorption rate data for reasonably fast reactions,which occur in the time range of approximately 0.4 to 60 s. The measured sorption rate curves were shown to be well fit to multi-exponential equations. The accuracy of the method is currently limited by the failure to meet shallow bed conditions with the apparatus. This systematic error in the experiment has the greatest effect on the steeply rising portion of the sorption rate curve. A possible solution to this problem is the use of solvent systems of lower viscosity or a solution delivery system capable of higher pressure. Both of these

measures would result in a higher linear velocity through the shallow bed. The weight of packing could also be reduced as long as a radially uniform bed is formed within the slider.

A second major source of error is the limited ability of the apparatus to measure sorption at very short exposure times. The smallest exposure time, limited by the lever system which moves the slider containing the shallow bed is about 0.4 s. Sorption reactions that are complete or near-complete before this time are inaccessible. For the sorption rate curves studied here, if one of the processes is fast, the steeply rising portion of the curve will be poorly defined, resulting in erroneous rate constants in this region. A modification of the lever system might make shorter exposure times possible.

One obvious avenue open for investigation is the link between diffusion characteristics of solute molecules and their rates of sorption on polymeric packings as measured by this experiment. The slow sorption of naphthalene on PRP-1 is suspected to be a result of slow diffusion within the micropores of the polymer. If the sorption rate of a sample which is large enough to be excluded from the micropores were found to be larger than that of naphthalene, this could be taken as evidence to support this concept. The study of sorption rates of compounds which have much larger and much smaller diffusion coefficients than naphthalene could be undertaken. Also of interest is the correlation of the measured sorption rates to observed efficiencies. Polyaromatic species are observed to give especially poor efficiencies on PRP-1. Sorption rate measurements for molecules with similar diffusion characteristics to those of naphthalene but which are not polyaromatic are therefore appropriate.

The shallow bed apparatus could also be used to measure sorption rates for materials on other types of packings. The sorption rates associated with ion-exchange or affinity chromatography might be investigated by this method, assuming that the rates are in the range accessible by the shallow bed technique.

The third major area of investigation was the development of a model which uses the results of the shallow bed experiments to predict elution profiles. The model was successfully applied only qualitatively or semi-quantitatively. However, by using only one of the three sorption terms measured, the main portion of the elution profile of naphthalene on PRP-1 was successfully modelled. Poor accuracy of sorption measurements at short-exposure times means that the first term in the tri-exponential is probably underestimated. Poor precision in the curve fit at long exposure times leads to large uncertainties in the constants describing the slowest process. Improvements in the shallow bed experiment that were suggested above, which may result in meeting shallow bed conditions, may also improve prove the quantitative accuracy of the model. Another possibility in testing the model is increasing the accuracy of the shallow bed experiment by studying slower sorption processes. If sorption is a diffusion-limited process, the rate can be decrease by increasing the particle diameter, effectively increasing the diffusion distance. This work is currently underway in this laboratory.

The application of sorption rate data to HPLC columns using the Giddings type model also appears to be limited because of the apparent difference in availability of the slowest "sites", depending on the column history. In columns that are "primed", that is, where sample has been injected and is occupying the "sites" associated with the slowest kinetic process, the fraction of sites available in subsequent injections is probably not the same fraction as measured by the sorption rate experiment. For the most part, except where elution occurs off of an "unprimed"column, the effect on the chromatogram of the slowest sorption process measured in the sorption rate may be small.

BIBLIOGRAPHY

1.1 L.C. Sander and S.A. Wise, "Recent Advances in Bonded Phases for Liquid Chromatography", CRC Critical Reviews in Analytical Chemistry, 18, 299-415 (1987).

1.2 M.P. Rigney, E.F. Funkenbusch and P.W. Carr, "Physical and Chemical Characterization of Microporous Zirconia", J. Chromatogr. , 499, 291-304 (1990).

1.3 U. Bien-Vogelsang et.al., "Synthesis of Stationary Phases for Reversed-Phase LC Using Silanization and Polymer Coating", Chromatogr. 19, 170-179 (1984).

1.4 R. M. Chicz, Z. Shi and F.E. Regnier, "Preparation and Evaluation of Inorganic Anion-Exchange Sorbents Not Based on Silica", J. Chromatogr. , 359, 121-131 (1986).

1.5 M.P. Rigney, T.P. Weber and P.W.Carr, "Preparation and Evaluation of Zirconia Reversed-phase Chromatographic Support", J. Chromatogr. , 484, 273-291 (1989).

1.6 B. Gawdzik, J. Gawdzik and U. Czerwinska-Bil, "Copolymer of Di(Methylacryloxymethyl) Naphthalene and Divinylbenzene as a Column Packing for High-Performance Liquid Chromatography", Chromatogr., 26, 399-407 (1990).

1.7 R. M. Smith et.al., "Determination of Trace Levels of Ethylenethiourea by HPLC Following Derivatisation with Phenacyl Halides", Chromatogr., 19, 411-414 (1984).

1.8 D.J. Pietrzyk, "Organic Polymeric Stationary Phases", Chem. Anal. (N.Y.), 98, 223-276 (1989).

1.9 K. Wolfs et.al., "Separation of Tetracycline and Related Substances by High-Performance Liquid Chromatography on Poly(Styrene-Divinylbenzene)", J. Chromatogr., 358, 444-447 (1986).

1.10 H.J.E.M. Reeuwijk, "High-Performance Liquid Chromatography of Tetracyclines", J. Chromatogr., 353, 339-350 (1986).

1.11 W.A. Moats, "Effect of the Silica Support of Bonded Reversed-Phase Columns on Chromatography of Some Antibiotic Compounds", J. Chromatogr., 366, 69-78 (1986).

1.12 K.A. Tweeten and T.N. Tweeten, "Reversed-Phase Chromatography of Proteins on Resin-Based Wide Pore Packings", J. Chromatogr., 359, 111-117 (1986).

1.13 I.O. Kibwage et.al., "Separation of Erythromycin and related substances by High-Performance Liquid Chromatography", J. Chromatogr., 330, 275-286 (1985).

1.14 S.E.Tett, D.J. Cutler and K.F. Brown, "High-Performance Liquid Chromatographic Assay for Hydroxychlorquine and Metabolites in Blood and Plasma using a Stationary Phase of Poly(Styrene-Divinylbenzene) and a Mobile Phase at pH 11, with Fluorometric Detection", J. Chromatogr., 344, 241-248 (1985).

1.15 R.M. Cassidy and S. Elchuk, "Dynamically Coated Columns for the Separation of Metal Ions and Anions by Ion Chromatography", Anal. Chem., 54, 1558-1563 (1982).

1.16 J.W. O'Laughlin, "Separation of Cationic Metal Chelates of 1,10 - Phenanthroline by Liquid Chromatography", Anal. Chem., 54, 178-181 (1982).

1.17 R.L. Smith and D.J. Pietrzyk, "Retention of Inorganic and Organic Cations on a Poly(styrene-divinylbenzene) Adsorbent in the Presence of Alkylsulfonate Salts", Anal. Chem., 56, 1572-1577 (1984).

1.18 M. Dreux and M. Lafosse, "Measurement of Sub Parts-per Million of Inorganic Anions in Water by Nonsuppressed Ion Exchange Chromatography with Conventional HPLC Instrumentation", J. High Resolut. Chrom., 9, 122-??? (1986).

1.19 P.G. Rigas and D.J. Pietrzyk, "Liquid Chromatographic Separation and Indirect Detection of Inorganic Anions Using Iron(II) 1,10- Phenanthroline as a Mobile Phase Additive", Anal. Chem., 58, 2226-2233 (1986).

1.20 S.Coppi and A. Betti, "Liquid Chromatographic Separation and Behaviour of some Triazines on Styrene-divinylbenzene Columns", J. Chromatogr., 472, 406-410 (1989).

1.21 J.R. Benson and D.J. Woo, "Polymeric Columns in Liquid Chromatography", J. Chromatogr. Sci., 22, 386-399 (1990).

1.22 D.P. Lee, "Reversed-Phase HPLC from pH 1 to 13", J. Chromatogr. Sci., 20, 203-208 (1982).

1.23 R.M. Smith and D.R. Garside, "Effect of Organic Modifier on the Separation and Efficiencies of Homologues on Porous Columns", J. Chromatogr., 407, 19-35 (1987).

1.24 F. Nevejans and M. Verzele, "On the Structure and Chromatographic Behaviour of Poystyrene Phases", J. Chromatogr., 406, 325-342 (1987).

1.25 C. Grobe-Rhode, H.G. Kicinski and A. Kettrup, "Modified Polystyrene, Stationary Phases for the Separation of Different Aromatic Hydrocarbon Types by HPLC", Chromatogr., 26, 209-214 (1990).

1.26 Y.B. Yang and M. Verzele, "New Water-Compatible Modified Polystyrene as a Stationary Phase for High-Performance Liquid Chromatography; Characterization and Application", J. Chromatogr., 387, 197-205 (1987).

1.27 D.P. Lee, "Chromatographic Evaluation of Large-Pore and Non-Porous

Poymeric Reversed Phases", J. Chromatogr., 443, 143-153 (1988).

1.28 F. Nevejans and M. Verzele, "Porous Polystyrene Packings: Characterization Through Pore Structure Determination", Chromatogr., 20, 173-178 (1985).

1.29 L.D. Bowers and S.Pedigo, "Solvent Strength on Polystyrene-Divinylbenzene Columns", J. Chromatogr., 371, 243-251 (1986).

2.1 J.C. Giddings, Dynamics of Chromatography, Marcel Dekker, New York, 1965.

2.2 C. Horvath and H.-J. Lin, "Band Spreading in Liquid Chromatography", J. Chromatogr., 149, 43-70 (1978).

2.3 J.-C. Chen and S.G. Weber, "Theoretical and Experimental Determination of Band Broadening in Liquid Chromatography", Anal. Chem. 55, 127-134, (1983).

2.4 J.C. Giddings, Dynamics of Chromatography, Marcel Dekker, New York, 1965, pps. 35, 36.

2.5 J.H. Knox and L. McLaren, "A New Gas Chromatographic Method for Measuring Gaseous Diffusion Coefficients and Obstructive Factors", Anal. Chem., 36, 1477-1482, (1964).

2.6 T. Dubetz, Ph.D. Thesis, "Study of the Origin of Excessive Bandbroadening on PRP-1", University of Alberta, Edmonton, Canada, 1988, pps. 54-59.

2.7 J.C. Giddings, Dynamics of Chromatography, Marcel Dekker, New York, 1965, pps. 49-52.

2.8 R.M. Miller, Separation Methods in Chemical Analysis, Wiley-Interscience, Toronto, 1975, pg. 123.

2.9 R. Endele, I. Halasz and K. Unger, "Influence of d_p on Column Efficiencies", J. Chromatogr., 99, 377-393 (1974).

2.10 J.C. Giddings, Dynamics of Chromatography, Marcel Dekker, New York, 1965, pps. 40-47.

2.11 R.P.W. Scott, "Contemporary Liquid Chromatography" in Techniques in Chemistry, Vol. XI, Wiley-Interscience, Toronto, !976, Chapter 2.

2.12 J.C. Giddings, Dynamics of Chromatography, Marcel Dekker, New York, 1965, pps. 52-61.

2.13 J.C. Giddings, " Isolation of Peak Broadening Factors in Exclusion Chromatography", Macromolecules, 10, 443-448 (1977).

2.14 D.J. Anderson and R.R. Walters, "Equilibrium and Rate Constants of Immobilized Concanavalin A Determined By High-Performance Affinity Chromatography", J. Chromatogr., 376, 69-85 (1986).

2.15 J.C. Giddings, Dynamics of Chromatography, Marcel Dekker, New York,

1965, pps. 36-39.

2.16 S.J. Hawkes, "Mass Transfer Terms in Porous Layers and Particles", J. Chromatogr., 68, 1-8 (1972).

2.17 E. Grushka, L.R. Snyder and J.H.Knox, "Advances in Band Spreading Theories", J. Chromatogr. Sci., 13, 25-36 (1975).

2.18 Rohm and Haas, personal communication.

2.19 T. Dubetz, Ph.D. Thesis, "Study of the Origin of Excessive Bandbroadening on PRP-1", University of Alberta, Edmonton, Canada, 1988.

2.20 F.G. Helfferich in Mass Transfer and Ion Exchange, L. Liberti and F.G. Helfferich, eds., Martinus Nijhoff Publishers, Boston, 1983, Chapter 5.

2.21 O. Grubner in Advances in Chromatography, Vol. 6, J.C. Giddings and R.A. Keller, eds., Dekker, NY, 1968, Chapter 4.

2.22 D.B. Marshall, J.W. Burns and D.E. Connolly, "Direct Measurement of Liquid Chromatographic Sorption-Desorption Kinetics and the Kinetic Contribution to Band Broadening," J. Chromatogr., 360, 13-25 (1986).

2.23 G.E. Boyd, A.W. Adamson and L.S.Myers, Jr., "The Exchange Adsorption of Ions from Aqueous Solutions by Organic Zeolites. II. Kinetics", J. Amer. Chem. Soc., 69, 2836-2848 (1947).

2.24 P.A. Riveros and W.C. Cooper, "Kinetic Aspects of the Ion Exchange Extraction of Gold, Silver, And Base Metal Cyano Complexes", Solvent Extraction and Ion Exchange, 6, 479-503 (1988).

2.25 G.M. Harris, Chemical Kinetics, D.C. Heath, Boston, 1966, pps 68-70.

2.26 J.R. Conder and C.L. Young, Physicochemical Measurement by Gas Chromatography, John Wiley and Sons, Toronto, 1976, p. 354.

2.27 C.H. Lochmuller et.al., "Bound Pyrene Excimer Photophysics and the Organization and Distribution of Reaction Sites on Silica", J. Amer. Chem. Soc., 106, 4077-4082 (1984).

2.28 D.B. Marshall, "Statistical Considerations in the Analysis of Dispersive Kinetics Data as Discrete or Continuous Distributions of Rate Constants", Anal. Chem., 61, 660-665 (1989).

2.29 J.C. Giddings, " Kinetic Origin of Tailing in Chromatography", Anal. Chem., 35, 1999-2002 (1963).

2.30 B.A. Bidlingmeyer and F.V. Warren, Jr., "Column Efficiency Measurements", Anal. Chem., 56, 1581A-1596A (1984)

2.31 D.J. Anderson and R.R. Walters, " Effect of Baseline Errors on the Calculation of Statistical Moments of Tailed Chromatographic Peaks", J. Chromatogr. Sci., 22, 353-359 (1984).

2.32 J.P. Foley and J.G. Dorsey, "A Review of the Exponentially Modified Gaussian (EMG) Function : Evaluation and Subsequent Calculation of Universal Data", J. Chromatogr. Sci., 22, 40-46 (1984).

2.33 S.N. Chesler and S.P. Cram, "Iterative Curve Fitting of Chromatographic Peaks", Anal. Chem., 45, 1354-1359 (1973).

3.1 S. May, R.A. Hux, and F.F. Cantwell, "Measurement of Sorption Isotherms by On-Stream Precolumn Equilibration Liquid Chromatography", Anal. Chem., 54, 1279-1282 (1980).

3.2 B.L. Karger, L.R. Snyder and C. Horvath, An Introduction to Separation Science, Interscience, New York, 1973, Chapter 3.

3.3 J.C. Giddings, Dynamics of Chromatography, Marcel Dekker, New York, 1965.

3.4 L.C. Sander, C. J. Glinka and S.A. Wise, "Recent Advances in the Characterization of Bonded Phases", National Bureau of Standards publication.

3.5 C.A. Lucy, Ph.D. Thesis, "Solvent Extraction - Flow Injection Analysis: Application and Speed of Analysis", University of Alberta, Edmonton, Alberta, Canada, 1988.

3.6 J.R. Conder and C.L. Young, Physicochemical Measurement by Gas Chromatography, Wiley, Toronto, 1979, pps. 57-62.

4.1 J. Marsden and A. Weinstein, Calculus: Single Variable, Benjamin/Cummings, Don Mills, Ont, 1981, pg. 531.

4.2 E. Grushka et.al., "Computer Characterization of Chromatographic Peaks by Plate Height and Higher Central Moments, Anal. Chem., 41, 889-892 (1969).

4.3 T. Petitclerc and G.Guichon, "Determination of Higher Moments of a Non-Symmetrical Chromatographic Signal" J. Chromatogr. Sci., 14, 531-535 (1976).

4.4 S.N. Chesler and S.P. Cram, "Effect of Peak Sensing and Random Noise on the Precision and Accuracy of Statistical Moment Analysis from Digital Chromatographic Data", Anal. Chem., 43, 1922-1933 (1971).

4.5 J.J Kirkland et.al., "Sampling and Extra-Column Effects on High-Performance Liquid Chromatography; Influence of Peak Skew on Plate Count Calculations", J. Chromatogr. Sci., 15, 303-316 (1977).

4.6 P.R. Rony and J.E. Funk, "Retention Time and the First Time Moment in Elution Chromatography", J. Chromatogr. Sci., 9, 215-219 (1971).

4.7 C. Vidal-Madjar and G. Guichon, "Experimental Characterization of Elution Profiles in Gas Chromatography Using Statistical Moments, " J. Chromatogr., 142, 61-86 (1977).

4.8 J.J. van Deemter, F.J. Zuiderweg and A. Klinkenberg, " Longitudinal Diffusion and Resistance to Mass Transfer as Causes of Non-ideality in

Chromatography". Chem. Eng. Sci., 5 271-289 (1956).

4.9 E. Katz, K. Logan and R.P.W. Scott, "Liquid Chromatographic Column Design", J. Chromatogr., 289, 65-83 (1984).

4.10 E. Katz, K. Logan and R.P.W. Scott, "Peak Dispersion and Mobile Phase Velocity in LC", J. Chromatogr., 270, 51-75 (1983).

4.11 J.C. Giddings and H. Eyring, "A Molecular Dynamic Theory of Chromatography", J. Chem. Phys., 59, 416-421 (1955).

4.12 D.M. Ottenstein, "Chromatographic Support in Gas Chromatography", J. Chromatogr. Sci., 11, 136-144 (1973).

4.13 L.R. Snyder and J.J. Kirkland, Introduction to Modern Liquid Chromatography, Wiley-Interscience, Toronto, 1979, pg. 838.

4.14 L.R. Snyder "A Rapid Approach to Selecting the Best Experimental Conditions for High-Speed Column Chromatography", J. Chromatogr. Sci., 15, 441-449 (1971).

4.15 J.G. Graselli and W.M. Ritchey, editors, Atlas of Spectral Data and Physical Constants for Organic Compounds, 2nd edition, CRC Press, Boca Raton, FA., 1975.

APPENDIX 1

Calculation of Contributions to the Total Plate Height from Individual Rate Processes

The contributions to the plate height that have been calculated for an HPLC column containing 10 μm spherical, porous particles are shown in the following discussion.

The diffusion coefficient was calculated from the Wilke-Chang equation [4.14] for naphthalene which was assumed to have a molar volume of 125 mL/mol. D_m is assumed to have a value of 1.0×10^{-5} cm^2/s. The mobile phase is considered to be 85 % MeOH. Section 4.6.3.3 describes the calculation for the diffusion coefficient of this sample molecule under these circumstances. The k' of the molecule is assumed to be 35 under these conditions. The linear velocity of the mobile phase, u_o is 0.4 cm/s.

1. Plate Height Contribution due to Longitudinal Diffusion

Using equation 2.2 and using an obstruction factor, γ, of 0.6 [2.5], H_{LD} is calculated be

$$H_{LD} = \frac{2\gamma D_m}{u_o} = \frac{2\,(0.6)\ 10^{-5}\ cm^2/s}{0.4\ cm/s} = 3 \times 10^{-5}\ cm$$

2. Plate Height Contribution due to Eddy Diffusion

Using equation 2.3 and a column packing factor of 2.5 [2.9], H_{eddy} is calculated to be

$$H_{eddy} = 2\lambda d_p = 2(2.5)(0.001\ cm) = 0.005\ cm$$

The packing factor was determined experimentally by Endele et.al. using spherical silica particles in the range of 5 to 35 μm. The value of the packing factor is calculated from a plot of plate height vs linear velocity at relatively high linear velocity. Equation 2.11 reduces to a linear function with an intercept equal to $2\lambda d_p$. This is an estimate, as the packing factor is expected to depend on the quality of packing as well

as the particle diameter.

3. Plate Height Contribution due to Resistance to Mass Transfer in the Mobile Phase

Using equation 2.4 and a packing factor of 1.3 [2.8], H_m is calculated to be

$$H_m = \frac{\omega d_p^2 u_o}{D_m} = \frac{1.3(0.001\text{cm})^2(0.4\text{ cm/s})}{10^{-5}\text{cm}^2/\text{s}} = 0.052\text{ cm}$$

This term is fairly large due to the small diffusion coefficient for the sample in the liquid mobile phase.

4. Plate Height Contribution due to Coupled Term

Using equation 2.5 and results shown above, H_{couple} is calculated to be

$$H_{couple} = \left[\frac{1}{H_{eddy}} + \frac{1}{H_m} \right]^{-1}$$

$$H_{couple} = \left[\frac{1}{0.005\text{ cm}} + \frac{1}{0.052\text{ cm}} \right]^{-1} = 0.0046\text{ cm}$$

5. Plate Height Contribution due to Resistance to Mass Transfer in the Stagnant Mobile Phase

In order to use equation 2.7, the fraction of mobile phase locate in the pores, f, must be calculated. This is given by the ratio of the pore volume of the column to the total pore and intraparticle volume. For PRP-1, the specific pore volume and the total specific volume are given by the manufacturer.

$$f = \frac{\text{pore vol.}}{\text{pore vol. + interparticle vol.}} = \frac{0.79\text{ mL/g}}{1.53\text{ mL/g}} = 0.52$$

The fct(f,k') can then be calculated using equation 2.8

$$fct(f,k') = \frac{(1 - f + k')^2}{30(1 - f)(1 + k')^2} = \frac{(1 - 0.52 + 35)^2}{30(1 - 0.52)(1 + 35)^2} = 0.067$$

This result can be used in equation 2.7 assuming γ' is 1.

$$H_{sm} = \frac{fct\,(f, k')\, d_p^2\, u_o}{\gamma' D_m}$$

$$= \frac{(0.067)\,(0.001\text{ cm})^2(0.4\text{ cm/s})}{1(10^{-5}\text{ cm}^2/\text{s})} = .0027\text{ cm}$$

6. Plate Height Contribution due to Resistance to Mass Transfer in the Stationary Phase

Equation 2.7 was used to calculate this contribution, assuming that the desorption rate constant was the inverse relaxation time found by Marshall et.al. to be on the order of 500 s^{-1} [2.22].

$$H_s = 2\,\frac{k'}{(1 + k')^2}\,\frac{u_o}{k_d}$$

$$= 2\,\frac{35}{(1 + 35)^2}\,\frac{(0.4\text{ cm/s})}{500\text{ s}^{-1}} = 4.3 \times 10^{-5}\text{ cm}$$

7. Total Plate Height

The total plate height is therefore the sum of the above individual contributions.

$$H = H_{LD} + H_{couple} + H_{sm} + H_s$$

$$= (3 \times 10^{-5} + 0.0046 + 0.0027 + 4.3 \times 10^{-5})\text{ cm}$$

$$H = 0.0073\text{ cm}$$

APPENDIX 2

Calculation of Specific Pore Volume for Partisil-10 ODS-3

Sander et.al. [3.4] used size exclusion chromatographic techniques to determine the specific pore volumes of a variety of bonded phase. They describe the synthesis of phases of different chain lengths in so-called monomeric and polymeric (which results in cross-linking of the stationary phase) syntheses. They demonstrate that the decrease in pore volume associated with surface derivatization of silica is independent of the type of synthesis used and is dependent only on the percentage carbon loading, % C. From their published data, equation A2.1 relates the pore volume of the bonded phase to % C.

$$v'_p = v_{p,Si} - \frac{0.0169\ mL}{g\ Si}(\%\ C) \qquad \text{eqn. A2.1}$$

Here, $v_{p,Si}$ is the specific pore volume of the original, underivatized silica. This is usually the only information available about pore volume for commercially available bonded phases. As further explained below, v'_p is the pore volume of the bonded phase with respect to the weight of the original silica in the bonded phase.

For the Partisil-10 ODS-3 used in the experiments, $v_{p,Si}$ is approximately 0.8 mL/g Si and the % C loading is 10.5 %. Therefore, v'_p is 0.62 mL/g Si. In order to calculate the pore volume with respect to the weight of the stationary phase as a whole, it is necessary to calculate the relative weight of original silica in the bonded phase.

In the derivatization process, octadecyl-silyl groups, Si-$C_{18}H_{37}$, are bonded to the silica surface by Si-O-Si linkages. The derivatization process is assumed to be the only source of C. In 100 g of derivatized packing, there are 10.5 g of carbon, corresponding to 0.874 mol. The amount of H added by the derivatization can be calculated from the ratio of C:H in ODS and is 1.8 g. Some silica is added in the derivatization process, in this case 0.049 mol or 1.4 g. In 100 g packing, the amount

of original silica is then given by equation A2.2

$$\text{g Si in pkg} = 100\ \text{g} - \text{g C} - \text{g H} - \text{g added Si} \qquad \text{eqn A2.2}$$

For Partisil-10 ODS-3, there are 86 g of original silica in 100 g of packing. The pore volume with respect to the weight of the bonded phase is calculated using A2.3

$$v_p = v_p' \frac{\text{g Si in pkg}}{\text{g pkg}} \qquad \text{eqn A2.3}$$

For Partisil-10 ODS-3, v_p is calculated to be 0.54 mL/ g pkg. A typical shallow bed with a weight of 1.06 ± .04 mg will have a pore volume of 0.57 µL.

PRP-1, the porous polymeric packing, has a specific pore volume of 0.79 mL/g pkg. A typical shallow bed with a weight of 1.82 ± .04 mg will have a pore volume of 1.43 µL.

APPENDIX 3.1

The program shown below, written in MATLAB by David Gowanlock is referred to in the text as EXPGAUSS and calculates the Exponentially-modified Gaussian function that best fits data from an elution curve. The data are entered with their time values in the brackets following the Data command.

```
echo off
clc
clear
Data = ...
[];
numberofpoints = 40;
t = Data(:,1);
y = Data(:,2);
[Ymax,indexYmax] = max(y);
[Ymin1,indexYmin1] = min(y(1:indexYmax));
[Ymin2,index] = min(y(indexYmax:length(y)));
indexYmin2 = index + indexYmax - 1;

[M0,M1,M2,M3] = moments(t,y);

retenttime_exp = (M3 ./ 2) .^ 0.3333
retenttime_gaus = M1 - retenttime_exp
variance_exp = retenttime_exp .^ 2
variance_gaus = M2 - variance_exp
fit_indecies = linspace(1,length(y),numberofpoints);
round(fit_indecies);
global FitData_t
FitData_t = t(fit_indecies);
global FitData_y
FitData_y = y(fit_indecies) ./ M0; % area of dist. normalized to unit area
axis([t(1) t(length(t)) 0 (Ymax ./ M0 .* 1.05)]);
plot(t,y ./ M0,FitData_t,FitData_y,'o');
```

```
lam = [retenttime_gaus retenttime_exp (variance_gaus .^ 0.5)]';
lam = fmins('fitmy',lam,.1)

FitData_y = y(fit_indecies);

global lam_global
lam_global = lam;
lin_scaling_factor = fzero('exp_fit_diff',M0)

mintime = min(t);
maxtime = max(t);
miny = 0.0;
maxy = max(y);
t_curvefit = mintime:10:maxtime;
y_curvefit = lin_scaling_factor .* (exp(lam(3).^2 ./ (2 .* lam(2).^2)) .* ...
exp((lam(1) - t_curvefit) ./ lam(2)) ./ (2 .* lam(2)) .* ...
(1 + erf((t_curvefit-lam(1)-lam(3).^2 ./ lam(2)) ./( sqrt(2) .* lam(3)))));
axis([mintime maxtime miny (maxy .* 1.05)]);
plot(t,y,FitData_t,FitData_y,'o',t_curvefit,y_curvefit);
xlabel('Time  [seconds]');
ylabel('Counts');
text(.65,.8,'numeric','sc')
text(.8,.8,'fit','sc')
text(.5,.7,'gaus  tr','sc')
text(.5,.65,'gs  sd.dv.','sc')
text(.5,.6,'exp  tr','sc')
text(.65,.7,num2str(retenttime_gaus),'sc')
text(.65,.65,num2str(variance_gaus .^ 0.5),'sc')
text(.65,.6,num2str(retenttime_exp),'sc')
text(.8,.7,num2str(lam(1)),'sc')
text(.8,.65,num2str(lam(3)),'sc')
text(.8,.6,num2str(lam(2)),'sc')
```

APPENDIX 3.2

The program shown below, called FITMY, is referred to in the EMG curve fitting routine shown in Appendix 3.1 and is written in MATLAB by David Gowanlock.

```
function f = fitfun(lam)
%       FITFUN is used by FITDEMO.  Fitfun(lam) returns the error
%       between the data and the values computed by the current
%       function of lam.  FITFUN assumes a function of the form

%y = lam(4).*(exp(lam(3) .^2 ./ (2 .* lam(2) .^2)) .* exp((lam(1) - t) ...
% ./ lam(2)) ./ (2 .* lam(2)) .* ...
%(1 + erf((t-lam(1)-lam(3) .^2 ./ lam(2)) ./( sqrt(2) .* lam(3)))));
% Global Data
t = FitData_t; y = FitData_y;
A = zeros(length(t),1);
for j = 1:1
A(:,j) = (exp(lam(3).^2 ./ (2 .* lam(2).^2)) .* exp((lam(1) - t) ...
 ./ lam(2)) ./ (2 .* lam(2)) .* ...
(1 + erf((t-lam(1)-lam(3).^2 ./ lam(2)) ./( sqrt(2) .* lam(3)))));

end
c = A\y;
z = A*c;
f = norm(z-y);

% Statements to plot progress of fitting:
%plot(t,z,t,y,'o')
%xt = max(t)/2;
%yt = max(y)/2;
%text(xt,1.2*yt,['lambda(1,2) = ' num2str(lam(1)) '  ' num2str(lam(2))])
%text(xt,1.0*yt,['lambda(3) = ' num2str(lam(3))])
%text(xt,0.8*yt,['err norm = ' num2str(f)])
```

APPENDIX 3.3

The program shown below, FZERO, is written in MATLAB by David Gowanlock and is referred to in the program peakshape shown in Appendix 4.1. It is used to find the minimum of a function.

```
function b = fzero(FunFcn,x,tol,trace)
%FZERO       Zero of a function of one variable.
%       FZERO(F,X) finds a zero of f(x). F is a string containing the
%       name of a real-valued function of a single real variable. X is
%       a starting guess. The value returned is near a point where F
%       changes sign. For example, FZERO('sin',3) is pi. Note the
%       quotes around sin. Ordinarily, functions are defined in M-files.
%       An optional third argument sets the relative tolerance for the
%       convergence test. The presence of an nonzero optional fourth
%       argument triggers a printing trace of the steps.
%       C.B. Moler 1-19-86
%       Revised CBM 3-25-87, LS 12-01-88.
%       Copyright (c) 1986-88 by the MathWorks, Inc.
% This algorithm was originated by T. Dekker. An Algol 60 version,
% with some improvements, is given by Richard Brent in "Algorithms for
% Minimization Without Derivatives", Prentice-Hall, 1973. A Fortran
% version is in Forsythe, Malcolm and Moler, "Computer Methods
% for Mathematical Computations", Prentice-Hall, 1976.

% Initialization
if nargin < 3, trace = 0; tol = eps; end
if nargin == 3, trace = 0; end
if trace, clc, end
if x ~= 0, dx = x/20;
else, dx = 1/20;
end
a = x - dx;  fa = feval(FunFcn,a);
if trace, home, init = [a fa], end
b = x + dx;  fb = feval(FunFcn,b);
```

```
if trace, home, init = [b fb], end

% Find change of sign.
while (fa > 0) == (fb > 0)
  dx = 2*dx;
  a = x - dx;  fa = feval(FunFcn,a);
  if trace, home, sign = [a fa], end
  if (fa > 0) ~= (fb > 0), break, end
  b = x + dx;  fb = feval(FunFcn,b);
  if trace, home, sign = [b fb], end
end

fc = fb;
% Main loop, exit from middle of the loop
while fb ~= 0
  % Insure that b is the best result so far, a is the previous
  % value of b, and c is on the opposite of the zero from b.
  if (fb > 0) == (fc > 0)
    c = a;  fc = fa;
    d = b - a;  e = d;
  end
  if abs(fc) < abs(fb)
    a = b;    b = c;    c = a;
    fa = fb;  fb = fc;  fc = fa;
  end

  % Convergence test and possible exit
  m = 0.5*(c - b);
  toler = 2.0*tol*max(abs(b),1.0);
  if (abs(m) <= toler) + (fb == 0.0), break, end

  % Choose bisection or interpolation
  if (abs(e) < toler) + (abs(fa) <= abs(fb))
  % Bisection
    d = m;  e = m;
  else
```

```
  % Interpolation
    s = fb/fa;
    if (a == c)
    % Linear interpolation
      p = 2.0*m*s;
      q = 1.0 - s;
    else
    % Inverse quadratic interpolation
      q = fa/fc;
      r = fb/fc;
      p = s*(2.0*m*q*(q - r) - (b - a)*(r - 1.0));
      q = (q - 1.0)*(r - 1.0)*(s - 1.0);
    end;
    if p > 0, q = -q; else p = -p; end;
    % Is interpolated point acceptable
    if (2.0*p < 3.0*m*q - abs(toler*q)) * (p < abs(0.5*e*q))
      e = d;  d = p/q;
    else
      d = m;  e = m;
    end;
  end % Interpolation
% Next point
  a = b;
  fa = fb;
  if abs(d) > toler, b = b + d;
  else if b > c, b = b - toler;
     else b = b + toler;
     end
  end
  fb = feval(FunFcn,b);
  if trace, home, step = [b fb], end
end % Main loop
```

APPENDIX 3.4

The program shown below, written in MATLABby David Gowanlock is called EXP_FIT_DIFF and is used in peakshape, the program shown in Appendix 3.1 to determine the difference between the experimental data points and those calculated by the fit equation.

```
function differ = exp_fit_diff(linscale)

% Global Data
t = FitData_t; y_experimental = FitData_y;
lam = lam_global;

y_fit = linscale .* (exp(lam(3).^2 ./ (2 .* lam(2).^2)) .* exp((lam(1) - t) ...
 ./ lam(2)) ./ (2 .* lam(2)) .* ...
(1 + erf((t-lam(1)-lam(3).^2 ./ lam(2)) ./( sqrt(2) .* lam(3)))));

differ = sum(y_experimental - y_fit);
```

APPENDIX 4.1

The program shown in Appendix 4.1 is written in MATLAB by David Gownalock and uses information from the sorption rate curves to calculate the elution chromatogram. The program is called PEAK SHAPE CALC. It is based on the data treatment discussed in Section 2.3.6.

```
clear
clc
% ELUTION CHROMATOGRAM FROM KINETIC CURVE
% David Gowanlock  May 31, 1991
%
% The following is written to predict elution chromatogram profiles
% from shallow bed kinetic plots. In this case the shallow bed kinetic
% plots have been fit to a triexponential of the following form:
%
% absorbance = n0 - (n1 * exp(-k1 * t)) - (n2 * exp(-k2 * t))
%              - (n3 * exp(-k3 * t))
%
%                        1 = fast sites
%                        2 = intermediate sites
%                        3 = slow sites
% The equation used to produce the elution profiles corresponding
% to each of the above type of sites is given in the following reference
% (see function probdist):
%  equation (1), page 1999
%  J. C. Giddings, Anal. Chem., Vol. 35, Page 1999, Dec. 1963
%
% Variable List
%  k_prime = k'
%  k = rate constant from kinetic curve
%  n = fraction of a particular type of site
%  ord = order of bessel function
%  ts = t - tm
%  tm = time for mobile phase
```

```
%   t = time from injection
%   ka = adsorption rate constant
%   kd = desorption rate constant
%   Pts = probability distribution with respect to time
%   nanalrt = used to detect NaN warnings that can arise in the
%         calculation of bessel values in the function probdist
%                                   stepsz = stepsize along the time axis
%   fr_no_sl = fraction not interacting with the slow sites
%          (fraction not slow)
%   fr_sl = fraction interacting with the slow sites
%        (fraction slow)
%   theor_ratio = theoretical ratio of solute iteracting with slow sites to
%             solute not interacting with slow sites
%   act_ratio = theoretical ratio of solute iteracting with slow sites to
%             solute not interacting with slow sites
%   maxsz = maximum value of range of ts1 and ts2 values
%-------------------------------------------------------------------
%  This section is where the inital parameters used throughout the rest
%  of the program are entered.

stepsz = 50;
maxsz = 3000;
k_prime = 35.7
k1 = 2.79
k2 = .642
k3 = .0572
n1 = 1.70e-7
n2 = .697e-7
n3 = .356e-7
tm = 37.32

n0 = n1 + n2 + n3

%-------------------------------------------------------------------
%  The following calculates the elution profile for the fast sites.
%
```

```
ord1 = 1;
ts1 = 1:stepsz:maxsz;
ka1 = k1 ./ (1 + (k_prime .^ (-1)))
kd1 = k1 ./ (k_prime + 1)
tm1 = tm .* n1 ./ n0

[Pts1,nanalrt1] = probdist(ts1,ka1,kd1,tm1,ord1);

%-----------------------------------------------------------------
% The following calculates the eleution profile for the intermediate sites.
%
ord2 = 1;
ts2 = 1:stepsz:maxsz;
ka2 = k2 ./ (1 + (k_prime .^ (-1)))
kd2 = k2 ./ (k_prime + 1)
tm2 = tm .* n2 ./ n0

[Pts2,nanalrt2] = probdist(ts2,ka2,kd2,tm2,ord2);

%-----------------------------------------------------------------
% The following convolves the elution profiles of sites 1 & 2 and
% calculates the maximum value of the ts3 array.
Pts1_2 = conv(Pts1,Pts2);
maxsz3 = length(Pts1_2) .* stepsz;

%-----------------------------------------------------------------
% The following calculates the elution profile for the slow sites
%
ord3 = 1;
ts3 = 1:stepsz:maxsz3;
ka3 = k3 ./ (1 + (k_prime .^ (-1)))
kd3 = k3 ./ (k_prime + 1)
tm3 = tm .* n3 ./ n0

[Pts3,nanalrt3] = probdist(ts3,ka3,kd3,tm3,ord3);
%-----------------------------------------------------------------
```

```
% The following convolves the elution profiles and plots the results
% along with the elution profiles for each type of site acting alone.
%
ts1_2 = 1:stepsz:maxsz3;
Pts1_2_3 = conv(Pts1_2,Pts3);
maxsz1_2_3 = length(Pts1_2_3) .* stepsz;
ts1_2_3 = 1:stepsz:maxsz1_2_3;
ymax = max([max(Pts1),max(Pts2),max(Pts3)]);
scale1_2 = 0.6 .* ymax ./ max(Pts1_2);
scale1_2_3 = 0.4 .* ymax ./ max(Pts1_2_3);

axis([0,maxsz1_2_3.*0.5,0,1.05.*ymax])
plot(ts2,Pts2,ts1,Pts1,ts1_2,Pts1_2 .* scale1_2,ts3,Pts3,ts1_2_3,Pts1_2_3 .* ...
scale1_2_3)
xlabel('ts'), ylabel('P(ts)')
pause
%-----------------------------------------------------------------------
% Integration of the peaks

area1_2 = integrate_2pt(ts1_2,Pts1_2)
area1_2_3 = integrate_2pt(ts1_2_3,Pts1_2_3)
%area1 = integrate_2pt(ts1,Pts1)
%area2 = integrate_2pt(ts2,Pts2)
%area3 = integrate_2pt(ts3,Pts3)
%-----------------------------------------------------------------------
% This section scales the convolution of 1 & 2 with the convolution of 1, 2, & 3

fr_no_sl = exp(-1 .* ka3 .* tm3);
fr_sl = 1.0 - fr_no_sl;
theor_ratio = fr_sl ./ fr_no_sl;
act_ratio = area1_2_3 ./ area1_2;
correction = theor_ratio ./ act_ratio;
Pts1_2_3 = Pts1_2_3 .* correction;
area1_2_3 = integrate_2pt(ts1_2_3,Pts1_2_3)
axis([0,maxsz1_2_3.*0.5,0,1.05.*max([max(Pts1_2),max(Pts1_2_3)])])
plot(ts1_2,Pts1_2,ts1_2_3,Pts1_2_3)
```

```
xlabel('ts'), ylabel('P(ts)')
pause

%-------------------------------------------------------------------------
%  This section addes the convolution of 1 & 2  to the convolution of 1, 2, & 3
%
for l= 1:length(Pts1_2);
Ptsnet(l) = Pts1_2(l) + Pts1_2_3(l);
end
axis([0,maxsz1_2_3.*0.5,0,1.05.*max(Ptsnet)])
plot(ts1_2,Pts1_2,ts1_2_3,Pts1_2_3,ts1_2,Ptsnet)
xlabel('ts'), ylabel('P(ts)')
pause

%-------------------------------------------------------------------------
%  This section plots the elution profile from time of injection, not ts
%  (ts = t - tm)
%
t1_2 = ts1_2 + tm;
axis;
plot(t1_2,Ptsnet)
xlabel('t'), ylabel('P(t)')
```

APPENDIX 4.2

The following program, called INTEGRATE_2PT, is used in the program PEAK SHAPE CALC shown in Appendix 4.1. It was written in MATLAB by David Gowanlock.

```
function area = integrate_2pt(X,Y)
%
%
if length(X) ~= length(Y)
  error('Can not integrate because X & Y of unequal length')
end
deltaX = X(2) - X(1);
runningarea = 0.0;
for l = 1:length(X)-1;
  Yave = (Y(l) + Y(l+1)) ./ 2;
  slicearea = deltaX .* Yave;
  runningarea = runningarea + slicearea;
end
area = runningarea;
```

APPENDIX 4.3

The program shown below, called PROBDIST is referred to in the program PEAK SHAPE CALC, shown in Appendix 4.1. It was written in MATLAB by David Gowanlock. This program calculates the function Pt_S.

```
function [Y,nanalrt] = probdist(ts,ka,kd,tm,n)
% PROBABILITY DISTRIBUTION
% The equation used to produce the eleution profile corresponding
% to each type of site
%   equation (1), page 1999
%   J. C. Giddings, Anal. Chem., Vol. 35, Page 1999, Dec. 1963
% Variable List
%   n = order of bessel function
%   ts = t - tm
%   tm = time for mobile phase
%   t = time from injection
%   ka = adsorption rate constant
%   kd = desorption rate constant
%   Pts = probability distribution with respect to time
%   nanalrt = used to detect NaN warnings that can arise in the
%             calculation of bessel values
term = sqrt(4 .* ka .* kd .* tm .* ts);
subterm = abs(((-1) .^n .* bessel(n,i .* term) .* i));
Y = ((ka .* kd .* tm) ./ ts) .^0.5 .* ...
exp(-1 .* ((ka .* tm) + (kd .* ts))) .* ...
subterm;
for l=1:length(Y);
 if Y(l) == NaN,
  Y(l) = 0.0;
       nanalrt(l) = 1;
 end;
end;
```